TUM School of Natural Sciences

Lewis Acid-Catalyzed Photochemical Reactions of Conjugated Carbonyl Compounds: Fundamental Studies and Application to Isomerization of Cycloheptene Derivatives

Daniel P. Schwinger

Vollständiger Abdruck der von der TUM School of Natural Sciences der Technischen Universität München zur Erlangung des akademischen Grades eines Doktors der Naturwissenschaften (Dr. rer. nat.) genehmigten Dissertation.

Vorsitz: Prof. Dr.-Ing. Kai-Olaf M. Hinrichsen

Prüfer*innen der Dissertation:
1. Prof. Dr. Thorsten Bach
2. Prof. Dr. Stephan A. Sieber

Die Dissertation wurde am 23.05.2023 bei der Technischen Universität München eingereicht und durch die TUM School of Natural Sciences am 15.06.2023 angenommen.

To my family,
all my friends, and my better half

This thesis was conducted under the direction of Prof. Dr. Thorsten Bach at the Technical University of Munich from November 2019 to May 2023.

Parts of this thesis have been published:

- D. P. Schwinger, T. Bach, *Acc. Chem. Res.* **2020**, *53*, 1933–1943.
- M. T. Peschel, P. Kabaciński, D. P. Schwinger, E. Thyrhaug, G. Cerullo, T. Bach, J. Hauer, R. de Vivie-Riedle, *Angew. Chem. Int. Ed.* **2021**, *60*, 10155–10163.
- T. Rigotti, D. P. Schwinger, R. Graßl, C. Jandl, T. Bach, *Chem. Sci.* **2022**, *13*, 2378–2384.
- D. P. Schwinger, M. T. Peschel, C. Jaschke, C. Jandl, R. de Vivie-Riedle, T. Bach, *J. Org. Chem.* **2022**, *87*, 4838–4851.
- D. P. Schwinger, M. T. Peschel, T. Rigotti, P. Kabaciński, T. Knoll, E. Thyrhaug, G. Cerullo, J. Hauer, R. de Vivie-Riedle, T. Bach, *J. Am. Chem. Soc.* **2022**, *144*, 18927–18937.

In this thesis, the relative configuration of racemates is represented with straight bonds (bold or hashed) and the absolute and relative configuration of enantiomerically pure or enantiomerically enriched compounds is represented with wedged bonds (bold or hashed).

racemate

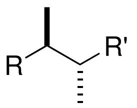

enantiomerically pure or

enantiomerically enriched compound

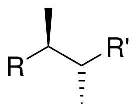

Acknowledgments

First and foremost, I would like to thank my supervisor Prof. Dr. Thorsten Bach for giving me the opportunity to conduct research in his lab and for his professional input on my work. I have learned a lot in the Bach Lab, not only about organic chemistry but also about myself.

I also want to thank:

- the members of my examining committee, Prof. Dr.-Ing. Kai-Olaf M. Hinrichsen and Prof. Dr. Stephan A. Sieber;
- my collaboration partners, including Martin Peschel, Piotr Kabaciński and Thomas Rigotti;
- my interns Aygün Celik, Daniela Krauss, Ekrem Suylu, Ilias Asimakopoulos, Robert Irle, Philipp Schloz and Veit Irl;
- the permanent staff, Anja Osterauer, Jürgen Kudermann, Kerstin Voigt, Olaf Ackermann and Stefan Breitenlechner, who all helped me on multiple occasions; and
- all my proofreaders, for taking the time and providing valuable feedback on my thesis.

Furthermore, I am grateful to my boxmates Christian Schiwek, Franziska Pecho, Morgane de Robichon, Simone Stegbauer and Yeshua Sempere Molina for tips on chemistry and the pleasant work atmosphere. It really was fun being in box 8.

In addition, I thank my labmates Johanna Prößdorf, Maximilian Iglhaut, Raphaela Graßl and Thilo Kratz, as I cannot imagine having that much fun as well as interesting discussions about chemistry and all other things in life with other people. Thank you also to all other former and current members of the Bach Lab for help and support during my PhD – you made this time very special!

Last but not least, I thank my family, my friends, and especially my boyfriend, who have all supported me along my journey.

Abstract

The impact of Lewis acids on photochemical reactions of conjugated carbonyl compounds was investigated within two projects. The first study focused on fundamental studies on Lewis acid–chromophore assemblies using model complexes, namely cyclohex-2-enone–BF_3 and benzaldehyde–BCl_3. A combination of experiments, spectroscopy and theory was used to evaluate mechanistic hypotheses. For the benzaldehyde–BCl_3 complex, photoinduced B – Cl bond fission was found and utilized for C – H bond activation. The second study focused on the application of Lewis acids to the photoinduced *E*–*Z* isomerization of cycloheptene derivatives, which generates strained intermediates for Diels-Alder and other reactions. For cyclohept-2-enone and cyclohept-1-enecarbaldehyde, the substrate scope was investigated. The method was applied to the total synthesis of *trans*-α-himachalene. With Lewis acids, thermal background reactions were unavoidable, making this substrate–catalyst combination unsuitable for photoinduced Diels-Alder reactions. The insights of these studies may benefit related studies on similar chromophores or other catalyst classes.

Zusammenfassung

Der Einfluss von Lewis-Säuren auf photochemische Reaktionen konjugierter Carbonylverbindungen wurde in zwei Projekten untersucht. Die erste Studie konzentrierte sich auf grundlegende Studien zu Lewis-Säure–Chromophor-Verbünden unter Verwendung von Modellkomplexen, speziell Cyclohex-2-enon–BF_3 und Benzaldehyd–BCl_3. Zur Bewertung mechanistischer Hypothesen wurde eine Kombination aus Experimenten, Spektroskopie und Theorie eingesetzt. Für den Benzaldehyd–BCl_3-Komplex wurde eine photoinduzierte B – Cl-Bindungsspaltung beobachtet und für eine C – H-Bindungsaktivierung genutzt. Die zweite Studie konzentrierte sich auf die Anwendung von Lewis-Säuren auf die photoinduzierte *E*-*Z*-Isomerisierung von Cycloheptenderivaten, die gespannte Zwischenprodukte für Diels-Alder-Reaktionen und andere Umsetzungen erzeugt. Für Cyclohept-2-enon und Cyclohept-1-encarbaldehyd wurde die Substratbreite untersucht. Die Methode wurde auf die Totalsynthese von *trans*-α-Himachalen angewendet. Mit Lewis-Säuren waren thermische Hintergrundreaktionen unvermeidbar, sodass diese Substrat-Katalysator-Kombination für photoinduzierte Diels-Alder-Reaktionen ungeeignet war. Die Erkenntnisse dieser Studien können verwandten Studien zu ähnlichen Chromophoren oder anderen Katalysatorklassen zugutekommen.

Contents

Acknowledgments **v**

Abstract / Zusammenfassung **vii**

Abbreviations **xi**

1 Introduction **1**

2 Theoretical Background **3**

2.1 General Photochemistry 3

2.2 Lewis Acids in Photochemical Reactions of Conjugated Carbonyl Compounds 6

2.3 *E*–*Z* Isomerization of Cyclic Alkenes and Subsequent Strain-Release Reactions 8

3 Experiments Conducted, Results and Discussion **11**

3.1 Fundamental Studies on Lewis Acids in Photocatalysis 11

3.2 Photochemical Isomerization of Cycloheptene Derivatives 15

4 Information on Original Publications **21**

4.1 Diels–Alder Reaction of Photochemically Generated (*E*)-Cyclohept-2-enones: Diene Scope, Reaction Pathway, and Synthetic Application . . . 21

4.2 Photoinduced B–Cl Bond Fission in Aldehyde-BCl_3 Complexes as a Mechanistic Scenario for C–H Bond Activation 22

5 Conclusions **23**

Bibliography **25**

A Diels–Alder Reaction of Photochemically Generated (*E*)-Cyclohept-2-enones: Diene Scope, Reaction Pathway, and Synthetic Application **29**

B Photoinduced B–Cl Bond Fission in Aldehyde-BCl_3 Complexes as a Mechanistic Scenario for C–H Bond Activation **45**

Abbreviations

aq.	aqueous
calcd	calculated
Cy	cyclohexyl
DFT	density functional theory
dr	diastereomeric ratio
ee	enantiomeric excess
e. g.	exempli gratia (for example)
Et	ethyl
equiv	equivalent
HAT	hydrogen atom transfer
$h\nu$	indicates light; h is Planck's constant, ν is photon frequency
IC	internal conversion
i. e.	id est (that is)
ISC	intersystem crossing
λ	wavelength
LED	light emitting diode
Me	methyl
n-Bu	*n*-butyl
NMR	nuclear magnetic resonance
PET	positron emission tomography
Ph	phenyl
Φ	quantum yield
rr	regioisomeric ratio
rfx	reflux
rsm	recovered starting material
rt	room temperature
SET	single electron transfer
THF	tetrahydrofuran (oxolane)
TMS	trimethylsilyl
UV	ultraviolet
Vis	visible

1 Introduction

Pharmaceutical agents and their development play a crucial role in society and economy. They are essential for treating various illnesses, ranging from cancer and cardiovascular diseases to bacterial and viral infections. Active pharmaceutical ingredients often have complex structures with defined stereochemical configurations. Many of them are chiral,[1] meaning their image and reflection are not congruent, like a human being's left and right hands. Enantiomers of active ingredients may have different effects, with only one enantiomer achieving the desired effect while the other causing unwanted side effects or no effect at all. Therefore, efficient methods are necessary to synthesize active ingredients from simple precursors in a controlled fashion.

Photochemical reactions (i. e. reactions that are induced by light)[2] are of particular interest since they provide means of accessing structurally complex molecular scaffolds from simple starting materials.[3,4] For years, photochemists have studied these reactions and tried to perform them enantioselectively. To achieve the desired enantioselectivity, chiral catalysts have been applied. A catalyst is a chemical compound that increases the reaction rate and/or induces a certain selectivity, without being consumed in the process.[5]

In the field of photochemistry, major research efforts are still needed to understand the interaction of chromophores and catalysts. Having a wide range of chiral catalysts would be extremely useful for science and industry. However, since excitation with light already forms extremely reactive species that react quickly to form the products, increased demands are placed on a catalyst for a photochemical reaction. The catalyst must already bind strongly to the substrate during the excitation or enable its exclusive excitation by binding to the substrate. Achieving this poses a challenging task and remains an active area of research.[6]

Lewis acids are catalysts that have been commonly employed in both thermal[7] and photochemical reactions.[8] They are electron-poor entities that can coordinate to electron-rich moieties and thereby form a defined assembly.[5] It stands to reason that this Lewis acid–substrate assembly has distinct photophysical and photochemical properties. Due to their electron-rich oxygen atom, conjugated carbonyl compounds are potential substrates for this kind of catalysis. These molecules have a carbonyl group as well as a system of alternating single and multiple bonds.[5] In this thesis, conjugation refers to molecules like α,β-unsaturated or aromatic aldehydes and ketones.

The aim of this research was to investigate how Lewis acid catalysts impact photochemical reactions of conjugated carbonyl compounds in two main projects. One study focused on fundamental studies of Lewis acid–chromophore assemblies, using two model complexes (Scheme 1a): The cyclohex-2-enone–BF_3 complex (**1**·BF_3) and the benzaldehyde–BCl_3 complex (**2**·BCl_3) served as representative models for *α*,*β*-unsaturated ketones and aromatic aldehydes. Through experiments, theory and spectroscopy, we gained insights into their photochemical mechanisms and found novel reactivity.

Another project focused on the application of Lewis acids to the photoinduced *E*–*Z* isomerization of cycloheptene derivatives (Scheme 1b). This isomerization generates strained intermediates that undergo Diels-Alder reactions at room temperature. Although few publications exist on this reaction with cyclohept-2-enone (**3**) and cyclooct-2-enone (**4**), it has not yet been carried out enantioselectively. As a comprehensive picture of the substrate scope had been missing, we investigated the scope and mechanism of this reaction as well as used the products as a starting point for the synthesis of the natural product *trans*-*α*-himachalene. Furthermore, we studied whether other cycloheptene derivatives like cyclohept-1-enecarbaldehyde (**5**) undergo the photoinduced *E*–*Z* isomerization. Finally, the impact of Lewis acids on the isomerization and strain release-cycloaddition reactions was studied.

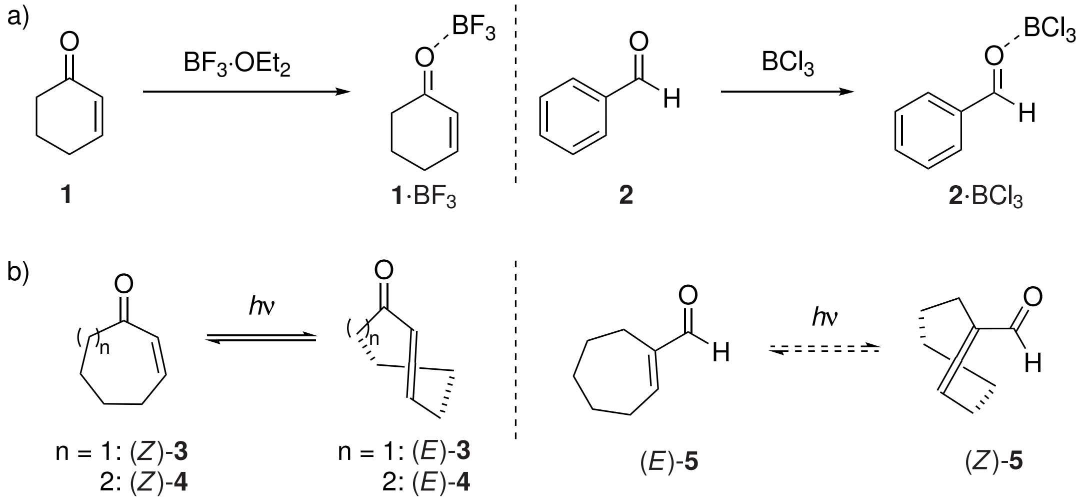

Scheme 1: Substrates investigated in this research study: a) **1** and **2** as model substrates for fundamental studies on Lewis acid-assemblies. b) Photoinduced *E*–*Z* isomerization of **3**, **4**, and potentially **5**.

2 Theoretical Background

2.1 General Photochemistry

The Italian chemist Giacomo Ciamician was a pioneer in the field of photochemistry and already proclaimed in 1912 that photochemistry will be an useful and sustainable field of chemistry in the future.[9] Since then, research in photochemistry has continuously been growing and photochemical reactions have found numerous applications, e. g. in natural product synthesis.[3] In recent years, modern theoretical and spectroscopical methods increased our fundamental understanding of photochemistry.

The foundation of any photochemical reaction is the absorption of a photon with energy $E = h\nu$. With this energy uptake, an excited state is reached, from which different physical or chemical pathways are available. These possibilities are summarized in a Jabłoński diagram (Figure 1).[10] For most organic molecules, their electrons are paired so the sum of the electron spins S is zero, resulting in a multiplicity ($M = 2S + 1$) of 1. States with this multiplicity are called singlet states. In case of a spin flip of a single electron, the multiplicity changes to 3, which means the molecule is in a triplet state. The transition between states of different multiplicities is called intersystem crossing (ISC), a slow process for most organic molecules. A transition between states of the same multiplicity is called internal conversion (IC). These two transitions are non-radiative and provide the molecule the opportunity to return to the ground state S_0. If a molecule returns to S_0 by emission of a photon, the transition is called fluorescence or phosphorescence, depending on the original multiplicity.[11]

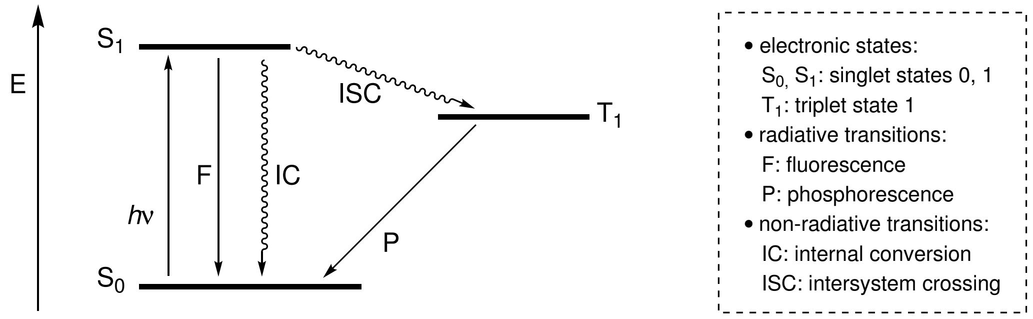
E
S1
S0
T1
hν
F
IC
ISC
P
• electronic states:
S0, S1: singlet states 0, 1
T1: triplet state 1
• radiative transitions:
F: fluorescence
P: phosphorescence
• non-radiative transitions:
IC: internal conversion
ISC: intersystem crossing

Figure 1: Simplified Jabłoński diagram showing energy levels and possible transitions.

All the discussed transitions are chemically non-productive. However, new and often distinct reaction pathways are available for organic molecules in their excited states (e. g.

S_1, T_1). Typical photoreactions include isomerization reactions,[12] and photocycloaddition reactions like [2+2] photocycloaddition of alkenes[13–15] or *ortho* photocycloaddition of arenes,[16–18] for which selected examples are shown in Scheme 2. Lewis acids on photochemical reactions as well as on photoinduced *E*–*Z* isomerization are provided in the next sections.

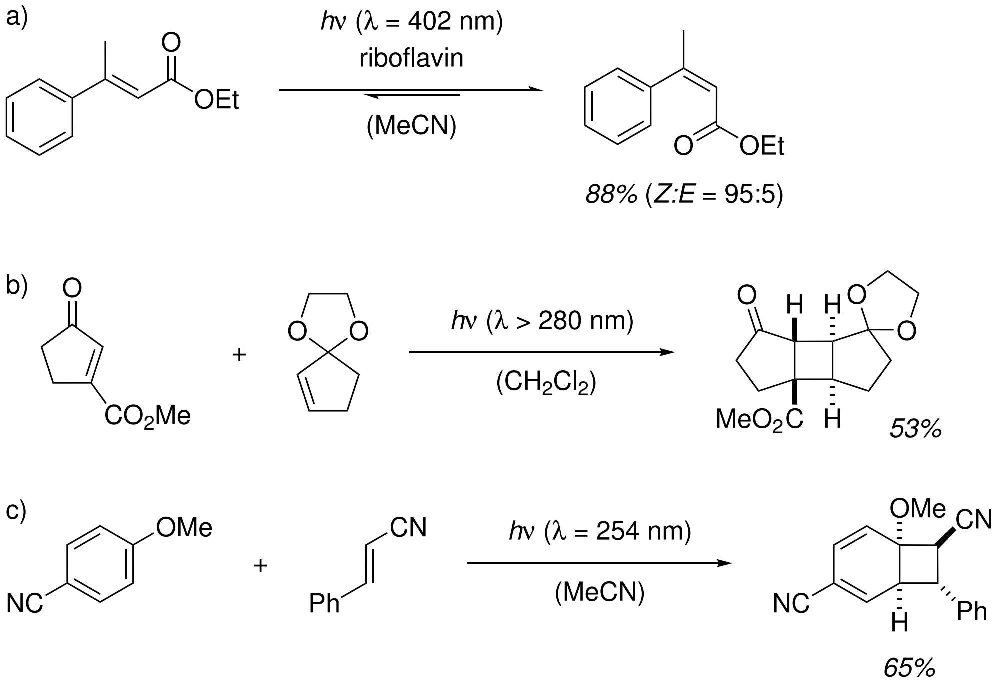

Scheme 2: Selected examples of typical photoreactions: a) Isomerization of a cinnamic acid derivative. b) [2+2] Photocycloaddition of a β-functionalized cyclopent-2-enone with an alkene. c) *ortho* Photocycloaddition of an electron-rich arene with cinnamonitrile.

To evaluate the efficiency of a photochemical reaction, its quantum yield Φ can be determined. This value is defined as the number of certain chemical events per absorbed photon:[5]

$$\Phi = \frac{\text{number of consumed starting material or formed product molecules}}{\text{number of absorbed photons}}$$

The value depends on several factors, as can be seen from the examples in Table 1. For a purely photochemical reaction, the quantum yield cannot exceed unity, as every absorbed photon can only lead to one chemical transformation. In case of radical chain reactions, one photon can lead to the conversion of several molecules of starting material, which results in a quantum yield greater than unity (also see Table 1, entry 7). Thus, the quantum yield can be an indicator if a radical chain mechanism operates in a photoinduced reaction. However, the quantum yield can be dependent on the light intensity in these reactions, which makes it difficult to replicate.[19]

Table 1: Overview of photoreactions for which their quantum yields were determined by our group (chronologically ordered). BArF = tetrakis[3,5-bis(trifluoromethyl)phenyl]borate, bpy = 2,2′-bipyridine, bpz = 2,2′-bipyrazine, TXT = thioxanthone.

#	Reaction and Quantum Yield	Reference
1	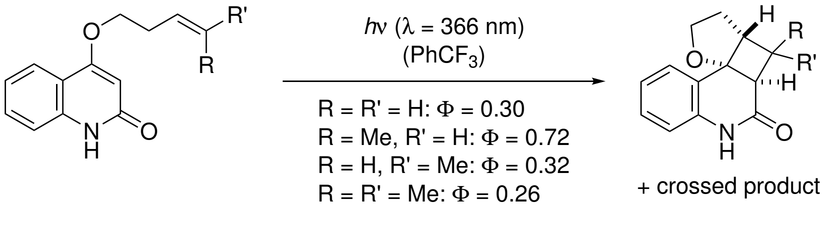 $h\nu$ (λ = 366 nm) ($PhCF_3$) R = R' = H: Φ = 0.30 R = Me, R' = H: Φ = 0.72 R = H, R' = Me: Φ = 0.32 R = R' = Me: Φ = 0.26 + crossed product 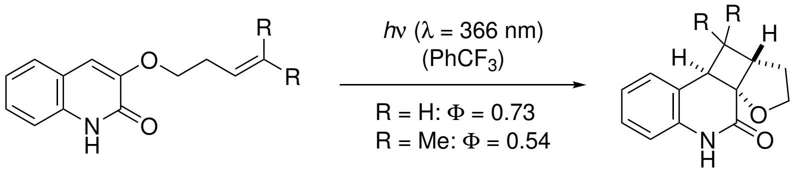 $h\nu$ (λ = 366 nm) ($PhCF_3$) R = H: Φ = 0.73 R = Me: Φ = 0.54	ref.[20]
2	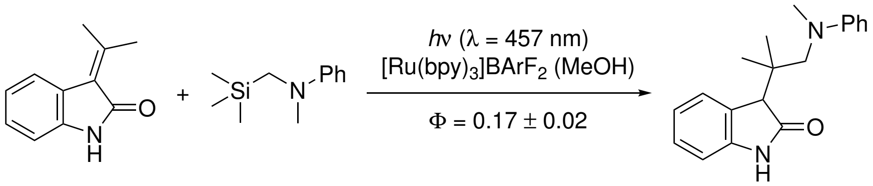 $h\nu$ (λ = 457 nm) $[Ru(bpy)_3]BArF_2$ (MeOH) $\Phi = 0.17 \pm 0.02$	ref.[21]
3	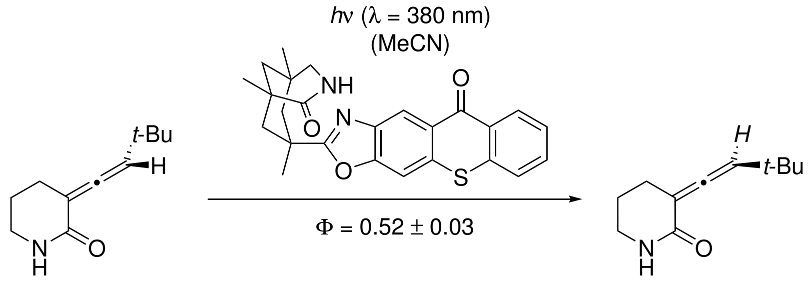 $h\nu$ (λ = 380 nm) (MeCN) $\Phi = 0.52 \pm 0.03$	ref.[22]
4	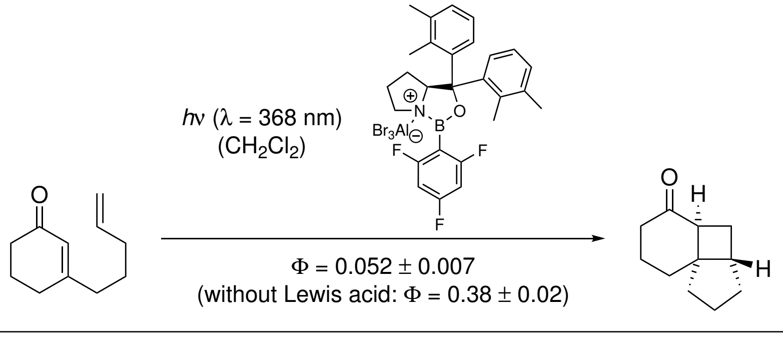 $h\nu$ (λ = 368 nm) (CH_2Cl_2) $\Phi = 0.052 \pm 0.007$ (without Lewis acid: $\Phi = 0.38 \pm 0.02$)	ref.[23]
5	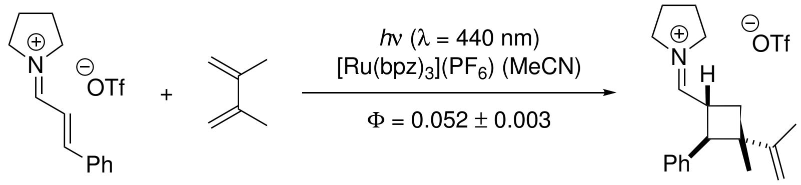 $h\nu$ (λ = 440 nm) $[Ru(bpz)_3](PF_6)$ (MeCN) $\Phi = 0.052 \pm 0.003$	ref.[24]

6	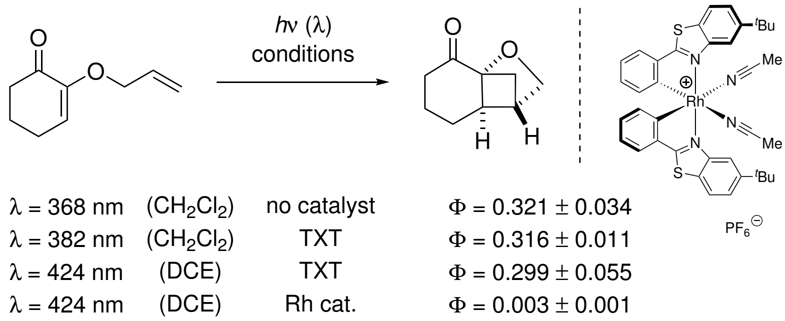 λ = 368 nm (CH$_2$Cl$_2$) no catalyst Φ = 0.321 ± 0.034 λ = 382 nm (CH$_2$Cl$_2$) TXT Φ = 0.316 ± 0.011 λ = 424 nm (DCE) TXT Φ = 0.299 ± 0.055 λ = 424 nm (DCE) Rh cat. Φ = 0.003 ± 0.001	ref.[25]
7	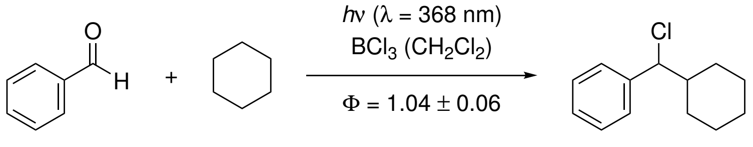 *hν* (λ = 368 nm) BCl$_3$ (CH$_2$Cl$_2$) Φ = 1.04 ± 0.06	ref.[26]

2.2 Lewis Acids in Photochemical Reactions of Conjugated Carbonyl Compounds

Already in the 1980s, a change in absorption and reactivity was reported for conjugated carbonyl compounds by addition of Lewis acids.[27,28] Since then, the activation of conjugated carbonyl compounds with Lewis acids and other compounds for photochemical transformations has been studied.[29–31] It has become clear that various facets can be modulated by Lewis acids: singlet and triplet state energies, absorptivity, redox potential, or the reaction pathway in general. For example, with chiral 1,3,2-oxazaborolidine catalysts, various substrates can undergo enantioselective photochemical reactions.[32]

Chiral oxazaborolidines have already been studied extensively in thermal reactions.[33] They can be tailored to a specific reaction by variation of the aryl substituents as these stem from condensation of a prolinol and a boronic acid, comparable to two variable modules being put together. The sterically demanding aryl residues allow side differentiation and thus enantioselectivity when the catalyst is bound to the substrate. A correspondingly strong bond to the substrate is therefore necessary. Calculations suggest that on the one hand the boron atom (Lewis acidic site) coordinates to the oxygen atom of the carbonyl group (Lewis basic site) and on the other hand the oxygen atom of the catalyst forms a non-classical hydrogen bond with either an olefinic *α*-hydrogen atom or an aldehyde hydrogen atom.[34] As conjugated carbonyl compounds share these structural features, many of them are suitable chromophores for activation with chiral 1,3,2-oxazaborolidine Lewis acids (Scheme 3).

In some cases, racemic background reactions prevent the use of low catalyst loadings (< 50 mol%, see Scheme 3a,b). For example, simple *α*,*β*-unsaturated ketones show a weak absorption band typically between 300 nm to 350 nm, where also the strong

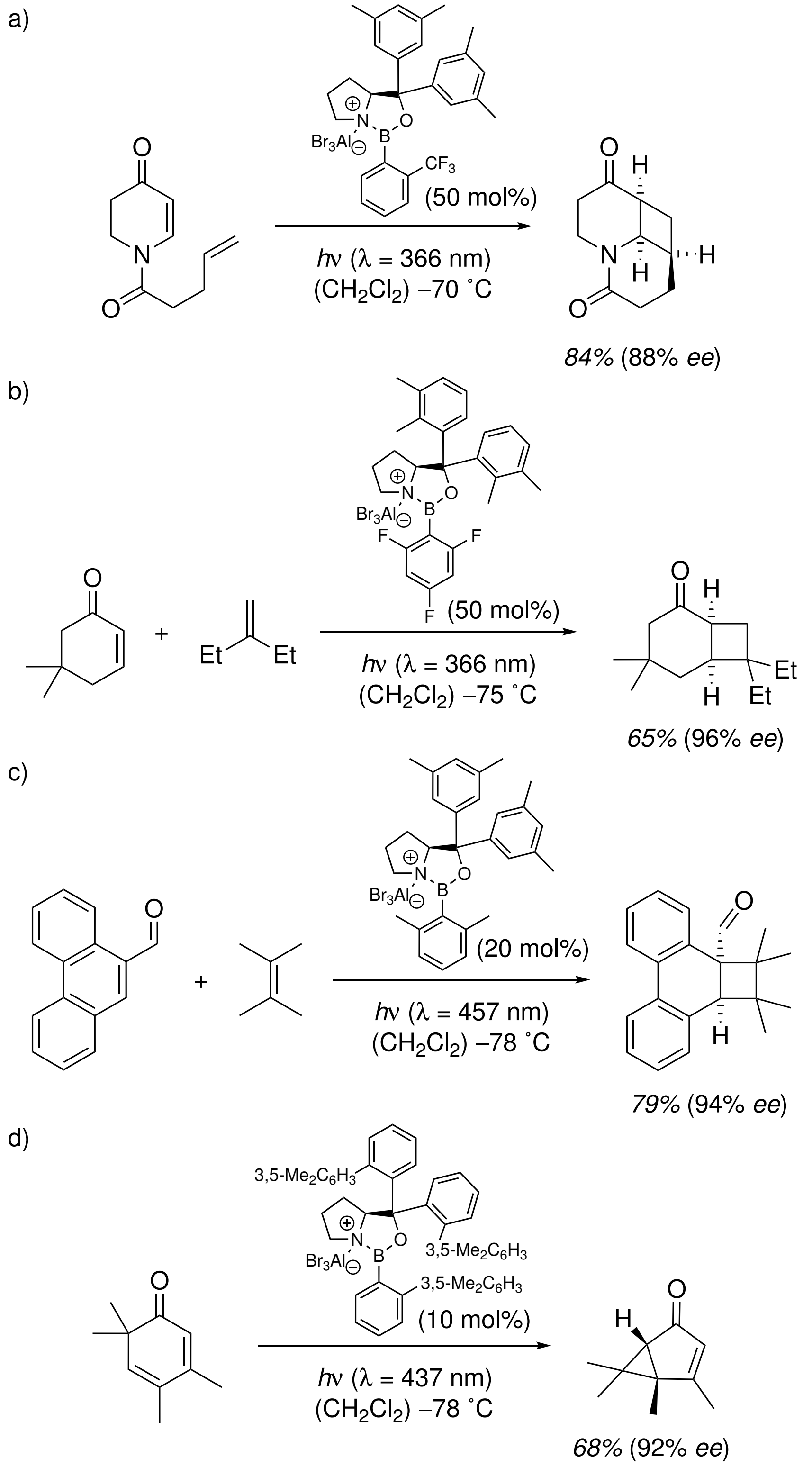
a)
Br$_3$Al
CF$_3$
(50 mol%)
hν (λ = 366 nm)
(CH$_2$Cl$_2$) –70 °C
84% (88% ee)
b)
Br$_3$Al
F
(50 mol%)
Et
hν (λ = 366 nm)
(CH$_2$Cl$_2$) –75 °C
65% (96% ee)
c)
Br$_3$Al
(20 mol%)
hν (λ = 457 nm)
(CH$_2$Cl$_2$) –78 °C
79% (94% ee)
d)
3,5-Me$_2$C$_6$H$_3$
Br$_3$Al
(10 mol%)
hν (λ = 437 nm)
(CH$_2$Cl$_2$) –78 °C
68% (92% ee)

Scheme 3: Selected examples of enantioselective photoreactions with 1,3,2-oxazaborolidine catalysts: a) [2+2] Photocycloaddition of a 2,3-dihydropyridin-4(1*H*)-one. b) [2+2] Photocycloaddition of a cyclohex-2-enone. c) *ortho* Photocycloaddition of phenanthrene-9-carbaldehyde. d) Oxadi-π-methane rearrangement of a cyclohexa-2,4-dienone.

absorption band of their Lewis acid assembly lies. Therefore, both the assembly and the uncomplexed substrate will be excited, leading to a loss of enantioselectivity.

Besides the possibility of stereoselectivity, Lewis acids can also enable new photoreactivity. As an example, 2-naphthaldeyhde (**6**) typically reacts with simple olefins like 2,3-dimethylbut-2-ene in a Paternò-Büchi reaction to oxetane **7**. In the presence of $AlBr_3$ as Lewis acid, the *ortho* photocycloaddition product **8** was obtained (Scheme 4).[35] In addition, a significant bathochromic shift was observed for the substrate–Lewis acid assembly, which enabled irradiation with visible light. This effect has also been observed for other chromophores, e. g. cyclohexa-2,4-dienones.[36] In these cases, high enaniomeric excesses can be achieved even with low loadings of chiral catalyst (see Scheme 3c,d).

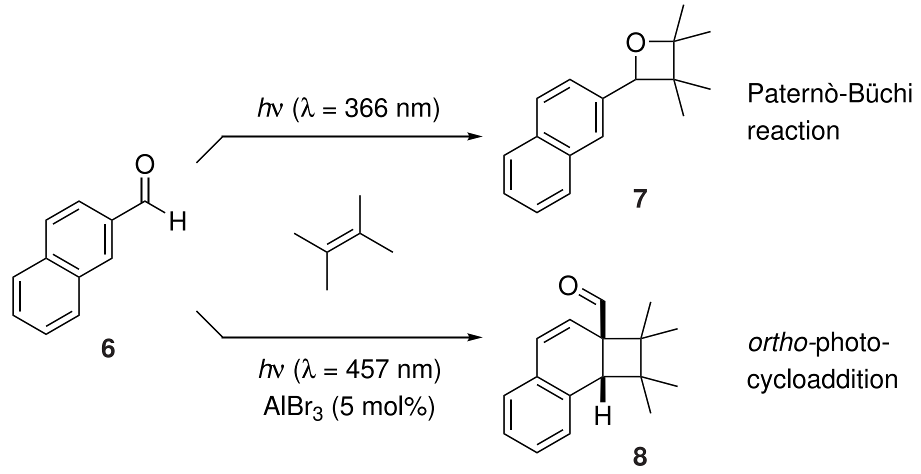

Scheme 4: Change of 2-naphthaldehyde's reactivity by addition of $AlBr_3$.

Gaining a better understanding of how Lewis acids interact with conjugated carbonyl compounds is therefore helpful to design new photochemical methods and expand the synthetic photochemistry toolbox.

2.3 *E–Z* Isomerization of Cyclic Alkenes and Subsequent Strain-Release Reactions

The photoinduced isomerization of olefinic double bonds is a topic of ongoing scientific research and even relevant for vision in mammals.[12] While substituents at a C=C double bond must be planar in the ground state, the double bond character is removed in the excited state, allowing rotation around the C–C bond (Scheme 5a). The molecule can then relax to either the *E*- or *Z*-configured isomer. Depending on the absorptivity of these two isomers (or the triplet energies in case of a sensitized isomerization), one of the two diastereomers will be enriched. In mammalian vision, 11-*cis*-retinal (**9**) is bound to a protein, opsin, and isomerizes upon excitation to **10** (Scheme 5b), which causes a neural signal and sets free all-*trans*-retinal (**11**). In a separate biochemical pathway, **11** is transformed back to **9**.

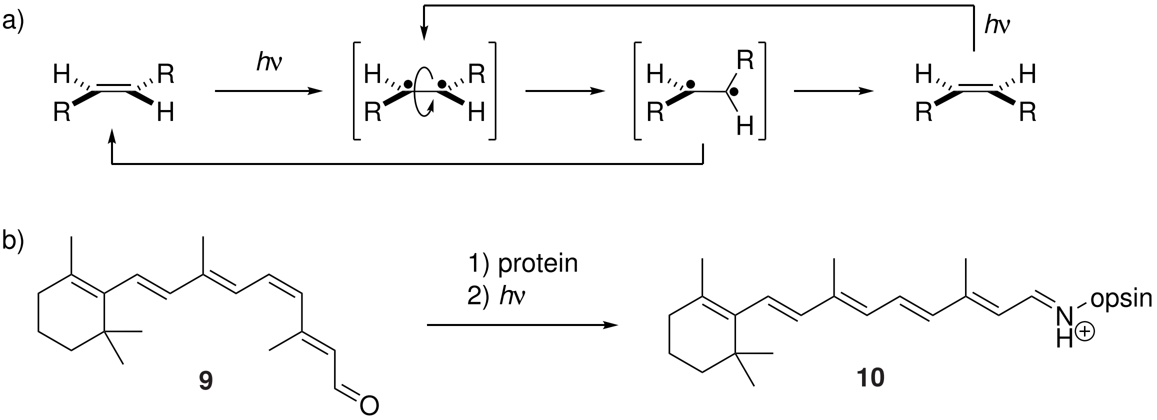

Scheme 5: a) Photoinduced *E*–*Z* isomerization of an alkene. b) Photoisomerization of retinal **9** as part of the visual cycle.

In cyclic systems, this isomerization is intrinsically limited. While isomerization is impossible for cyclopentene, the flexibility of the chain increases with the number of carbon atoms, so that larger rings like cyclooctene can adopt a highly twisted state from which they can also relax to the corresponding (*E*)-isomer. For example, Swenton described the photoisomerization of (*Z*)-cyclooctene to (*E*)-cyclooctene in 1969.[37] Its ring strain can be used for reactions at room temperature that would otherwise require elevated temperatures. This has been employed in the field of bioconjugation.[38–40] (*E*)-Cyclooctene derivatives readily undergo bioorthogonal Diels-Alder reactions with tetrazine derivatives (with bioorthogonal meaning rapid and selective, under physiological conditions and tolerating functional groups of living systems).[41] For example, the Diels-Alder reactions of (*E*)-cyclooctene derivatives can be employed in pre-targeted positron emission tomography (Scheme 6).[42,43]

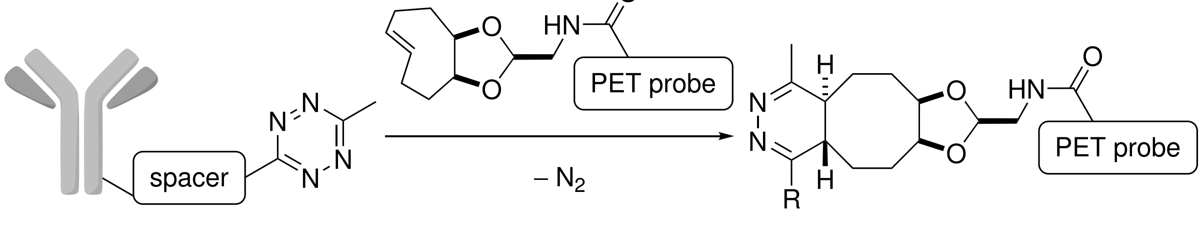

Scheme 6: Bioorthogonal Diels-Alder reaction between a tetrazine attached to an antibody and an (*E*)-cyclooctene derivative with a PET probe. R = spacer + antibody.

Isomerization of simple cycloalkenes requires irradiation with highly energetic UV-C light, which limits functional group tolerance. In contrast, cycloalk-2-enones can absorb UV-A light, as typical for α,β-unsaturated ketones. From their excited state, isomerization and relaxation into their strained isomers are possible. For example, photoisomerization of (*Z*)-cycloheptenone [(*Z*)-**3**] and (*Z*)-cyclooctenone [(*Z*)-**4**] were studied.[44,45] (*E*)-Cycloheptenone and (*E*)-cyclooctenone possess significant ring strain, which enables chemical reactions that normally require separate activation of their (*Z*)-isomers. This includes Diels–Alder reactions with dienes,[46,47] conjugate additions of nucleophiles[44,48–50] or dimerization reactions[51] (Scheme 7).

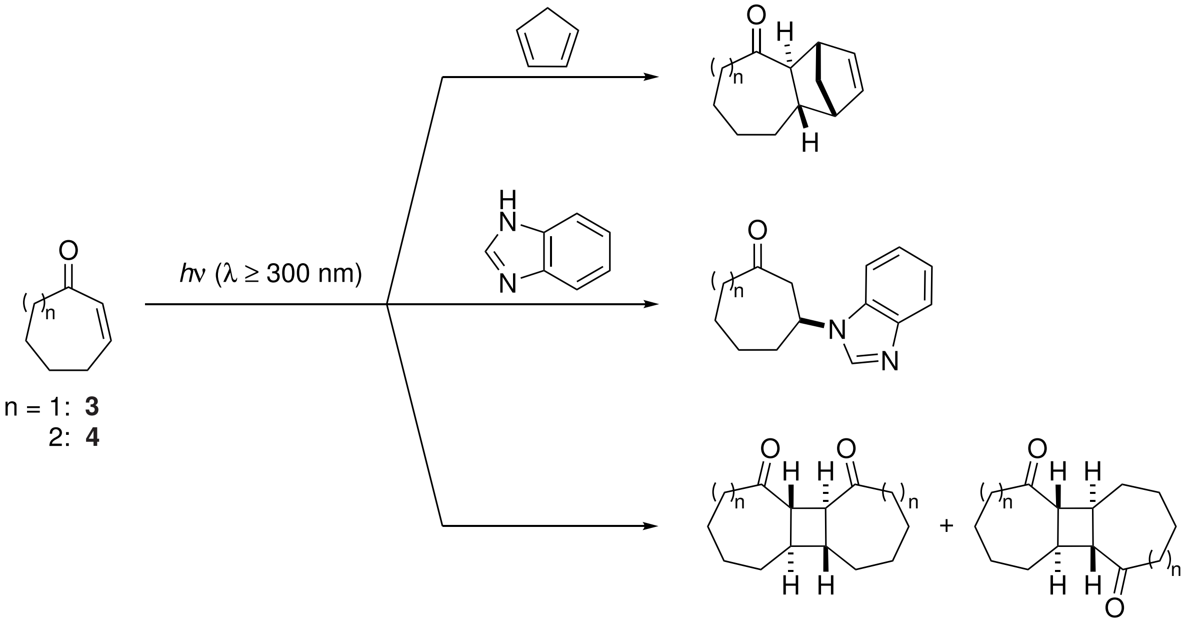

Scheme 7: Examples of photoinduced reactions of **3** (n = 1) and **4** (n = 2).

Since the (*E*)-isomers are chiral and the ring chain shields one face of the C=C double bond, attack of the nucleophile or diene occurs from the more accessible face. So far, this aspect has not been exploited for enantioselective reactions. Again, chiral Lewis acids could be employed to enantioselectively form (*E*)-cycloalkenones for use in a subsequent Diels–Alder reaction. Since an attack would be stereospecific, the stereoinformation would be transferred to the product.

3 Experiments Conducted, Results and Discussion

3.1 Fundamental Studies on Lewis Acids in Photocatalysis

As chiral boron-based Lewis acids have been frequently employed in photochemistry, e. g. with α,β-unsaturated ketones,[23,52] we wanted to investigate their influence on a substrate's pathway after photoexcitation. But as the chiral 1,3,2-oxazaborolidines are too large to be adequately treated on a high level of theory, smaller analogues had to be studied instead. For α,β-unsaturated carbonyl compounds, cyclohex-2-enone (**1**) was chosen as a suitable model substrate.

State-of-the-art transient absorption spectroscopy and high level calculations were therefore conducted on the cyclohex-2-enone–BF_3 complex.[53] Experiment and theory were in good agreement and showed that the complex relaxes to its triplet state after excitation with BF_3 still attached. Likely, this applies also to the more complex chiral 1,3,2-oxazaborolidines and corroborates their mode of action. In addition, we investigated whether we can selectively excite the Lewis acid–substrate assembly $\mathbf{1}\cdot BF_3$ by judicious choice of irradiation wavelength [Figure 2; $\lambda_{max}(\mathbf{1}) = 224\,nm, 329\,nm$; $\lambda_{max}(\mathbf{1}\cdot BF_3) = 250\,nm$]. With irradiation at $\lambda = 272\,nm$, no conversion of cyclohex-2-enone could be detected with isobutene as reactant, due to the ketone alone showing almost no absorption at that wavelength. However, the BF_3-complex showed steady conversion, forming **12** (Scheme 8), due to its significant absorptivity. This highlights how a change in absorptivity, induced by a Lewis acid, can be used for selective excitation and reactivity.

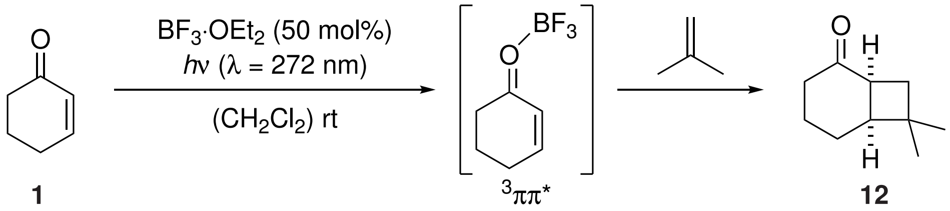

Scheme 8: Selective excitation of $\mathbf{1}\cdot BF_3$ results in a reactive triplet state ($\pi\pi^*$) that undergoes [2+2] photocycloaddition with isobutene to cyclobutane **12**.

Similarly to α,β-unsaturated carbonyl compounds, aromatic aldehydes can form assemblies with Lewis acids that have shown distinct photochemistry compared to their uncomplexed chromophores.[35,54,55] As a next study,[26] we selected benzaldehyde (**2**),

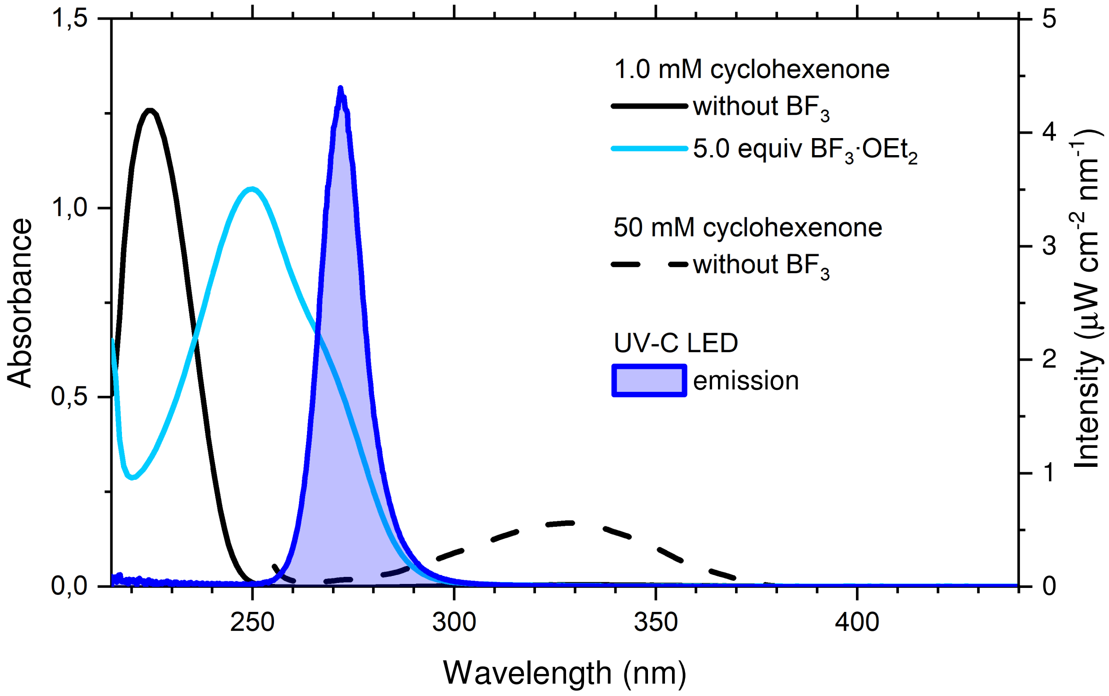

Figure 2: UV/Vis absorption spectrum of **1** and its BF_3 complex (1.0 mm quartz cuvette, in CH_2Cl_2) as well as emission spectrum of the 272 nm LED.

the simplest representative of this class. Due to the lower Lewis basicity of aldehyde **2**, BCl_3 was chosen as a suitable Lewis acid for effective formation of the assembly.[56]

By non-adiabatic dynamics calculations, we predicted a homolytic cleavage of the B–Cl bond after excitation with UV light ($\lambda > 300$ nm), which forms ketyl radical **13** and a chlorine radical (Scheme 9). These radicals were calculated to undergo single electron transfer (SET) to cation **14** and a chloride anion. Both radicals and ions can potentially recombine and tautomerize to the original complex.

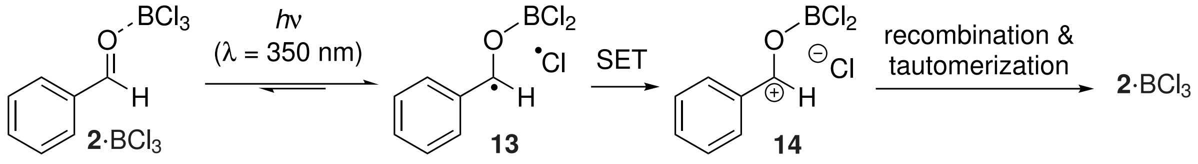

Scheme 9: Photoinduced B–Cl bond fission upon UV irradiation of **2**·BCl_3 and consecutive reactivity as proposed by theory.

UV/Vis titration experiments confirmed that the assembly is a 1:1 complex [Figure 3; λ_{max}(**2**) = 246 nm, 281 nm, 323 nm; λ_{max}(**2**·BCl_3) = 297 nm]. In addition, the calculated spectrum matched the experimental one, confirming that the complex can be adequately described by theory. UV/Vis ultrafast transient absorption spectroscopy revealed that radical **13** was formed with a lifetime of approximately 400 ps. Also cation **14** was identified at approximately 1 ns.

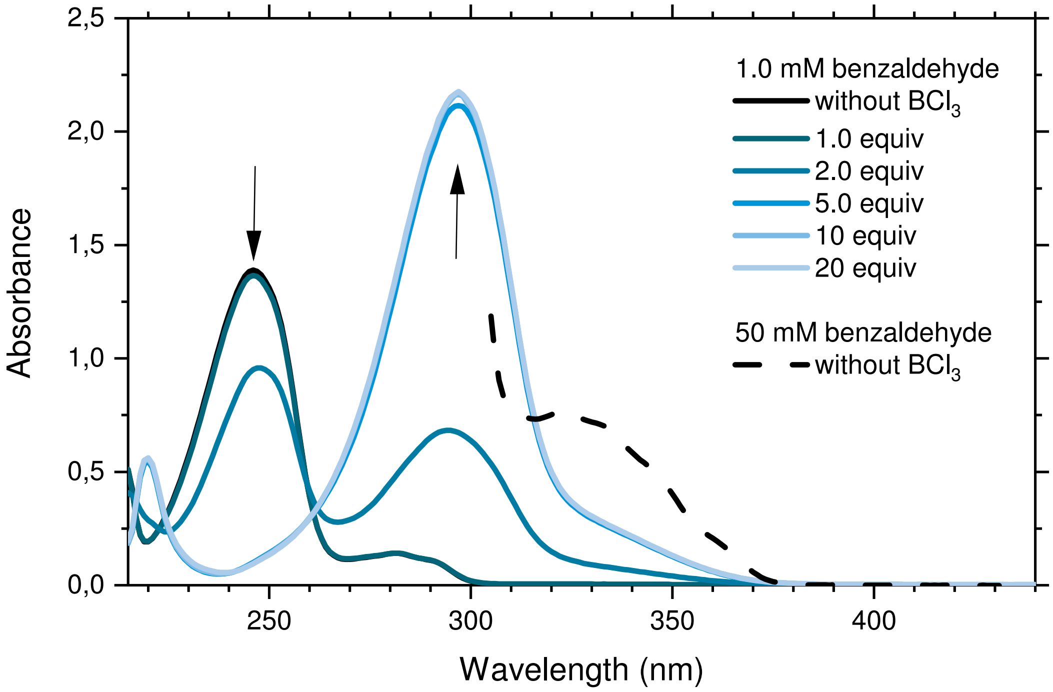

Figure 3: UV/Vis absorption spectrum of **2** and its BCl_3 complex (1.0 mm quartz cuvette, in CH_2Cl_2).

To use this reactivity synthetically, the benzaldehyde–BCl_3 complex was irradiated in the presence of cyclohexane (Scheme 10). The formed chlorine radical was expected to abstract an hydrogen atom from the alkane (hydrogen atom transfer, HAT), forming a cyclohexyl radical.[57] This alkyl radical can then either recombine with a ketyl radical **13** or react with another molecule of the complex, so that a chlorine radical is formed. The latter pathway corresponds to a chain mechanism. In both cases, a borylated alcohol is formed that can undergo nucleophilic substitution with a chloride anion. This hypothesis was confirmed as product **15** was isolated in good yield after irradiation of **2**·BCl_3 with cyclohexane. Because **15** is very non-polar, separation from minor impurities was difficult. This fact sparked the desire to isolate the intermediate alcohol.

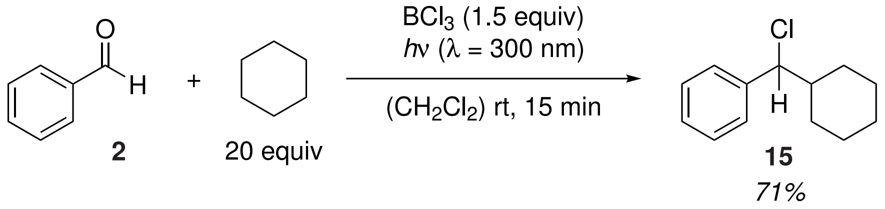

Scheme 10: Formation of **15** by irradiation of **2**·BCl_3 with cyclohexane.

To avoid the nucleophilic substitution and isolate alcohol **16**, inorganic bases as additives were screened. Indeed, with 10 equivalents of K_3PO_4, the reaction stopped at the alcohol stage. Best yields were obtained with 20 equivalents of the alkane, 1.5 equivalents of

BCl_3 and irradiation with a 368 nm LED at 0 °C. Different aromatic aldehydes and alkanes were probed under these optimized conditions and their alcohols were isolated in 42-76% yield (19 examples, 0.200 mmol to 1.00 mmol, Figure 4).

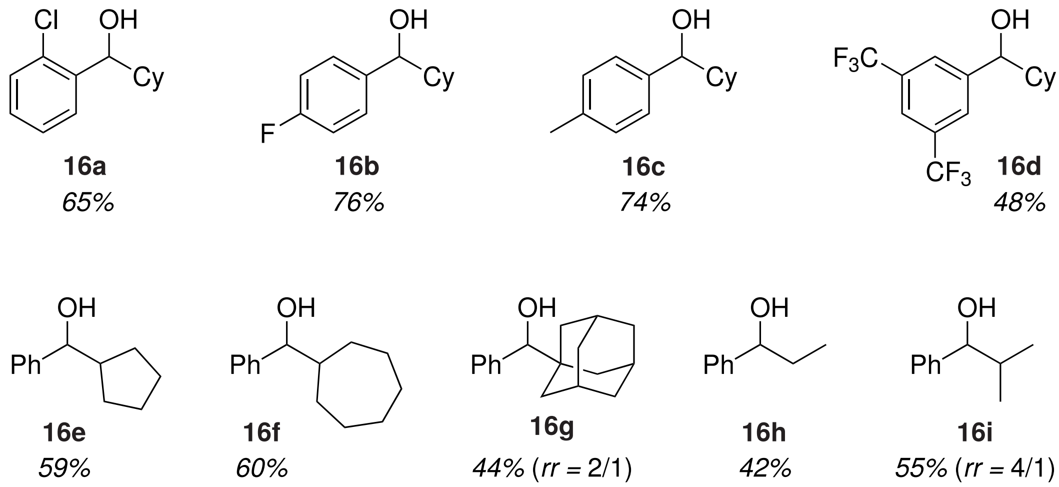

Figure 4: Selected examples of alcohols **16** obtained through the BCl_3-mediated photoreaction with base. Major regioisomers are depicted.

Besides the synthetic scope, we were also interested in the reaction mechanism. Therefore, different mechanistic studies were conducted. H/D experiments with PhCDO or C_6D_{12} showed that deuterium was incorporated into **15** as expected. With a 1:1 mixture of C_6H_{12} and C_6D_{12} (Scheme 11), 50% of the isolated product featured a d_{11}-deuterated cyclohexane ring, suggesting no kinetic isotope effect.

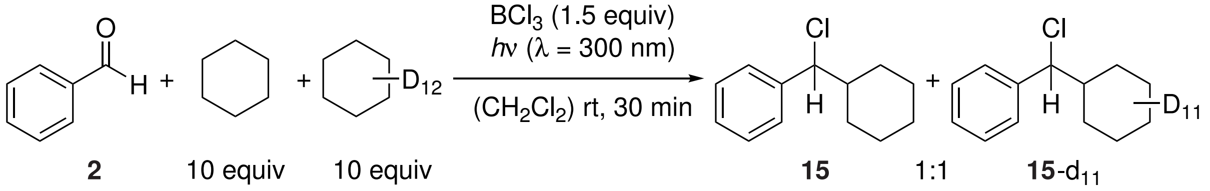

Scheme 11: Irradiation of **2**·BCl_3 with an equimolar mixture of C_6H_{12} and C_6D_{12}, providing **15** and **15**-d_{11} in a 1:1 ratio.

In a set of kinetic experiments, the effect of various parameters on the reaction of **2**·BCl_3 with C_6H_{12} was studied. We found that a higher alkane concentration leads to a faster reaction. This can be attributed to competing loss channels, e. g. radical recombination to **2** or single electron transfer of the radicals, so that a higher concentration of alkane can contribute to a productive reaction by enabling the HAT. When the light intensity was decreased with neutral density filters, the reaction rate decreased proportionally, which stands to reason for a photochemical reaction that is photon-limited.

By light on–off experiments, we found that a small amount of starting material is consumed also in the dark. This thermal reactivity could be due to a radical chain pathway. In addition, the obtained quantum yield after 120 s of continuous irradiation was determined as 1.036 ± 0.062, which confirmed that a radical chain pathway operates in this reaction. By calculations, we found that an attack of a cyclohexane radical to complex **2**·BCl_3 can propagate the chain (Scheme 12). The key step is an intramolecular SET that restores aromaticity and provides a free chlorine radical.

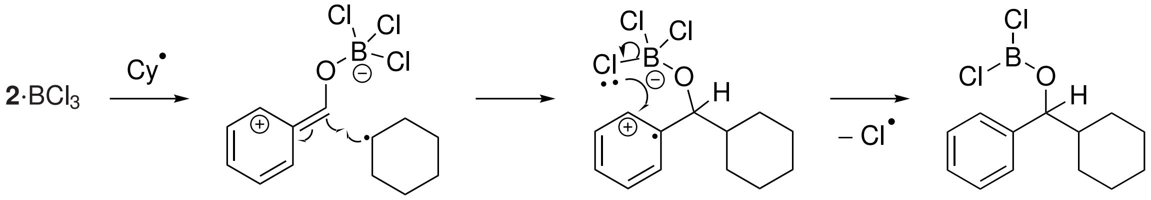

Scheme 12: Radical chain mechanism proposed via calculations.

In summary, these fundamental studies showcased the diversity of Lewis acid-modified photochemistry and the fruitful interplay of theory, spectroscopy and synthesis. With the study on the cyclohex-2-enone–BF_3 complex, existing mechanistic hypotheses on the activation of enones by Lewis acids could be corroborated. With the study on the benzaldehyde–BCl_3 complex, photoinduced bond fission in a substrate–Lewis acid assembly was established as a possibility for C–H bond activation.

3.2 Photochemical Isomerization of Cycloheptene Derivatives

With our interest in enantioselective photochemistry of α,β-unsaturated ketones, we became intrigued by the *Z*–*E* isomerization of cyclohept-2-enone (**3**) and focussed on the photoinduced Diels-Alder reaction of **3** (Scheme 13). This transformation would provide structurally intriguing bi- or tricyclic products with multiple defined stereogenic centers. Therefore, we wanted to study its diene scope, reaction pathway, and synthetic applications.[58] Also effects of Lewis acids on the reaction were investigated.

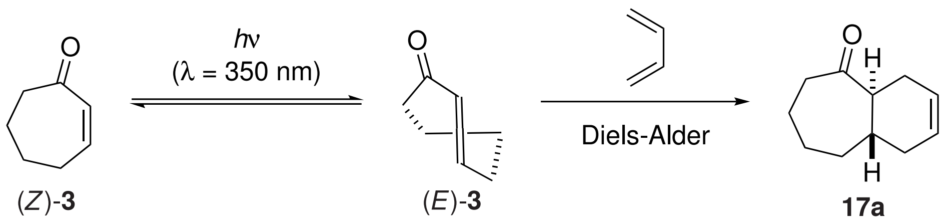

Scheme 13: Photoinduced isomerization of (*Z*)-**3** that enables a Diels-Alder reaction.

Theoretical studies revealed the isomerization of (*Z*)-**3** to proceed by two competitive reaction channels on either the singlet or triplet hypersurface. In both cases, the molecule can end up in the *E*-configuration with a dihedral angle (H–C=C–H) of 170°, which is 120 kJ mol^{-1} higher in energy compared to the *Z*-configuration (in S_0) and which allows for a consecutive Diels-Alder reaction.

While this strain energy enables various reactions, it prohibits isolation of (*E*)-**3** and leads to its consumption when no suitable reaction partner is present, as (*E*)-**3** can react with (*Z*)-**3** in a thermal $[_{\pi}2_s+_{\pi}2_a]$ cycloaddition reaction. We studied this reaction spectroscopically: (*Z*)-**3** was irradiated without other reactants and the solution monitored by UV/Vis or NMR spectroscopy. In both cases, signals of (*Z*)-**3** disappeared while signals of dimers emerged. This dimerization occurs within a typical time period of a photo-induced Diels-Alder reaction. Therefore, if the Diels-Alder reaction with a certain diene is comparatively slow, the dimerization becomes dominant and consumes the material. Both the dimerization of **3** and thermal re-isomerization to (*Z*)-**3** preclude the isolation of pure (*E*)-**3**.

With suitable dienes, a clean Diels-Alder reaction was observed. Various dienes and cycloalk-2-enones were probed (17 examples, 0.100 mmol to 1.00 mmol) and provided the products **17** in 68-98% yield (Figure 5).

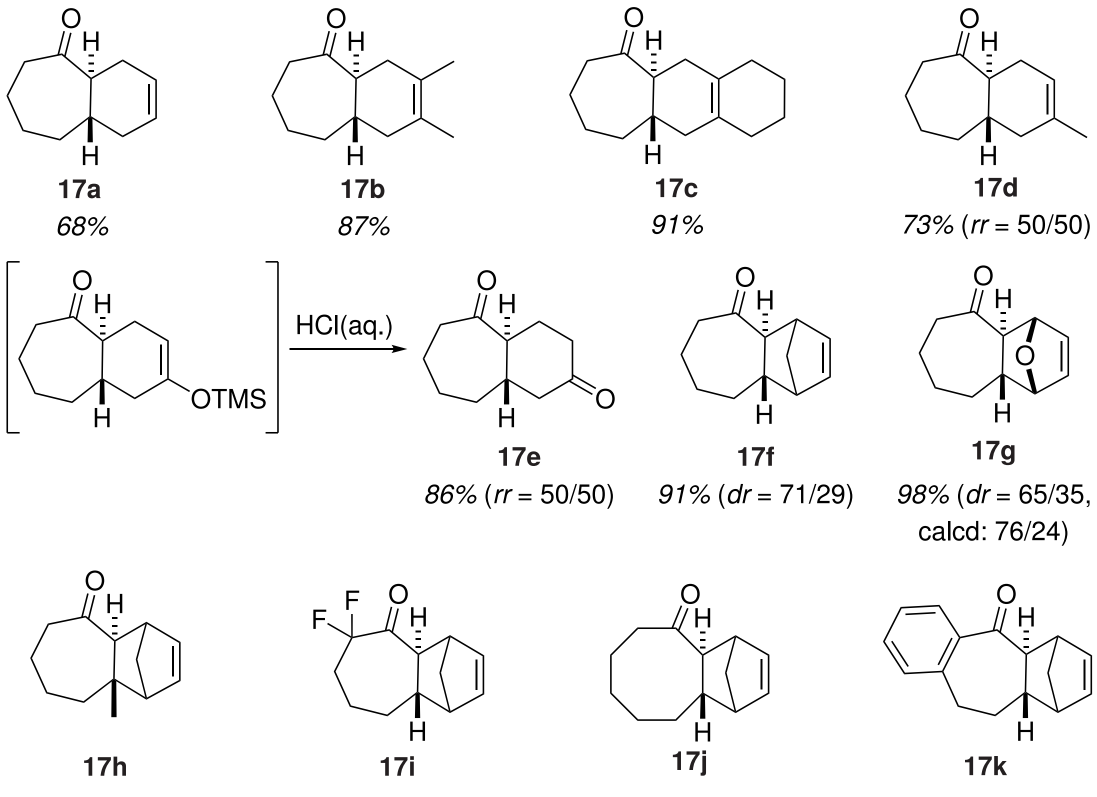

17a
68%

17b
87%

17c
91%

17d
73% (*rr* = 50/50)

17e
86% (*rr* = 50/50)

17f
91% (*dr* = 71/29)

17g
98% (*dr* = 65/35, calcd: 76/24)

17h
89% (*dr* = 39/61)

17i
84% (*dr* = 72/28)

17j
94% (*dr* = 80/20)

17k
80% (*dr* = 62/38)

Figure 5: Selected examples of products **17** obtained through photoinduced Diels-Alder reaction. Major regioisomers and diastereomers are depicted.

The reaction with furan was studied in detail by theory and the calculated diastereomeric ratio matched the experimental ratio. Additionally, product **17g** gave access to single crystals for X-ray analysis, by which the relative configuration of the product could be proven.

To highlight the applicability, racemic *trans*-α-himachalene (**18**) was synthesized in four steps (14% overall yield, Scheme 14). After the Diels-Alder reaction of ketone **19** with diene **20**, alcohol **17l** was directly obtained by treating the crude product with hydrochloric acid. Methylation and Wittig methylenation provided ether **21**. Reductive treatment with lithium in ammonia furnished the natural product **18**.

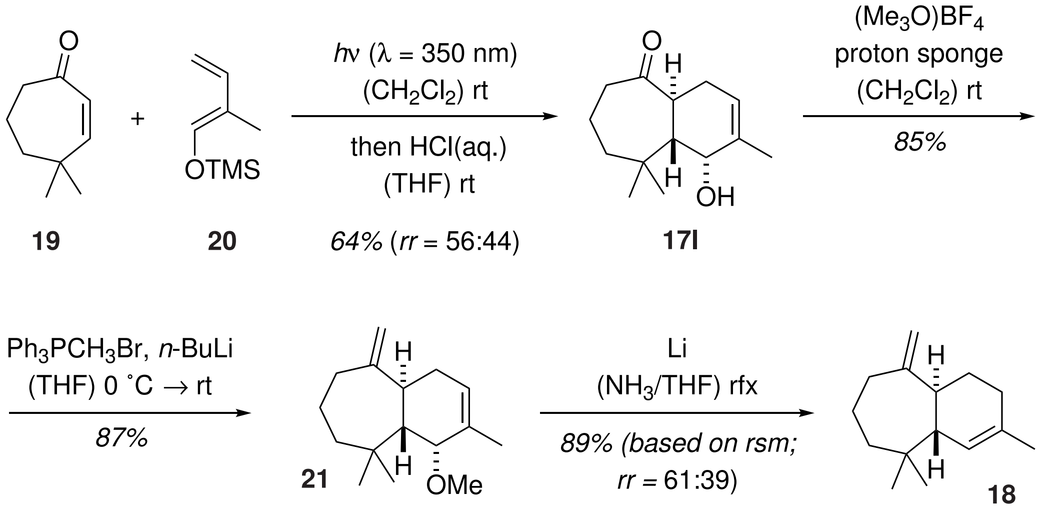

Scheme 14: Total synthesis of *trans*-α-himachalene with the photoinduced Diels-Alder reaction as key step.

As we were pleased with the scope of the photoinduced Diels-Alder reaction of **3**, we studied the effects of Lewis acids on the reaction. Therefore, chiral 1,3,2-oxazaborolidines were tested as Lewis acid catalysts for the reaction of **3** with cyclopenta-1,3-diene. Unfortunately, an inseparable mixture of multiple stereoisomers was obtained. While the *trans*-configured product **17f** was formed with up to 42% *ee*, also the *cis*-configured Diels-Alder product was found. The latter can be explained by a Lewis acid-induced thermal background reaction. Even when the reaction was conducted at low temperatures (−78 °C), this issue remained. We deemed **3** unsuitable for Lewis acid-catalysis and hypothesized that a potentially less reactive trisubsituted dienophile could be an alternative to **3**, as this could avoid the undesired thermal background reaction.

As aldehyde moieties are possible handles for Lewis acids in photochemistry (see Section 2.2 on page 6), we wondered if cyclohept-2-enecarbaldehyde (**5**) could act as a viable alternative for **3**. To the best of our knowledge, the photochemistry of **5** has not been explored. Due to its structural similarity to previously studied cycloheptene[59] and **3** (see above), we expected photochemical isomerization of (*E*)-**5** to (*Z*)-**5** and a subsequent Diels-Alder reaction as depicted in Scheme 15. Therefore, we studied the photoinduced isomerization of **5** and subsequent strain-release reactions.

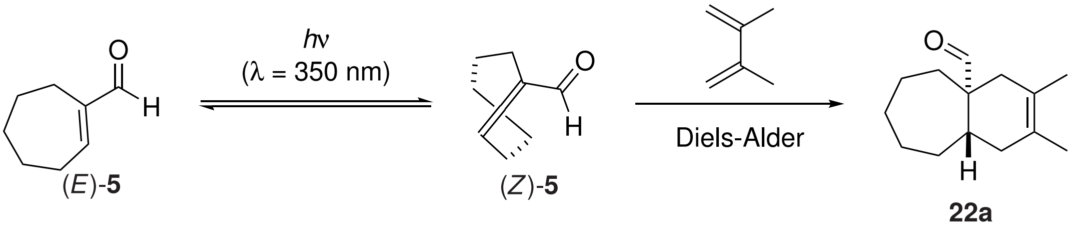

(*E*)-**5** (*Z*)-**5** **22a**

Scheme 15: Photoinduced isomerization of (*E*)-**5** that enables a Diels-Alder reaction.

Indeed, upon irradiation of **5** with 2,3-dimethylbuta-1,3-diene, we saw starting material consumption. Surprisingly, two structurally different products were obtained. The major product was the Diels-Alder product **22a**, whose structure was corroborated through reduction and esterification with *para*-bromobenzoyl chloride and X-ray analysis. The minor product was the Alder-ene product **23a**. Gratifyingly, **5** underwent the Diels-Alder reaction with other 1,3-dienes or in case of methylenecyclopentane the Alder-ene reaction (Figure 6). When 1,3-dipoles were used as reaction partners, [3+2] cycloaddition products like **24** were formed, similar to **3**.[60] In total, 12 different photoproducts could be isolated.

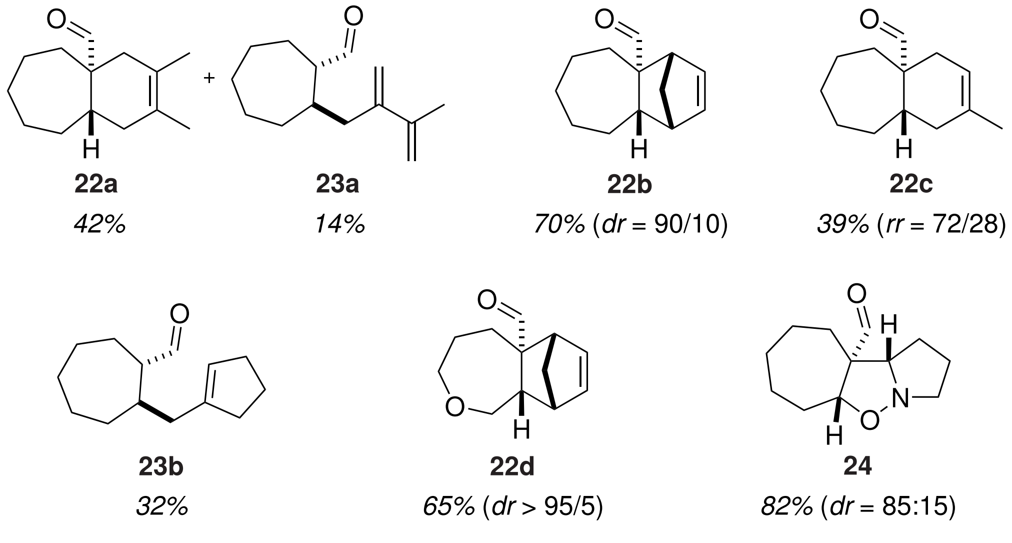

22a *42%*

23a *14%*

22b *70%* (*dr* = 90/10)

22c *39%* (*rr* = 72/28)

23b *32%*

22d *65%* (*dr* > 95/5)

24 *82%* (*dr* = 85:15)

Figure 6: Selected examples of products obtained through photoinduced Diels-Alder, Alder-ene or [3+2] cycloaddition reactions of **5**. Major regioisomers and diastereomers are depicted.

When comparing the reactivity of **3** with **5**, two aspects were noticeable: The reactions with **5** were slower and the products were obtained in lower yields. This could be explained through the decreased ring strain of (*Z*)-**5** compared to (*E*)-**3**. To quantify the different efficiencies, the quantum yields of the photoinduced Diels-Alder reactions with cyclopenta-1,3-diene were determined. For the consumptions of **3** and **5**, quantum yields of 0.50 ± 0.09 and 0.096 ± 0.005 were obtained, respectively. This means that (*Z*)-**5** is 81% less reactive than (*E*)-**3**. Nevertheless, the quantum yields for these Diels-Alder reactions are in the same order of magnitude of other, relatively efficient photoreactions like the intramolecular [2+2] photocycloaddition reaction of 2-(allyloxy)cyclohexenone.[25] In the latter case, we obtained quantum yields of approximately 0.3 both for directly excited or sensitized reactions. Only with a chiral Lewis acid, the quantum yield dropped to 0.003.

Also for **5**, the effect of Lewis acids was studied. Unfortunately, **5** was rapidly consumed in the dark with $EtAlCl_2$ as Lewis acid and cyclopenta-1,3-diene as reactant. In addition, we found that ketone **25** was formed with BF_3 or $EtAlCl_2$ and 2,3-dimethylbuta-1,3-diene (Scheme 16). This can be mechanistically explained through a thermal Diels-Alder reaction to **26** followed by a rearrangement cascade.

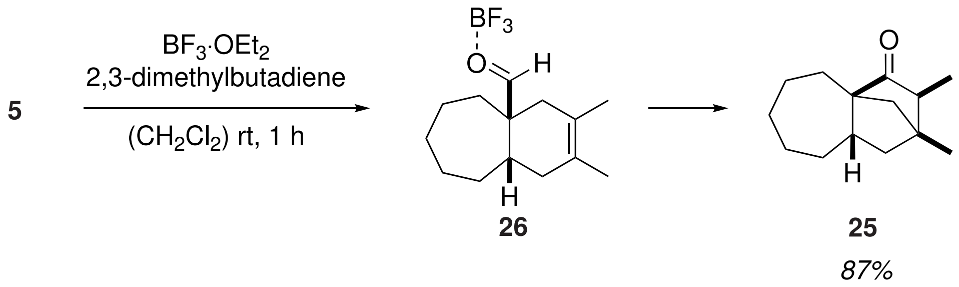

Scheme 16: Lewis acid-induced Diels-Alder/rearrangement reaction to ketone **25**.

As, again, thermal reactions were induced by Lewis acids, no experiments regarding enantioselective photocatalysis were conducted with **5**. Our findings indicate that Lewis acids are too strong activators for *α*,*β*-unsaturated carbonyl compounds to allow for exclusively photoinduced Diels-Alder reactions. In summary, we could show that the *E*–*Z* isomerization/Diels–Alder sequence is a versatile tool to obtain *trans*-fused ring systems from cycloheptene derivatives **3** and **5**.

4 Information on Original Publications

4.1 Diels–Alder Reaction of Photochemically Generated (*E*)-Cyclohept-2-enones: Diene Scope, Reaction Pathway, and Synthetic Application

Bibliographic information:

D. P. Schwinger, M. T. Peschel, C. Jaschke, C. Jandl, R. de Vivie-Riedle, T. Bach, *J. Org. Chem.* **2022**, *87*, 4838–4851. Published on 22 March 2022 (see A on page 29).

Summary:

(*Z*)-Cyclohept-2-enones can undergo isomerization to their strained (*E*)-isomers upon UV-irradiation. We studied this process theoretically by calculations and experimentally by subsequent Diels–Alder reactions. The calculations revealed that the isomerization can occur on both the singlet and triplet hypersurface. In the Diels–Alder reactions, various dienes served as suitable reaction partners and provided the corresponding products in good yields (up to 98%) and with *trans*-configuration of the bridgehead substituents. For furan, the relative configuration of all stereogenic centers could be established by X-ray diffraction analyses and the experimental results matched the calculated ones. In addition to cyclohept-2-enone, substituted cyclohept-2-enones and cyclooct-2-enone were studied with cyclopenta-1,3-diene. The method was also used to synthesize the natural product *trans*-α-himachalene in four steps.

Author contributions:

D. P. Schwinger and T. Bach developed the project. D. P. Schwinger designed and performed synthetic experiments as well as generated and evaluated the analytical data. M. T. Peschel and C. Jaschke developed the theory and performed the calculations with input from R. de Vivie-Riedle. C. Jandl performed X-ray crystallographic analyses. D. P. Schwinger validated all data. T. Bach administered the project, acquired funding and supervised the research. D. P. Schwinger and T. Bach wrote, reviewed and edited the manuscript with critical input from the other authors.

4.2 Photoinduced B–Cl Bond Fission in Aldehyde-BCl_3 Complexes as a Mechanistic Scenario for C–H Bond Activation

Bibliographic information:

D. P. Schwinger, M. T. Peschel, T. Rigotti, P. Kabaciński, T. Knoll, E. Thyrhaug, G. Cerullo, J. Hauer, R. de Vivie-Riedle, T. Bach, *J. Am. Chem. Soc.* **2022**, *144*, 18927–18937. Published on 7 October 2022 (see B on page 45).

Summary:

Lewis acids are established catalysts for photochemical reactions. In previous studies, the induced changes of a substrate's photophysical and -chemical properties were in the spotlight. We could show that the assembly of an aromatic aldehyde with BCl_3 as Lewis acid exhibits completely different reactivity compared to the sole substrate. Upon UV-irradiation, the B–Cl bond is homolytically cleaved, which forms a borylated ketyl radical as well as a chlorine radical. This was established by transient absorption spectroscopy and time-dependent DFT calculations. These radicals were synthetically used in a hydroalkylation reaction with alkanes. As the chlorine can abstract an H atom from simple alkanes, alkyl radicals are formed that can either recombine with a ketyl radical or react with an aromatic aldehyde–BCl_3 assembly via addition and then elimination of a chlorine radical. The latter process leads to radical chains and was confirmed by DFT and quantum yield measurements. As products of this reaction, various alcohols were obtained in moderate to good yield (up to 76%).

Author contributions:

D. P. Schwinger, M. T. Peschel and T. Bach developed the project. D. P. Schwinger and T. Rigotti designed and performed synthetic and mechanistic experiments as well as generated and evaluated the analytical data. M. T. Peschel and T. Knoll developed the theory and performed the calculations with input from R. de Vivie-Riedle. P. Kabaciński designed and performed the transient absorption measurements with guidance from G. Cerullo. E. Thyrhaug evaluated the transient absorption data and performed the kinetic analysis with input from J. Hauer. D. P. Schwinger, M. T. Peschel and T. Rigotti validated all data. J. Hauer, R. de Vivie-Riedle and T. Bach administered the project, acquired funding and supervised the research. D. P. Schwinger, M. T. Peschel, T. Rigotti, J. Hauer, R. de Vivie-Riedle and T. Bach wrote, reviewed and edited the manuscript with critical input from the other authors.

5 Conclusions

This research study focused on the use of Lewis acids to modulate the reactivity of conjugated carbonyl compounds in photochemical reactions. Therefore, we investigated model substrates together with boron-based Lewis acids, involving mechanistic experiments, theory and spectroscopy. Within our study on the cyclohex-2-enone–BF_3 complex, we discovered that selective excitation of a Lewis acid–chromophore assembly with UV light is possible, as long as the absorption of the complex lies in-between absorption bands of the uncomplexed chromophore and a suitable irradiation source is used. In addition, we could corroborate the photophysical and -chemical mechanism of Lewis acid–enone assemblies. We also found a new photochemical method for $C-H$ bond activation through our study on the benzaldehyde–BCl_3 complex. Its reaction mechanism includes $B-Cl$ bond fission, subsequent hydrogen abstraction and radical chain propagation. These steps were not only supported by mechanistic experimental studies and high level calculations but were also predicted by theory before any experiments were conducted. This theory-driven approach to synthetic discovery might prove useful for other substrate classes, e. g. photochemical reactions of heteroarene–Lewis acid assemblies.[18,61]

Furthermore, we investigated the application of Lewis acid-catalysis to *E*–*Z* isomerization of cycloheptene derivatives. The scope of the photoinduced Diels-Alder reaction with cyclohept-2-enone was explored, the structures of certain products were confirmed by X-ray analysis, and the reaction pathway analyzed by theory. In addition, *trans*-α-himachalene was synthesized applying this method. As Lewis acids triggered a thermal reaction of cyclohept-2-enone in the dark, we investigated the more hindered cylohept-2-enecarbaldehyde. Its photochemical behavior was so far unknown. Similar to cyclohept-2-enone, it underwent different strain release-promoted cycloaddition reactions. Also an Alder-ene reaction was observed. With Lewis acids, thermal reactions of cylohept-2-enecarbaldehyde with 1,3-dienes were detected. Taken together, our findings suggest that Lewis acids may be unsuitable for photoinduced Diels-Alder reactions of cycloheptene derivatives. However, other catalyst classes[62,63] could allow for these ring strain-promoted reaction to occur enantioselectively, which warrants further investigations. In summary, the findings as part of this thesis shed light on the fundamental aspects of Lewis acid-catalyzed photochemical reactions of conjugated carbonyl compounds and offer insights for future research in this area.

Bibliography

[1] M. R. Islam, J. G. Mahdi, I. D. Bowen, *Drug Saf.* **1997**, *17*, 149–165.

[2] N. J. Turro, V. Ramamurthy, J. C. Scaiano, *Modern molecular photochemistry of organic molecules*, Univ. Science Books, Sausalito, **2010**.

[3] M. D. Kärkäs, J. A. Porco, C. R. J. Stephenson, *Chem. Rev.* **2016**, *116*, 9683–9747.

[4] T. Bach, J. P. Hehn, *Angew. Chem. Int. Ed.* **2011**, *50*, 1000–1045.

[5] Compiled by A. D. McNaught and A. Wilkinson, online version created by S. J. Chalk, *The IUPAC Compendium of Chemical Terminology*, 2nd ed. (the "Gold Book"), Blackwell Scientific Publications, Oxford, **2019**.

[6] R. Brimioulle, D. Lenhart, M. M. Maturi, T. Bach, *Angew. Chem. Int. Ed.* **2015**, *54*, 3872–3890.

[7] H. Yamamoto, *Lewis Acids in Organic Synthesis*, Wiley-VCH, Weinheim, **2000**.

[8] K. L. Skubi, T. R. Blum, T. P. Yoon, *Chem. Rev.* **2016**, *116*, 10035–10074.

[9] G. Ciamician, *Science* **1912**, *36*, 385–394.

[10] A. Jablonski, *Nature* **1933**, *131*, 839–840.

[11] B. Wardle, *Principles and Applications of Photochemistry*, Wiley, Chichester, **2009**.

[12] T. Neveselý, M. Wienhold, J. J. Molloy, R. Gilmour, *Chem. Rev.* **2022**, *122*, 2650–2694.

[13] T. Bach, *Synthesis* **1998**, 683–703.

[14] S. Poplata, A. Tröster, Y.-Q. Zou, T. Bach, *Chem. Rev.* **2016**, *116*, 9748–9815.

[15] D. Sarkar, N. Bera, S. Ghosh, *Eur. J. Org. Chem.* **2020**, *2020*, 1310–1326.

[16] P. J. Wagner, *Acc. Chem. Res.* **2001**, *34*, 1–8.

[17] N. Hoffmann, *Photochem. Photobiol. Sci.* **2012**, *11*, 1613–1641.

[18] R. Remy, C. G. Bochet, *Chem. Rev.* **2016**, *116*, 9816–9849.

[19] B. Reiß, Q. Hu, E. Riedle, H.-A. Wagenknecht, *ChemPhotoChem* **2021**, *5*, 1009–1019.

[20] M. M. Maturi, M. Wenninger, R. Alonso, A. Bauer, A. Pöthig, E. Riedle, T. Bach, *Chem. Eur. J.* **2013**, *19*, 7461–7472.

[21] D. Lenhart, A. Bauer, A. Pöthig, T. Bach, *Chem. Eur. J.* **2016**, *22*, 6519–6523.

[22] A. Hölzl-Hobmeier, A. Bauer, A. V. Silva, S. M. Huber, C. Bannwarth, T. Bach, *Nature* **2018**, *564*, 240–243.

[23] S. Poplata, A. Bauer, G. Storch, T. Bach, *Chem. Eur. J.* **2019**, *25*, 8135–8148.

[24] F. M. Hörmann, C. Kerzig, T. S. Chung, A. Bauer, O. S. Wenger, T. Bach, *Angew. Chem. Int. Ed.* **2020**, *59*, 9659–9668.

[25] T. Rigotti, D. P. Schwinger, R. Graßl, C. Jandl, T. Bach, *Chem. Sci.* **2022**, *13*, 2378–2384.

[26] D. P. Schwinger, M. T. Peschel, T. Rigotti, P. Kabaciński, T. Knoll, E. Thyrhaug, G. Cerullo, J. Hauer, R. de Vivie-Riedle, T. Bach, *J. Am. Chem. Soc.* **2022**, *144*, 18927–18937.

[27] F. D. Lewis, D. K. Howard, J. D. Oxman, *J. Am. Chem. Soc.* **1983**, *105*, 3344–3345.

[28] T. Ogawa, Y. Masui, S. Ojima, H. Suzuki, *Bull. Chem. Soc. Jpn.* **1987**, *60*, 423–425.

[29] C. Brenninger, J. D. Jolliffe, T. Bach, *Angew. Chem. Int. Ed.* **2018**, *57*, 14338–14349.

[30] T. Rigotti, J. Alemán, *Chem. Commun.* **2020**, *56*, 11169–11190.

[31] C. Prentice, J. Morrisson, A. D. Smith, E. Zysman-Colman, *Beilstein J. Org. Chem.* **2020**, *16*, 2363–2441.

[32] D. P. Schwinger, T. Bach, *Acc. Chem. Res.* **2020**, *53*, 1933–1943.

[33] E. J. Corey, *Angew. Chem. Int. Ed.* **2009**, *48*, 2100–2117.

[34] M. N. Paddon-Row, L. C. H. Kwan, A. C. Willis, M. S. Sherburn, *Angew. Chem. Int. Ed.* **2008**, *47*, 7013–7017.

[35] S. Stegbauer, N. Jeremias, C. Jandl, T. Bach, *Chem. Sci.* **2019**, *10*, 8566–8570.

[36] M. Leverenz, C. Merten, A. Dreuw, T. Bach, *J. Am. Chem. Soc.* **2019**, *141*, 20053–20057.

[37] J. S. Swenton, *J. Org. Chem.* **1969**, *34*, 3217–3218.

[38] M. F. Debets, S. S. van Berkel, J. Dommerholt, A. T. J. Dirks, F. P. J. T. Rutjes, F. L. van Delft, *Acc. Chem. Res.* **2011**, *44*, 805–815.

[39] R. Selvaraj, J. M. Fox, *Curr. Opin. Chem. Biol.* **2013**, *17*, 753–760.

[40] S. Mayer, K. Lang, *Synthesis* **2017**, *49*, 830–848.

[41] E. M. Sletten, C. R. Bertozzi, *Angew. Chem. Int. Ed.* **2009**, *48*, 6974–6998.

[42] E. Ruivo, F. Elvas, K. Adhikari, C. Vangestel, G. van Haesendonck, F. Lemière, S. Staelens, S. Stroobants, P. van der Veken, L. Wyffels, K. Augustyns, *ACS Omega* **2020**, *5*, 4449–4456.

[43] R. García-Vázquez, U. M. Battisti, M. M. Herth, *Pharmaceuticals* **2022**, *15*, 685.

[44] P. E. Eaton, K. Lin, *J. Am. Chem. Soc.* **1965**, *87*, 2052–2054.

[45] E. J. Corey, M. Tada, R. LaMahieu, L. Libit, *J. Am. Chem. Soc.* **1965**, *87*, 2051–2052.

[46] H. Shinozaki, S. Arai, M. Tada, *Bull. Chem. Soc. Jpn.* **1976**, *49*, 821–822.

[47] R.-B. Wang, S.-G. Ma, C. S. Jamieson, R.-M. Gao, Y.-B. Liu, Y. Li, X.-J. Wang, Y.-H. Li, K. N. Houk, J. Qu, S.-S. Yu, *Chem. Sci.* **2021**, *12*, 7003–7011.

[48] R. Noyori, M. Katô, *Bull. Chem. Soc. Jpn.* **1974**, *47*, 1460–1466.

[49] H. Hart, E. Dunkelblum, *J. Am. Chem. Soc.* **1978**, *100*, 5141–5147.

[50] J. Moran, P. Dornan, A. M. Beauchemin, *Org. Lett.* **2007**, *9*, 3893–3896.

[51] P. E. Eaton, K. Lin, *J. Am. Chem. Soc.* **1964**, *86*, 2087–2088.

[52] S. Poplata, T. Bach, *J. Am. Chem. Soc.* **2018**, *140*, 3228–3231.

[53] M. T. Peschel, P. Kabaciński, D. P. Schwinger, E. Thyrhaug, G. Cerullo, T. Bach, J. Hauer, R. de Vivie-Riedle, *Angew. Chem. Int. Ed.* **2021**, *60*, 10155–10163.

[54] S. Stegbauer, C. Jandl, T. Bach, *Angew. Chem. Int. Ed.* **2018**, *57*, 14593–14596.

[55] S. Stegbauer, C. Jandl, T. Bach, *Chem. Sci.* **2022**, *13*, 11856–11862.

[56] R. J. Mayer, N. Hampel, A. R. Ofial, *Chem. Eur. J.* **2021**, *27*, 4070–4080.

[57] S. Bonciolini, T. Noël, L. Capaldo, *Eur. J. Org. Chem.* **2022**, e202200417.

[58] D. P. Schwinger, M. T. Peschel, C. Jaschke, C. Jandl, R. de Vivie-Riedle, T. Bach, *J. Org. Chem.* **2022**, *87*, 4838–4851.

[59] R. Hoffmann, Y. Inoue, *J. Am. Chem. Soc.* **1999**, *121*, 10702–10710.

[60] H. Yang, T. Zeng, S. Xi, S. Hu, Y. Wu, Y. Tang, *Green Chem.* **2020**, *22*, 7023–7030.

[61] J. Zou, P. S. Mariano, *Photochem. Photobiol. Sci.* **2008**, *7*, 393–404.

[62] F. Burg, T. Bach, *J. Org. Chem.* **2019**, *84*, 8815–8836.

[63] M. J. Genzink, J. B. Kidd, W. B. Swords, T. P. Yoon, *Chem. Rev.* **2022**, *122*, 1654–1716.

A Diels–Alder Reaction of Photochemically Generated (*E*)-Cyclohept-2-enones: Diene Scope, Reaction Pathway, and Synthetic Application

Reprinted (adapted) with permission from D. P. Schwinger, M. T. Peschel, C. Jaschke, C. Jandl, R. de Vivie-Riedle, T. Bach, *J. Org. Chem.* **2022**, *87*, 4838–4851. Copyright 2022 American Chemical Society.

JOC The Journal of Organic Chemistry

pubs.acs.org/joc Article

Diels–Alder Reaction of Photochemically Generated (*E*)-Cyclohept-2-enones: Diene Scope, Reaction Pathway, and Synthetic Application

Daniel P. Schwinger, Martin T. Peschel, Constantin Jaschke, Christian Jandl, Regina de Vivie-Riedle, and Thorsten Bach*

Cite This: *J. Org. Chem.* 2022, 87, 4838–4851 Read Online

ACCESS | Metrics & More | Article Recommendations | SI Supporting Information

Downloaded via TU MUENCHEN on August 16, 2022 at 10:16:58 (UTC).
See https://pubs.acs.org/sharingguidelines for options on how to legitimately share published articles.

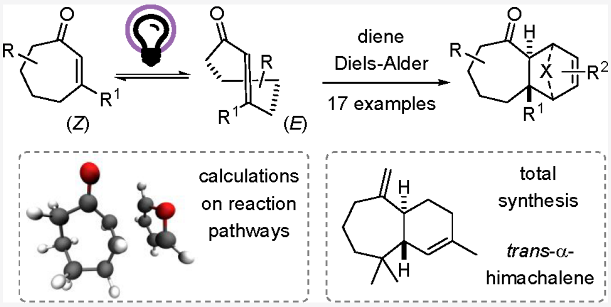

ABSTRACT: Upon irradiation at $\lambda = 350$ nm, cyclohept-2-enone undergoes an isomerization to the strained (*E*)-isomer. The process was studied by XMS-CASPT2 calculations and found to proceed by two competitive reaction channels on either the singlet or the triplet hypersurface. (*E*)-Cyclohept-2-enone is a reactive dienophile in thermal [4 + 2] cycloaddition reactions with various dienes. Ten different dienes were probed, most of which—except for 1,3-cyclohexadiene—underwent a clean Diels–Alder reaction and gave the respective *trans*-fused six-membered rings in good yields (68–98%). The reactions with furan were studied in detail, both experimentally and by DLPNO–CCSD(T) calculations. Two diastereoisomers were formed in a ratio of 63/35 with the *exo*-product prevailing, and the configuration of both diastereoisomers was corroborated by single crystal X-ray crystallography. The outcome of the photoinduced Diels–Alder reaction matched both qualitatively and quantitatively the calculated reaction pathway. Apart from cyclohept-2-enone, five additional cyclic hept-2-enones and cyclooct-2-enone were employed in their (*E*)-form as dienophiles in the Diels–Alder reaction with 1,3-cyclopentadiene (80–98% yield). The method was eventually applied to a concise total synthesis of racemic *trans*-*α*-himachalene (four steps, 14% overall yield).

■ INTRODUCTION

Photochemical reactions are particularly useful if they provide access to intermediates that cannot be generated by conventional (thermal) transformations. They open unprecedented reaction channels, which in turn can lead to novel, structurally unique products.[1] Along these lines, the *Z*/*E* isomerization of cyclic alkenes has received intensive attention,[2] and outstanding contributions were made by the group of Y. Inoue,[3] who focused on the preparation of chiral (*E*)-cycloalkenes in enantiomerically enriched form.[4] In recent years, the ring strain of cyclic (*E*)-alkenes has been favorably used to facilitate biochemical ligation reactions.[5] From a synthetic perspective, the high ring strain in (*E*)-cycloalkenes and specifically (*E*)-cycloalk-2-enones allows for consecutive reactions that are not feasible thermally or require activation by a catalyst. In back-to-back publications, the groups of Corey[6] and Eaton[7] reported in 1965 on the photochemical formation of (*E*)-cyclohept-2-enone[8] and its consecutive reaction with either 1,3-cyclopentadiene or furan as diene components in a Diels–Alder reaction (Scheme 1).[9] Despite the fact that the Diels–Alder adducts, which are—unlike thermal products[10]—intrinsically *trans*-fused,[11] hold promise for the total synthesis of naturally occurring cycloheptanes, the number of subsequent publications on the topic has remained limited. Hiraku et al. studied the photochemical reaction of cyclohept-2-enone with cyclopentadiene and isoprene claiming the formation of structurally defined products as single isomers.[12] Dorr and Rawal recognized that the regioselectivity of the reaction can be

Scheme 1. Photochemical Isomerization of (*Z*)-Cyclohept-2-enone [(*Z*)-1] to Its (*E*)-Isomer [(*E*)-1] and Structures of Dienes Known to Undergo a Diels–Alder Reaction with (*E*)-1

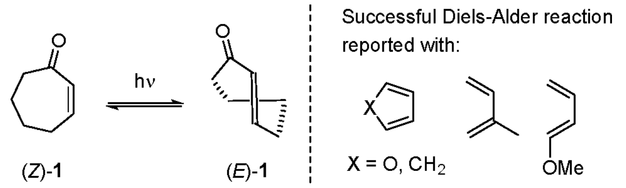

Received: January 26, 2022
Published: March 22, 2022

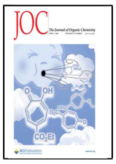

ACS Publications

© 2022 The Authors. Published by American Chemical Society

https://doi.org/10.1021/acs.joc.2c00186
J. Org. Chem. 2022, 87, 4838–4851

favorably controlled in an intramolecular reaction and reported on the formation of polycyclic cyclohept-2-enone adducts by a cascade of photochemical *Z*/*E* isomerization and intramolecular Diels−Alder reaction.[13]

The hitherto most comprehensive study on the photochemical reaction of cyclohept-2-enones with dienes was performed by Autschbach, Davies, and co-workers.[14] In the context of a projected total synthesis of vibsanin E, they studied the reaction of various cyclohept-2-enones with isoprene, 2,4-hexadiene, and 1-methoxy-1,3-butadiene. For the parent compound cyclohept-2-enone (**1**), they observed upon reaction with neat 1-methoxy-1,3-butadiene two major products in a ratio of 4/1 to which they assigned the structures **2a** and **2a′** (Scheme 2). On the basis of DFT calculations on the B3LYP/6-31G(d) level of theory, they could rationalize the outcome of the reactions by analyzing the transition state energies for the approach of the diene to substrate (*E*)-**1**.

Scheme 2. Previous Study[14] on the Diels−Alder Reaction of 1-Methoxy-1,3-butadiene with (*E*)-Cyclohept-2-enone [(*E*)-1] to Regioisomeric Bicyclic Products 2a and 2a′

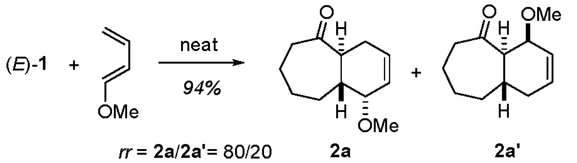

Ghosh, Datta, and co-workers studied the photochemical reaction of chiral cyclohept-2-enones with various dienes focusing on its use for diterpene total synthesis. For furan as diene, they found a single addition product, the selective formation of which was explained by the fact that its formation was most exothermic according to DFT calculations.[15] With nonsymmetric dienes, the formation of regioisomeric products was observed. In a recent study, Wang et al. employed the photoinduced Diels−Alder reaction for the construction of a spirooliganin library.[16] They also analyzed structures and relative energies of Diels−Alder products and transition states for the reaction of isoprene and 4,4-dimethylcyclohept-2-enone by DFT calculations at the ωB97X-D/def2-QZVPP//ωB97X-D/def2-TZVP level of theory.

Our interest in the photochemistry of cyclohept-2-enone and its derivatives was kindled by the intrinsic chirality of (*E*)-cyclohept-2-enones (vide supra), which could potentially be exploited for enantioselective transformations.[17] Since a procedure to access racemic compounds was needed and since it seemed desirable to establish the constitution and relative configuration of the Diels−Alder products, we studied the photoinduced reaction of various cyclohept-2-enones with dienes in detail. We herein describe the results of our experiments, which were combined with computational studies and which led to the application of the photoinduced Diels−Alder reaction to the synthesis of the natural product *trans-α*-himachalene.

■ RESULTS AND DISCUSSION

Cyclohept-2-enone displays two notable absorption bands in the UV−vis spectrum. At λ = 226 nm, a strong absorption (ε = 10 475 L mol^{-1} cm^{-1}) is recorded in dichloromethane solution, while the long-wavelength absorption at λ = 325 nm is weak (ε = 64.4 L mol^{-1} cm^{-1}). The spectrum calculated at XMS-CASPT2(6,5)/cc-pvtz level of theory matched the experimental data well and allowed us to assign the blue-shifted absorption (λ_{calc} = 220 nm) to a bright $\pi\pi^*$ transition and the red-shifted absorption (λ_{calc} = 336 nm) to an almost dark, forbidden $n\pi^*$ transition (see the SI for further details). The XMS-CASPT2 optimizations of critical points in the excited states of cyclohept-2-enone indicated two ultrafast relaxation pathways that allow for the observed *Z*/*E* isomerization, a triplet pathway via intersystem crossing (ISC) as well as a singlet pathway via internal conversion (Figure 1). After photoexcitation to the $S_1(n\pi^*)$ state, the (*Z*)-isomer of cyclohept-2-enone, (*Z*)-**1**, starts to relax. Already close to the

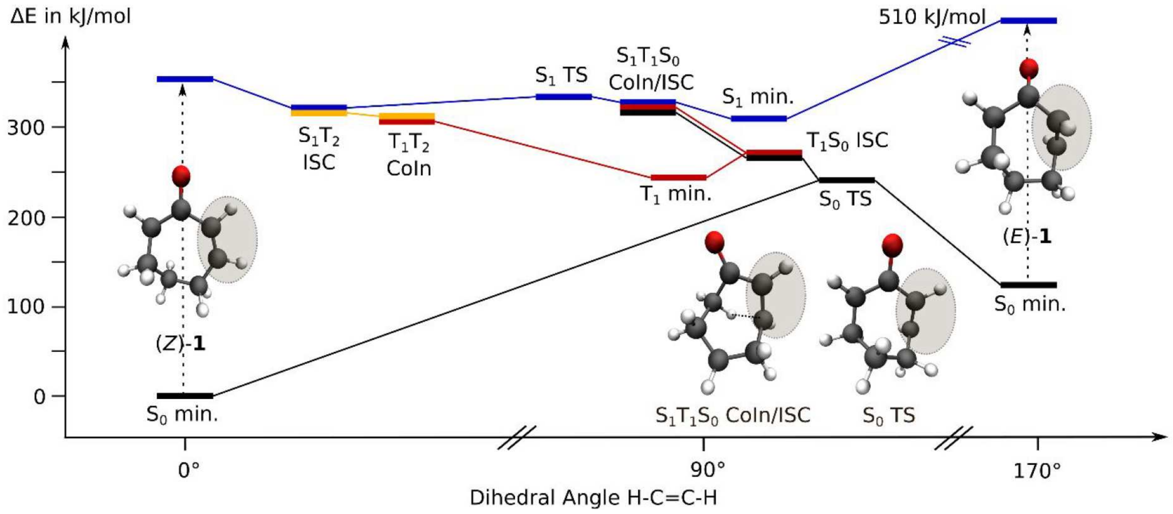

Figure 1. Critical points in the S_0 (black), S_1 (blue), T_1 (red), and T_2 (yellow) states along the *Z*/*E* photoisomerization pathways of cyclohept-2-enone optimized using XMS-CAPT2(6,5)/cc-pvtz.[21] The three most critical points on the left lie close to the Franck−Condon region with H—C═C—H torsion angles (indicated by gray ellipses) close to 0°, the six critical points in the middle have torsion angles close to 90° and the lowest lying (*E*)-conformer has a torsion angle of 170°. As examples, we explicitly show the molecular structures of the lowest lying (*Z*)- and (*E*)-isomer, the transition state (TS) connecting them, as well as the structure of the $S_1T_1S_0$ CoIn/ISC, where a transannular interaction between C-3 and the hydrogen atom at C-7 is indicated.

Franck–Condon region, intersystem crossing between S_1 and T_2 can occur as both states become degenerate (S_1T_2 ISC). From there, following the T_2, the system arrives at a conical intersection between T_1 and T_2 (T_1T_2 CoIn), allowing a transition to T_1. Relaxation in the T_1 leads to a torsion of the double bond by 90° and a T_1 minimum of $\pi\pi^*$ character is reached. A barrier of 27.7 kJ mol^{-1} has to be overcome to reach the crossing region with the S_0 state (T_1S_0 ISC). This region is geometrically close to the thermal Z/E transition state in the S_0 (S_0 TS). Two pathways are now possible, either back to (Z)-**1** or continuing the rotation toward the (E)-isomer, (E)-**1**. The final geometry of (E)-**1** is characterized by a double bond torsion of 170°, which deviates from the classical value of 180° due to ring strain. For smaller enones[18] this ring strain is even stronger and prevents full isomerization. Only the larger and more flexible cyclohept-2-enone can undergo complete isomerization in the triplet states as has already been shown by García-Expósito et al. at the CASSCF level.[19] At the XMS-CASPT2 level, we identified another possible isomerization pathway exclusively via singlet states. Only a small barrier in the S_1 state (S_1 TS), lying 20.5 kJ mol^{-1} below the Franck–Condon point, has to be overcome to reach a three state crossing between S_1, T_1, and S_0. Here the double bond torsion is also close to 90°. Furthermore, the structure is stabilized by a transannular interaction of C-3 and the hydrogen at C-7. As internal conversion is typically faster than intersystem crossing, we expect preferential population of the S_0 state and the possibility of Z/E isomerization by relaxation in the S_0 toward (E)-**1**. In case of the studied Diels–Alder reactions, dienes are used in excess, which can act as efficient triplet quenchers.[20] This would lead to an additional loss channel when following the triplet pathway. However, the excited molecules might have sufficient energy and momentum to overcome the barrier associated with the T_1S_0 ISC before quenching can occur. Thus, the possibility of isomerization along the triplet path should still be considered.

A first set of preparative experiments were performed with cyclohept-2-enone (**1**) and some substituted 1,3-butadienes (Scheme 3). It was found that the reactions worked best in dichloromethane solution at an irradiation wavelength of λ = 350 nm (emission maximum of the fluorescent lamps). The diene component was used in excess to secure an efficient trapping of the strained (E)-intermediate. With 1,3-butadiene itself (product **3a**) and symmetrical 2,3-disubstituted dienes (products **3b**, **3c**), only a single product was obtained for each reaction. [2 + 2] Photocycloaddition reactions between the enone and 1,3-dienes were not observed.[22]

The *trans*-fusion of the newly formed cyclohexene ring was corroborated by a single crystal X-ray analysis of product **3b** derived from 1,2-bis(methylene)cyclohexane. The reaction with 2-substituted 1,3-butadienes led to a mixture of regioisomers, and no preference was observed (*rr* = regioisomeric ratio). The minor differences in the spectroscopic properties of the isoprene adducts **3d** and **3d′** may have been difficult to detect by the techniques available in the 1970s, which in turn accounts for a previous report on regioselective formation of **3d**.[12] A similar observation as with isoprene was also made with myrcene which gave the *trans*-fused products **3e** and **3e′** as a mixture of inseparable regioisomers. The reaction scale was irrelevant for the yields, which were consistently good to excellent. The limited regiocontrol exerted by the alkyl substituent in 2-position appeared to be due to its low electron-donating properties, and a better regiocontrol was expected for more electron-donating substituents.[23] However, the lack of regioselectivity persisted for stronger electron donors. 2-Trimethylsiloxy-1,3-butadiene, for example, is known to react with (Z)-enones under thermal conditions with high regioselectivity, even in the absence of a Lewis acid.[24] In contrast, no selectivity was observed in the reaction with photochemically generated (E)-enone (E)-**1**. Ketones **2b** and **2b′** were obtained after hydrolysis of the silyl enol ether in an equimolar ratio (Scheme 4).

Scheme 3. Photoinduced Diels–Alder Reaction of Cyclohept-2-enone (1) with 1,3-Butadiene and Related Alkyl-substituted 1,3-Dienes[c]

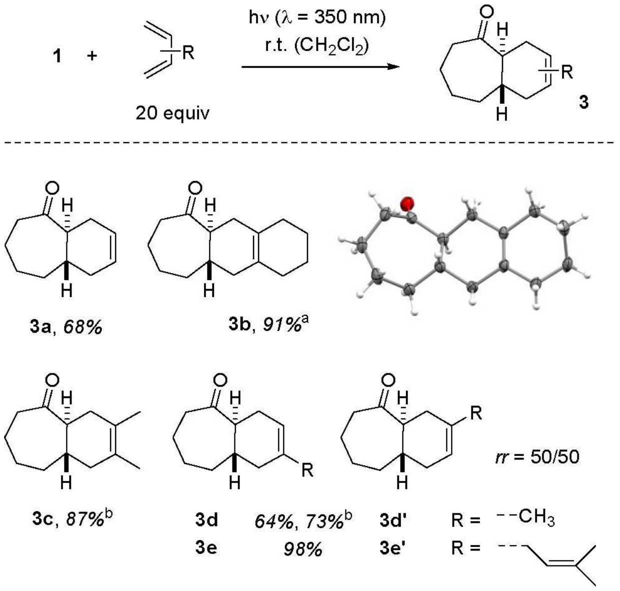

[a]0.1 mmol scale. [b]1.0 mmol scale. [c]0.2 mmol scale. Molecular structure of **3b** in the solid state with ellipsoids at the 50% probability level.

Scheme 4. Photoinduced Diels–Alder Reaction of Cyclohept-2-enone (1) with 2-Trimethylsiloxy-1,3-butadiene Delivering *trans*-Fused Products 2b and 2b′

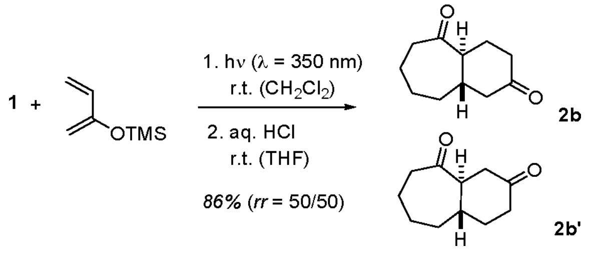

It seems reasonable to assume that stereoelectronic parameters play a smaller role in the reaction of the twisted (E)-enone as compared to reactions of cyclic (Z)-enone. We thus anticipated that the *endo*/*exo*-selectivity might also be less pronounced. The reaction with furan had been previously studied by Eaton and Lin who reported the formation of two diastereomeric products when irradiating cyclohept-2-enone in furan as the solvent.[7] Under our conditions, the high yield of the reaction was confirmed (Scheme 5) and the products were further analyzed (*dr* = diastereomeric ratio). The minor diastereoisomer **4′** gave crystals that were suitable for X-ray

Scheme 5. Photoinduced Diels–Alder Reaction of Cyclohept-2-enone (1) with Furan: Structure Proof and Subsequent Diastereoselective Reactions to Alcohol 5 and Epoxide 6[a]

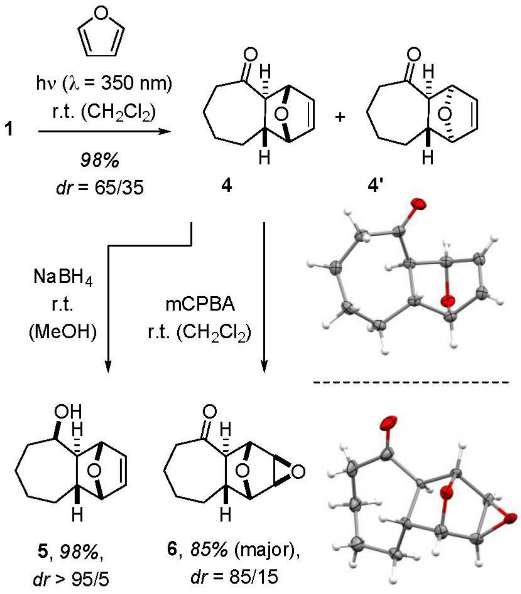

[a]Molecular structures of **4′** and **6** in the solid state with ellipsoids at the 50% probability level.

crystallographic analysis. In this tricyclic product, the former α-hydrogen atom of the α,β-unsaturated enone is positioned *exo* to the double bond, the former β-hydrogen atom *endo*. The keto group is also positioned *endo* to the double bond, which is why we refer to **4′** and related products as *endo*-products. The *exo*-product **4** was the major diastereoisomer the relative configuration of which was established by X-ray crystallographic analysis of its epoxidation product **6**. Unlike the reduction of the ketone to alcohol **5**, which proceeded with perfect diastereoselectivity, the epoxidation led to two diastereoisomers in a ratio of 85/15.

Since the photoinduced Diels–Alder reaction is irreversible, product formation occurs under kinetic control. For the furan cycloaddition, we probed the predictive character of DLPNO–CCSD(T) calculations by comparing their results with the experimental data. The calculations (Figure 2) confirmed that the (*E*)-isomer of cyclohept-2-enone, (*E*)-**1**, can undergo an uncatalyzed Diels–Alder reaction with furan. The activation barrier was calculated to be between 80 and 90 kJ mol^{-1}. Similar barrier heights were obtained in previous work for the reaction of isoprene with (*E*)-4,4-dimethylcyclohept-2-enone.[16]

The respective lowest transition states for an *exo*- vs an *endo*-approach of furan to (*E*)-**1** are depicted in Figure 2. They are energetically close to each other and lead to products **4** and **4′**. The reaction is found to be exergonic with a Gibbs free reaction energy $\Delta_rG°$ of −105.1 and −102.7 kJ mol^{-1}, respectively. The *endo*-transition state is higher in energy and the expected *dr* can be calculated from the relative barrier heights $\Delta^{\ddagger}G°$. The calculated value (*dr* = 76/24) is in remarkably good agreement with the experiment. The optimized molecular structure of **4′** matches closely the experimental structure of the compound in its crystal.

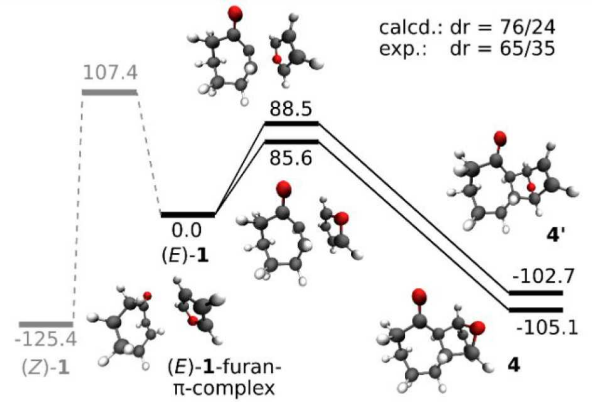

Figure 2. Transition states for the Diels–Alder reaction of (*E*)-**1** with furan to form products **4** and **4′** (black) and for the thermal isomerization back to (*Z*)-**1** (gray). Gibbs free activation energies $\Delta^{\ddagger}G°$ for the Diels–Alder reactions and Gibbs free reaction energies $\Delta_rG°$ for all reactions were calculated using DLPNO–CCST(D)/CBS(3/4, cc)[25]//ωB97xD/aug-cc-pvtz.[26] Gibbs free activation energies $\Delta^{\ddagger}G°$ for the *Z*/*E* Isomerization were calculated using XMS-CASPT2(6,5)/cc-pVTZ//UωB97xD/aug-cc-pvtz. All values are given in kJ mol^{-1}. The calculated diastereomeric ratio *dr* and the experimental *dr* are shown, as well as the structure of a π-complex of (*E*)-**1** and furan.

Scheme 6. Photoinduced Diels–Alder Reaction of Cyclohept-2-enone (1) with Various Bridged Dienes Delivering *trans*-Fused Products 7 and 7′

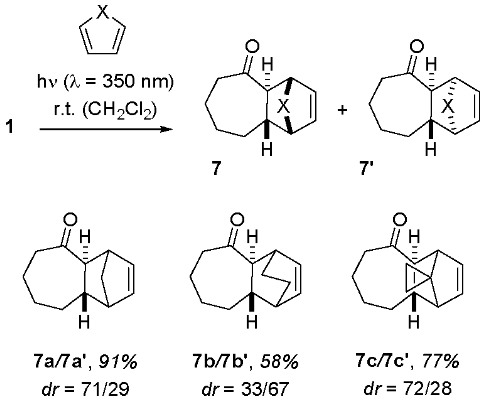

Expectedly, 1,3-cyclopentadienes reacted well in the Diels–Alder reaction with (*E*)-cyclohept-2-enone (Scheme 6, products **7a**/**7a′** and **7c**/**7c′**). The configuration assignment was based on analogy to the furan products, which means that the major product was *exo*-configured. This assignment is in line with previous work[6] in which the *exo*-isomer was described. We could further corroborate the analogous assignment by comparison of the experimental with calculated ^{1}H NMR data for both **4**/**4′** and **7a**/**7a′**; in both cases the olefinic signals of the *exo*-isomer are well separated while those of the *endo*-isomer overlap and lie in-between the signals of the *exo*-isomer (see SI for more details). However, we could not confirm that the product with cyclopentadiene was a single diastereoisomer,[6] even if the reaction was performed at low temperature (*dr* = 75/25 at −70 °C). This is again in agreement with the DLPNO–CCSDT calculations, which predict a barrier height of 77.7 kJ mol^{-1} for the *exo* approach leading to **7a** and a barrier height of 81.7 kJ mol^{-1} for the *endo* approach leading to **7a′**, corresponding to a predicted diastereomeric ratio of *dr* = 83/17.

The reaction with 1,3-cyclohexadiene was sluggish, as expected from the poor reactivity of this diene[27] in thermal Diels–Alder reactions. On the basis of the ^{1}H NMR data we assign the *endo*-isomer **7b′** to be the major diastereoisomer. In general, if trapping with a diene was not successful (e.g., with thiophene), a series of polar spots were detected on TLC, stemming from $[_{\pi}2_s + {}_{\pi}2_a]$ dimerization products[8] of cyclohept-2-enone. When a solution of cyclohept-2-enone was irradiated without diene, the substrate was consumed within the same time period typically required for completion of a photoinduced Diels–Alder reaction (2–4 h; see SI for more information on corresponding studies). This dimerization—in addition to thermal reisomerization to the (*Z*)-isomer—precludes an isolation of (*E*)-**1** at noncryogenic temperatures.

Scheme 7. Photoinduced Diels–Alder Reaction of Various Cycloalk-2-enones 8 with Cyclopentadiene to *trans*-Products 9 and 9′

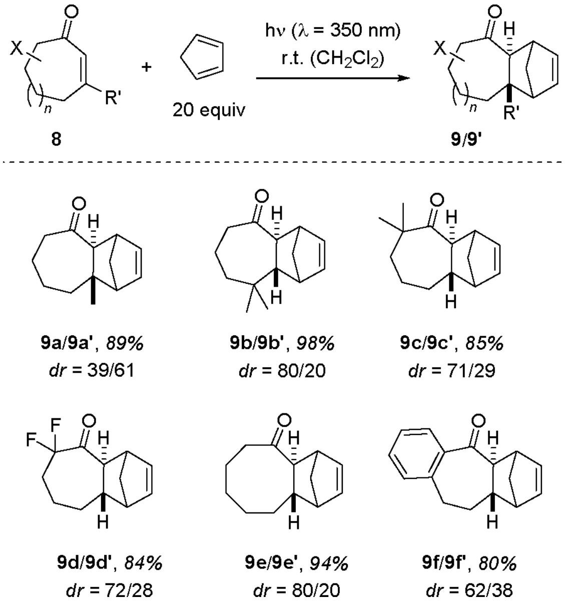

The scope section of this study was completed by submitting other readily available, seven-membered cyclic enones to the conditions of the photoinduced Diels–Alder reaction. 1,3-Cyclopentadiene was employed as the diene component (Scheme 7). In all cases, a mixture of *exo*- (**9**) and *endo*-products (**9′**) was obtained. The reaction proved remarkably robust toward a potential steric hindrance by methyl substituents. Yields remained high irrespective whether a methyl or dimethyl substitution was introduced in the 3-, 4-, or 7-position of the cyclohept-2-enone (products **9a**/**9a′**, **9b**/**9b′**, and **9c**/**9c′**). A difluorosubstitution was also well tolerated and gave the respective tricyclic products **9d**/**9d′** in high yield. The result is relevant for possible applications since it enables the introduction of fluorine atoms into a strained scaffold by a photochemical method. The reaction of cyclooct-2-enone with 1,3-cyclopentadiene was previously reported to yield a single product.[12] Under our conditions, we did not observe a single product but a mixture of two diastereoisomers (**9e**/**9e′**) in a ratio that was similar to the *dr* of the cyclohept-2-enone addition (Scheme 6, **7a**/**7a′**). Eventually, the Diels–Alder reaction was performed with 8,9-dihydrobenzocyclohepten-5-one which also reacted cleanly to products **9f**/**9f′** upon irradiation. In all cases but **9a**/**9a′**, the *exo*-product was again the major diastereoisomer.

As mentioned in the introduction, applications of the photoinduced Diels–Alder reaction in total synthesis are infrequent despite the fact that several natural products display *trans*-annulated bicyclo[5.4.0]undecane skeletons. As a potential target, the sesquiterpene *trans*-α-himachalene (**14**) was selected, which was isolated as (+)-**14** by Bartelt and coworkers[28] in 2001 from the male flea beetle *Phyllotreta cruciferae* and which had been previously synthesized from (*R*)-carvone by Srikrishna and Kumar.[29] The literature-known[16] starting material **8b** was shown to be a competent substrate for the reaction (cf. Scheme 7) despite its geminal dimethylsubstitution at C-4. Reaction with silylenolether **10**[30] was initiated by irradiation at λ = 350 nm and resulted in a mixture of regioisomeric cycloaddition products **11** and **11′** (*rr* = 56/44). Remarkably, the major regioisomer of the reaction, which was isolated in a yield of 36% after hydrolysis, was found to be diastereomerically pure (Scheme 8).

Scheme 8. Concise Total Synthesis of *trans*-α-Himachalene (14) by a Photoinduced Diels–Alder Reaction as Key Step

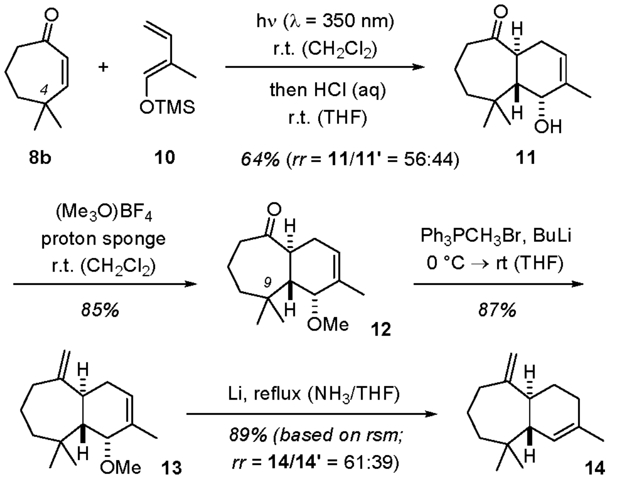

The relative configuration could be assigned after methylation of the free hydroxy group with a strong methylating agent (Meerwein salt) in the presence of 1,8-bis(dimethylamino)-naphthalene (proton sponge) as Brønsted base. NOE contacts were observed between one C-9 methyl group and the bridgehead hydrogen atom in α-position to the carbonyl group as well as between the other C-9 methyl group and the hydrogen atom geminal to the methoxy group. Consequently, these hydrogen atoms need to be on opposite sides of the ring system confirming the depicted relative configuration of product **11**. In turn, this means that the attack of the diene had occurred with *exo*-selectivity on the intermediate (*E*)-enone. The result is in good agreement with the outcome of the above-mentioned reaction of 1-methoxycyclobutadiene (product **2a**, Scheme 2).[14] Methylenation of the carbonyl group of ketone **12** was performed by a Wittig olefination, which produced diene **13** in 87% yield. The final step of the synthesis followed a literature-known[29] elimination under strongly reducing conditions. After release of the methoxide, the allylic anion is not protonated with perfect selectivity, which required separation of the natural product **14** from its regioisomer by column chromatography using $AgNO_3$-impregnated silica. The brevity of the synthesis is mainly due to the fact that the *trans*-junction of the annulated ring does not require a sequential introduction of the two stereogenic centers but was established in the [4 + 2] cycloaddition step.

■ CONCLUSION

In summary, we have shown that the sequence of *Z*/*E* isomerization/Diels−Alder reaction is a versatile tool to obtain *trans*-fused bicyclic ring systems from cyclohept-2-enones. Formation of the (*E*)-isomer can occur on the triplet or on the singlet hypersurface. The high ring strain of (*E*)-cyclohept-2-enones is responsible for their high reactivity toward dienes and the Diels−Alder reaction occurs in the absence of any catalyst. If cyclic dienes were employed, a notable *exo*/*endo* selectivity was recorded, mostly in favor of the *exo*-isomer. With substituted acyclic 1,3-dienes the regioselectivity was not very pronounced. Still, the method invites applications in total synthesis due to the unique bond formation it entails.

■ EXPERIMENTAL SECTION

General Methods. All air or moisture sensitive reactions were carried out in heat gun-dried glassware under an argon atmosphere using standard Schlenk techniques. Photochemical experiments were carried out in heat gun-dried Duran tubes in a positive geometry setup (cylindrical array of 16 fluorescent light tubes, see SI for datasheet) with the sample placed in the center of the illumination chamber. As cooling baths, ice/water (0 °C) and dry ice/isopropanol (−78 °C) mixtures were used. Commercially available chemicals were used without further purification unless otherwise noted. The following compounds were synthesized according to literature procedures: 1,2-dimethylenecyclohexane,[31] trimethyl((2-methylbuta-1,3-dien-1-yl)-oxy)silane.[32] For moisture sensitive reactions, tetrahydrofuran (THF), diethyl ether (Et_2O), and dichloromethane (CH_2Cl_2) were dried by a MBSPS 800 MBraun solvent purification system. All other dry solvents were purchased from Acros Organics (extra dry, over molecular sieves) and used without further purification. For photochemical reactions, dry dichloromethane was degassed by three freeze−pump−thaw cycles and stored over 3 Å molecular sieves (10% w/v), and all dienes were degassed by three freeze−pump−thaw cycles. For extractions or column chromatography, technical solvents were distilled prior to use. Flash column chromatography was performed on silica 60 (Merck, 230−400 mesh) with the indicated eluent mixtures. Thin layer chromatography (TLC) was performed on silica-coated glass plates (Merck, silica 60 F_{254}) with detection by UV-light (λ = 254 nm) [UV] and/or by staining with a potassium permanganate solution (3.00 g $KMnO_4$, 20.0 g K_2CO_3 and 5.00 mL of 5% aq. NaOH solution in 300 mL H_2O) [$KMnO_4$] followed by heat treatment. Melting points were determined using a Büchi M-565 melting point apparatus. Nuclear magnetic resonance spectra were recorded at room temperature on a Bruker AVHD-400, AVHD-500, or AV-III-500 (equipped with a CyroProbe). ^1H NMR spectra were referenced to the residual proton signal of the deuterated solvent [$\delta(CHCl_3)$ = 7.26 ppm, $\delta(CHDCl_2)$ = 5.32 ppm, $\delta(C_6HD_5)$ = 7.16 ppm, $\delta(CHD_2CN)$ = 1.94 ppm]. ^{13}C NMR spectra were referenced to the carbon signal of the deuterated solvent [$\delta(CDCl_3)$ = 77.16 ppm, $\delta(CD_2Cl_2)$ = 53.84 ppm, $\delta(C_6D_6)$ = 128.06 ppm, $\delta(CD_3CN)$ = 118.26 ppm]. ^{19}F NMR spectra were not referenced. Apparent multiplets that occur as a result of coupling constant equality between magnetically nonequivalent protons are marked as virtual (*virt.*). The following abbreviations for single multiplicities were used: br (broad), s (singlet), d (doublet), t (triplet), q (quartet), m (multiplet). Composition of isomeric mixtures was determined by ^1H NMR analysis of the crude product. Infrared spectra (IR) were recorded on a PerkinElmer Frontier IR-FTR spectrometer by ATR technique. The signal intensity is assigned using the following abbreviations: br (broad), vs (very strong), s (strong), m (medium), w (weak). UV−vis spectra were recorded on a PerkinElmer Lambda 35 UV−vis spectrometer, using a Hellma precision cell made of quartz SUPRASIL with a pathway of 1.0 mm. Mass spectrometry (MS) and high resolution mass spectrometry (HRMS) was performed on a Thermo Scientific DFS-HRMS spectrometer (EI).

Synthetic Procedures and Analytical Data. *3-Methylcyclohept-2-en-1-one (**8a**).* Based on a literature procedure.[33] 3.75 mL of a solution of MeLi (1.6 M, 6.00 mmol, 1.2 equiv) was added dropwise to a solution of 551 mg cyclohept-2-en-1-one (5.00 mmol, 1.0 equiv) in dry Et_2O (10 mL) at −78 °C. After stirring for 4 h, H_2O (5.0 mL) was added and the mixture allowed to warm to rt. The layers were separated and the aqueous layer was extracted with Et_2O (3 × 10 mL). The combined organic layers were washed with brine (10 mL), dried over Na_2SO_4, filtered, and concentrated in vacuo. The crude tertiary allylic alcohol was dissolved in dry CH_2Cl_2 (15 mL) and 2.07 g pyridinium dichromate (5.50 mmol, 1.1 equiv) were added. The mixture was vigorously stirred for 18 h. Et_2O (10 mL) was added and the mixture filtered through a pad of silica gel with Et_2O as eluent. After removing the solvent in vacuo and subsequent purification by column chromatography (2.5 cm × 20 cm, P/Et_2O = 4/1 → 2/1), 321 mg enone **8a** (2.59 mmol, 52%) were obtained as a colorless oil. TLC R_f = 0.50 (Hex/EtOAc = 3/1) [UV, $KMnO_4$]. ^1H NMR (500 MHz, $CDCl_3$, 300 K) δ [ppm] = 5.93 (q, *J* = 1.3 Hz, 1H), 2.58 (dd, *J* = 7.2, 5.2 Hz, 2H), 2.41 (dd, *J* = 6.9, 4.6 Hz, 2H), 1.96 (d, *J* = 1.3 Hz, 3H), 1.86−1.73 (m, 4H). ^{13}C NMR{^1H} (126 MHz, $CDCl_3$, 300 K) δ [ppm] = 204.0, 158.7, 130.0, 42.7, 34.7, 27.8, 25.3, 21.6. UV−vis (CH_2Cl_2) λ_{max} (ε) = 235 (11576), 322 nm (72.3 M^{-1} cm^{-1}). The data obtained matched those reported in the literature.[34]

2,2-Dimethyl-6-oxoheptanoic acid. Based on a literature procedure.[35] 6.10 mL β-Ionone (5.77 g, 30.0 mmol, 1.0 equiv) were dissolved in acetone (150 mL) and cooled at 0 °C. 47.4 g $KMnO_4$ (300 mmol, 10 equiv) were added in small portions so that the temperature of the solution stayed below 10 °C. The mixture was stirred for 2 h at rt. After removing the solvent carefully in vacuo, the residue was suspended in water and cooled at 0 °C. Then, 15 g Na_2SO_3 and 150 mL of a diluted aqueous H_2SO_4 solution (conc. H_2SO_4/H_2O = 1/2) were added in portions. While more diluted aqueous H_2SO_4 solution was added until the solution became clear, portions of Na_2SO_3 were added to keep the pH-value between 2 and 7. Once gas evolution stopped and the solution was clear, the pH-value was adjusted to pH = 2 with conc. H_2SO_4. The solution was extracted with CH_2Cl_2 (6 × 100 mL) and the combined organic layers were dried over $MgSO_4$, filtered, and concentrated in vacuo. After purification by Kugelrohr distillation (0.1 mbar, 150 °C), 1.06 g 2,2-dimethyl-6-oxoheptanoic acid (6.17 mmol, 21%) were obtained as a yellowish oil. ^1H NMR (500 MHz, $CDCl_3$, 300 K) δ [ppm] = 2.45 (t, *J* = 6.9 Hz, 2H), 2.16 (s, 3H), 1.66−1.52 (m, 5H), 1.24 (s, 6H). ^{13}C NMR{^1H} (126 MHz, $CDCl_3$, 300 K) δ [ppm] = 209.0, 183.9, 43.9, 42.1, 39.6, 30.0, 24.9, 19.2. The data obtained matched those reported in the literature.[35]

2,2-Dimethyl-6-oxoheptanal. Based on literature procedures.[36] To a stirred suspension of 661 mg $LiAlH_4$ (17.4 mmol, 3.0 equiv) in dry THF (60 mL) at 0 °C was added a solution of 1.00 g 2,2-dimethyl-6-oxoheptanoic acid (5.81 mmol, 1.0 equiv) in dry THF (10 mL). After stirring for 30 min at rt, the mixture was heated at 80 °C for 2.5 h. The mixture was allowed to cool to rt and was diluted with wet Et_2O (60 mL). 6.6 g Celite were added and the mixture vigorously was stirred. H_2O was added until gas evolution ceased. The mixture was filtered and concentrated in vacuo. The crude diol was dissolved in wet CH_2Cl_2 (450 mL) and cooled at 0 °C. A mixture of 16.0 g Dess−Martin periodinane (37.7 mmol, 6.5 equiv) and 6.34 g $NaHCO_3$ (75.5 mmol, 13 equiv) was added in portions. After the resulting suspension was stirred for 2 h at 0 °C and for 2 h at rt, 450 mL of a sat. aq. $NaHCO_3/Na_2S_2O_3$ solution (1:1) were added and the solution stirred for 15 min. The aqueous layer was extracted with Et_2O (3 × 200 mL). The combined organic layers were washed with brine (200 mL), dried over Na_2SO_4, filtered, and concentrated in vacuo. After purification by column chromatography (4.0 cm × 20 cm, P/Et_2O = 4/1), 823 mg 2,2-dimethyl-6-oxoheptanal (5.27 mmol, 91%) were obtained as a yellowish oil. TLC R_f = 0.21 (P/Et_2O = 4/1) [$KMnO_4$]. ^{1}H NMR (500 MHz, $CDCl_3$, 300 K) δ [ppm] = 9.45 (s, 1H), 2.43 (t, J = 6.9 Hz, 3H), 2.13 (d, J = 1.2 Hz, 4H), 1.54−1.38 (m, 6H), 1.06 (s, 6H). ^{13}C NMR{^{1}H} (126 MHz, $CDCl_3$, 300 K) δ [ppm] = 208.5, 206.2, 45.8, 43.8, 36.4, 30.0, 21.3, 18.5.

3-Hydroxy-4,4-dimethylcycloheptan-1-one. Based on a literature procedure.[37] 50.0 mg 2,2-dimethyl-6-oxoheptanal (320 μmol, 1.0 equiv) and 314 mg NPh_3 (1.28 mmol, 4.0 equiv) were dissolved in dry PhMe (40 mL) and cooled at −78 °C. 960 μL of a 1.0 M LiHMDS in PhMe solution (960 μmol, 3.0 equiv) were added dropwise and the solution was stirred for 2 h. After allowing the solution to warm to rt, sat. aq. NH_4Cl (10 mL) was added, the layers separated and the aqueous one extracted with EtOAc (3 × 20 mL). The combined organic layers were washed with brine (20 mL), dried over Na_2SO_4, filtered, and concentrated in vacuo. After purification by column chromatography (1.5 cm × 20 cm, P/Et_2O = 1/1), 33.1 mg 3-hydroxy-4,4-dimethylcycloheptan-1-one (212 μmol, 66%) were obtained as a yellow oil. TLC R_f = 0.16 (P/Et_2O = 1/1) [$KMnO_4$]. ^{1}H NMR (500 MHz, $CDCl_3$, 300 K) δ [ppm] = 3.62 (dd, J = 8.0, 1.9 Hz, 1H), 2.85 (dd, J = 15.3, 1.9 Hz, 1H), 2.69 (dd, J = 15.3, 8.0 Hz, 1H), 2.55−2.39 (m, 2H), 1.79−1.61 (m, 4H), 1.04 (s, 3H), 1.01 (s, 3H). ^{13}C NMR{^{1}H} (126 MHz, $CDCl_3$, 300 K) δ [ppm] = 212.9, 75.0, 47.2, 44.2, 38.2, 38.0, 26.6, 25.8, 19.2. IR (ATR) $\tilde{\nu}$ [cm^{-1}] = 3438 (*br* m), 2952 (s), 2932 (s), 2871 (m), 1691 (vs). MS (EI, 70 eV) m/z (%) = 95 (100), 109 (38), 123 (50), 139 (71), 156 (4) [M]$^+$. HRMS (EI, 70 eV) calcd for $C_9H_{16}O_2$ [M]$^+$: 156.1145, found 156.1136.

*4,4-Dimethylcyclohept-2-en-1-one (**8b**).* 50.0 mg 3-hydroxy-4,4-dimethylcycloheptan-1-one (320 μmol, 1.0 equiv) were dissolved in dry PhMe (25 mL) and 6.09 mg *p*-toluenesulfonic acid monohydrate (32.0 μmol, 10 mol %) were added. A Dean−Stark trap filled with dry PhMe was attached and the mixture heated at 150 °C for 1 h. After allowing the solution to cool to rt, sat. aq. $NaHCO_3$ (5.0 mL) was added. The aqueous layer was extracted with EtOAc (3 × 10 mL). The combined organic layers were washed with brine (10 mL), dried over Na_2SO_4, filtered, and concentrated in vacuo. After purification by column chromatography (2.0 cm × 20 cm, P/Et_2O = 4/1), 36.7 mg ketone **8b** (266 μmol, 83%) were obtained as a yellowish oil. TLC R_f = 0.51 (H/EtOAc = 3/1) [UV, $KMnO_4$]. ^{1}H NMR (500 MHz, $CDCl_3$, 300 K) δ [ppm] = 6.04 (d, J = 12.9 Hz, 1H), 5.76 (d, J = 12.9 Hz, 1H), 2.64−2.57 (m, 2H), 1.85−1.77 (m, 2H), 1.76−1.70 (m, 2H), 1.12 (s, 6H). ^{13}C NMR{^{1}H} (126 MHz, $CDCl_3$, 300 K) δ [ppm] = 204.9, 153.9, 127.6, 45.2, 40.7, 39.7, 29.9, 18.8. UV−vis (CH_2Cl_2) λ_{max} (ε) = 226 (11311), 292 nm (89.7 M^{-1} cm^{-1}). The data obtained matched those reported in the literature.[16]

General Procedure for α-Derivatization of Enones. Based on a literature procedure.[38] A solution of 165 mg cyclohept-2-en-1-one (1.50 mmol, 1.0 equiv) in dry THF (7.5 mL) was cooled at −78 °C and 2.0 mL of a 1.0 M LiHMDS solution in THF (1.95 mmol, 1.3 equiv) were added dropwise. After stirring for 30 min, the electrophile (2.25 mmol, 1.5 equiv) was added as a 500 mM solution in dry THF. The solution was allowed to warm to rt and stirred for 1 h. After cooling at −78 °C for 15 min, another 2.0 mL of a 1.0 M LiHMDS solution (1.95 mmol, 1.3 equiv) were added dropwise. After stirring for 30 min, a second portion of the electrophile (2.25 mmol, 1.5 equiv) was added as a 500 mM solution in dry THF. The solution was allowed to warm to rt and stirred for 1 h. Then, sat. aq. NH_4Cl (10 mL) was added, the layers were separated and the aqueous one extracted with Et_2O (3 × 10 mL). The combined organic layers were washed with brine (10 mL), dried over Na_2SO_4, filtered, and concentrated in vacuo. The crude product was purified by column chromatography.

*7,7-Dimethylcyclohept-2-en-1-one (**8c**).* Following the general procedure, 165 mg cyclohept-2-en-1-one (1.50 mmol, 1.0 equiv) were converted with two times 0.14 mL MeI (319 mg, 2.25 mmol, 1.5 equiv). After purification by column chromatography (2.0 cm × 20 cm, P/Et_2O = 95/5), 85.9 mg ketone **8c** (622 μmol, 41%) were obtained as a yellowish liquid. TLC R_f = 0.57 (Hex/EtOAc = 3/1) [UV, $KMnO_4$]. ^{1}H NMR (500 MHz, CD_2Cl_2, 300 K) δ [ppm] = 6.28 (dt, J = 12.6, 4.3 Hz, 1H), 5.88 (dt, J = 12.6, 2.0 Hz, 1H), 2.37 (tdd, J = 6.2, 4.3, 2.0 Hz, 2H), 1.80−1.66 (m, 4H), 1.56 (s, 2H), 1.12 (s, 6H). ^{13}C NMR{^{1}H} (126 MHz, CD_2Cl_2, 300 K) δ [ppm] = 209.9, 142.4, 130.2, 49.0, 38.2, 33.4, 27.1, 22.8. UV−vis (CH_2Cl_2) λ_{max} (ε) = 225 (9034), 321 nm (112 M^{-1} cm^{-1}). The data obtained matched those reported in the literature.[39]

*7,7-Difluorocyclohept-2-en-1-one (**8d**).* Following the general procedure, 165 mg cyclohept-2-en-1-one (1.50 mmol, 1.0 equiv) were converted with two times 710 mg *N*-fluorobenzenesulfonimide (2.25 mmol, 1.5 equiv). After purification by column chromatography (2.0 cm × 20 cm, P/Et_2O = 7/1), 51.8 mg ketone **8d** (355 μmol, 24%) were obtained as a yellowish liquid. TLC R_f = 0.33 (Hex/EtOAc = 3/1) [UV, $KMnO_4$]. ^{1}H NMR (500 MHz, CD_2Cl_2, 300 K) δ [ppm] = 6.84−6.76 (m, 1H), 6.10−6.03 (m, 1H), 2.54−2.46 (m, 2H), 2.34−2.22 (m, 2H), 1.93−1.84 (m, 2H). ^{13}C NMR{^{1}H} (126 MHz, CD_2Cl_2, 300 K) δ [ppm] = 190.6 (t, J = 28.3 Hz), 150.2, 127.1, 118.2 (t, J = 247.7 Hz), 33.5 (t, J = 23.9 Hz), 30.6, 20.8 (t, J = 6.0 Hz). ^{19}F NMR (376 MHz, CD_2Cl_2, 300 K) δ [ppm] = −98.3 (t, J = 16.6 Hz). IR (ATR) $\tilde{\nu}$ [cm^{-1}] = 2941 (w), 1670 (vs), 1686 (vs), 1627 (w). UV−vis (CH_2Cl_2) λ_{max} (ε) = 235 (8351), 305 nm (167 M^{-1} cm^{-1}). MS (EI, 70 eV) m/z (%) = 109 (100), 115 (18), 125 (14), 146 (4) [M]$^+$. HRMS (EI, 70 eV) calcd for $C_7H_8OF_2$ [M]$^+$: 146.0538, found 146.0536.

General Procedure for the α-Bromination of Ketones. Based on a literature procedure.[40] A solution of a cycloalkanone (1.0 equiv) in dry Et_2O (1.0 M) was placed in a water bath. *N*-Bromosuccinimide (1.05 equiv; recrystallized from 10 mL water per g NBS: dissolved at approximately 90 °C, cooled in ice bath for 3 h, colorless crystals filtered and washed with water, dried in vacuo overnight, stored dark under inert gas in fridge) and subsequently NH_4OAc (10 mol %) were added to the solution. The mixture was stirred at rt until full conversion was reached as determined by TLC. After filtration (Et_2O as eluent), the filtrate was washed with water and brine, dried over Na_2SO_4, filtered, and concentrated in vacuo. The crude product was purified by column chromatography.

General Procedure for the Elimination of α-Bromoketones to Enones. Based on literature procedures.[41] LiBr (2.5 equiv) and Li_2CO_3 (2.5 equiv) were added to a solution of a 2-bromocycloalkanone (1.0 equiv) in dry DMF (500 mM). The mixture was stirred at 130 °C until full conversion was reached as determined by TLC. After cooling to rt, the mixture was diluted to double its volume with EtOAc and filtered over a pad of Celite (EtOAc as eluent). The filtrate was washed with water (3×) and brine (2×), dried over Na_2SO_4, filtered, and concentrated in vacuo. The crude product was purified by column chromatography.

2-Bromocyclooctan-1-one. Following the general procedure, 2.52 g cyclooctanone (20.0 mmol, 1.0 equiv) were converted with 154.0 mg NH_4OAc (2.00 mmol, 10 mol %) and 3.74 g NBS (21.0 mmol, 1.05 equiv) within 4 h. After purification by column chromatography (5.0 cm × 20 cm, P/Et_2O = 95/5), 3.29 g ketone 2-bromocyclooctan-1-one (16.0 mmol, 80%) were obtained as a yellowish oil. TLC R_f = 0.67 (Hex/EtOAc = 2/1) [$KMnO_4$]. ^{1}H NMR (500 MHz, $CDCl_3$, 300 K) δ [ppm] = 4.27 (dd, J = 11.3, 4.0 Hz, 1H), 2.87 (*virt.* td, J = 12.1, 3.7 Hz, 1H), 2.44−2.26 (m, 3H), 1.98−1.87 (m, 1H), 1.83−1.63 (m, 3H), 1.63−1.50 (m, 2H), 1.46−1.35 (m, 1H), 1.24−1.12 (m, 1H). ^{13}C NMR{^{1}H} (126 MHz, $CDCl_3$, 300 K) δ [ppm] = 208.9, 54.5, 36.3, 32.8, 28.9, 26.7, 25.5, 24.1. The data obtained matched those reported in the literature.[42]

*(Z)-Cyclooct-2-en-1-one (**8e**).* Following the general procedure, 3.08 g ketone **S3** (15.0 mmol, 1.0 equiv) were converted with 3.26 g LiBr (37.5 mmol, 2.5 equiv) and 2.77 g Li_2CO_3 (37.5 mmol, 2.5 equiv) within 5 h. After purification by column chromatography (4.5 cm × 20 cm, P/Et_2O = 5/1), 513 mg enone **8e** (4.13 mmol, 28%) were obtained as a yellowish oil. TLC R_f = 0.58 (Hex/EtOAc = 2/1) [UV, $KMnO_4$]. ^{1}H NMR (300 MHz, $CDCl_3$, 300 K) δ [ppm] = 6.35 (dt, J = 12.4, 7.0 Hz, 1H), 6.06−5.95 (m, 1H), 2.65 (t, J = 6.8 Hz, 2H), 2.58−2.45 (m, 2H), 1.90−1.75 (m, 2H), 1.71−1.51 (m, 4H). ^{13}C NMR{^{1}H} (126 MHz, $CDCl_3$, 300 K) δ [ppm] = 214.1, 131.5, 124.2, 44.3, 42.2, 27.1, 25.7, 24.7. UV−vis (CH_2Cl_2) λ_{max} (ε) = 227

(8222), 315 nm (77.3 M^{-1} cm^{-1}). The data obtained matched those reported in the literature.[43]

6-Bromo-6,7,8,9-tetrahydro-5H-benzo[7]annulen-5-one. Following the general procedure, 1.60 g 1-benzosuberone (10.0 mmol, 1.0 equiv) were converted with 77.0 mg NH_4OAc (1.00 mmol, 10 mol %) and 1.87 g NBS (10.5 mmol, 1.05 equiv) within 5 h. After purification by column chromatography (4.0 cm × 20 cm, P/Et_2O = 95/5), 1.23 g ketone 6-bromo-6,7,8,9-tetrahydro-5*H*-benzo[7]annulen-5-one (5.14 mmol, 51%) were obtained as a yellow oil. TLC R_f = 0.40 (Hex/EtOAc = 9/1) [$KMnO_4$]. ^{1}H NMR (500 MHz, $CDCl_3$, 300 K) δ [ppm] = 7.60 (dd, *J* = 7.7, 1.5 Hz, 1H), 7.42 (*virt.* td, *J* = 7.5, 1.5 Hz, 1H), 7.30 (*virt.* td, *J* = 7.6 Hz, 1.2, 1H), 7.23−7.16 (m, 1H), 4.86 (dd, *J* = 7.8, 4.1 Hz, 1H), 3.10−2.84 (m, 2H), 2.52−2.19 (m, 2H), 2.09−1.95 (m, 2H). ^{13}C NMR{^{1}H} (126 MHz, $CDCl_3$, 300 K) δ [ppm] = 200.2, 139.7, 137.8, 132.3, 129.8, 129.7, 126.9, 54.5, 33.9, 33.4, 24.1.

8,9-Dihydro-5H-benzo[7]annulen-5-one ***(8f)***. Following the general procedure, 1.08 g ketone **S4** (4.50 mmol, 1.0 equiv) were converted with 977 mg LiBr (11.3 mmol, 2.5 equiv) and 831 mg Li_2CO_3 (11.3 mmol, 2.5 equiv) within 3 h. After purification by column chromatography (2.5 cm × 20 cm, P/Et_2O = 9/1), 265 mg enone **8f** (1.67 mmol, 37%) were obtained as a yellow oil. TLC R_f = 0.30 (Hex/EtOAc = 9/1) [UV, $KMnO_4$]. ^{1}H NMR (500 MHz, $CDCl_3$, 300 K) δ [ppm] = 7.68 (dd, *J* = 7.8, 1.5 Hz, 1H), 7.44−7.32 (m, 1H), 7.28−7.19 (m, 1H), 7.13 (d, *J* = 7.3 Hz, 1H), 6.69 (dt, *J* = 12.0, 4.7 Hz, 1H), 6.21 (dt, *J* = 12.0, 1.9 Hz, 1H), 3.03−2.97 (m, 2H), 2.57−2.50 (m, 2H). ^{13}C NMR{^{1}H} (126 MHz, $CDCl_3$, 300 K) δ [ppm] = 195.2, 147.2, 140.1, 139.9, 132.6, 132.3, 129.8, 129.0, 126.9, 34.6, 29.9. UV−vis (CH_2Cl_2) λ_{max} (ε) = 232 (8287), 351 nm (178 M^{-1} cm^{-1}). The data obtained matched those reported in the literature.[44]

General Procedure for the Photoinduced Diels−Alder Reaction. The dienophile (1.0 equiv) was transferred as a solution in dry CH_2Cl_2 (1.5 mL) to a Duran phototube. Then, the diene (20 equiv) was added and the solution diluted with dry CH_2Cl_2 to reach a total volume of 10 mL. The mixture was irradiated with fluorescent light tubes (λ_{max} = 350 nm) until full conversion of dienophile was reached as determined by TLC (2−4 h), concentrated in vacuo, and purified by column chromatography.

(4aS,9aS*)-1,4,4a,6,7,8,9,9a-Octahydro-5H-benzo[7]annulen-5-one* ***(3a)***. Following the general procedure, 22.0 mg cyclohept-2-en-1-one (200 μmol, 1.0 equiv) were converted with 2.35 mL butadiene in hexanes (15% w/w, 4.00 mmol, 20 equiv). After purification by column chromatography (1.5 cm × 20 cm, P/Et_2O = 9/1), 22.2 mg ketone **3a** (135.1 μmol, 68%) were obtained as a colorless oil. TLC R_f = 0.58 (Hex/EtOAc = 3/1) [$KMnO_4$]. ^{1}H NMR (500 MHz, $CDCl_3$, 300 K) δ [ppm] = 5.69−5.65 (m, 2H), 2.66 (*virt.* td, *J* = 11.3, 3.2 Hz, 1H), 2.44−2.34 (m, 1H), 2.30 (*virt.* td, *J* = 10.8, 6.3 Hz, 1H), 2.19−2.04 (m, 3H), 1.99−1.87 (m, 2H), 1.87−1.78 (m, 1H), 1.76−1.65 (m, 2H), 1.53−1.45 (m, 2H), 1.30−1.17 (m, 1H). ^{13}C NMR{^{1}H} (126 MHz, $CDCl_3$, 300 K) δ [ppm] = 216.9, 127.2, 125.6, 55.1, 41.2, 36.8, 35.6, 33.8, 29.6, 29.2, 26.5. The data obtained matched those reported in the literature.[10]

(5aS,10aS*)-1,2,3,4,5,5a,7,8,9,10,10a,11-Dodecahydro-6H-cyclohepta[b]naphthalen-6-one* ***(3b)***. Following the general procedure, 11.0 mg cyclohept-2-en-1-one (100 μmol, 1.0 equiv) were converted with 216 mg 1,2-dimethylenecyclohexane (2.00 mmol, 20 equiv). After purification by column chromatography (1.5 cm × 15 cm, P/Et_2O = 9/1), 19.8 mg ketone **3b** (90.5 μmol, 91%) were obtained as a colorless oil. TLC R_f = 0.65 (Hex/EtOAc = 3/1) [$KMnO_4$]. mp 74.9 °C. ^{1}H NMR (500 MHz, $CDCl_3$, 300 K) δ [ppm] = 2.67 (*virt.* td, *J* = 11.4, 3.2 Hz, 1H), 2.40−2.32 (m, 1H), 2.27 (ddd, *J* = 11.7, 10.5, 5.3 Hz, 1H), 2.08−1.80 (m, 9H), 1.80−1.63 (m, 5H), 1.52−1.43 (m, 4H), 1.28−1.17 (m, 1H). ^{13}C NMR{^{1}H} (126 MHz, $CDCl_3$, 300 K) δ [ppm] = 217.2, 128.2, 126.7, 55.8, 41.3, 39.1, 37.3, 35.5, 34.6, 30.0, 29.8, 29.3, 26.5, 23.2, 23.1. IR (ATR) $\tilde{\nu}$ [cm^{-1}] = 2919 (s), 2857 (s), 2824 (m), 1694 (vs). MS (EI, 70 eV) *m*/*z* (%) = 91 (96), 131 (40), 145 (38), 161 (29), 189 (23), 218 (100) $[M]^+$. HRMS (EI, 70 eV) calcd for $C_{15}H_{22}O$ $[M]^+$: 218.1665, found 218.1669. Crystals for X-ray analysis were obtained through preparing a concentrated solution of **3b** in CH_2Cl_2 and allowing the solvent to slowly evaporate at room temperature (see SI for information on crystal measurement).

(4aS,9aS*)-2,3-Dimethyl-1,4,4a,6,7,8,9,9a-octahydro-5H-benzo[7]annulen-5-one* ***(3c)***. Following the general procedure, 110 mg cyclohept-2-en-1-one (1.00 mmol, 1.0 equiv) were converted with 2.26 mL 2,3-dimethylbuta-1,3-diene (20.0 mmol, 20 equiv). After purification by column chromatography (2.0 cm × 20 cm, P/Et_2O = 9/1), 168 mg ketone **3c** (874 μmol, 87%) were obtained as a colorless oil. TLC R_f = 0.71 (Hex/EtOAc = 3/1) [$KMnO_4$]. ^{1}H NMR (500 MHz, $CDCl_3$, 300 K) δ [ppm] = 2.66 (*virt.* td, *J* = 11.4, 3.2 Hz, 1H), 2.39−2.32 (m, 1H), 2.24 (*virt.* td, *J* = 11.4, 5.3 Hz, 1H), 2.16−2.03 (m, 1H), 2.02−1.76 (m, 5H), 1.77−1.62 (m, 2H), 1.60 (s, 6H), 1.51−1.42 (m, 2H), 1.28−1.15 (m, 1H). ^{13}C NMR{^{1}H} (126 MHz, $CDCl_3$, 300 K) δ [ppm] = 217.1, 125.9, 124.3, 55.8, 41.3, 40.4, 37.4, 35.8, 35.4, 29.3, 26.4, 18.9, 18.6. IR (ATR) $\tilde{\nu}$ [cm^{-1}] = 2911 (s), 2858 (m), 2826 (w), 1699 (vs). MS (EI, 70 eV) *m*/*z* (%) = 91 (37), 107 (53), 119 (36), 135 (23), 159 (39), 177 (28), 192 (100) $[M]^+$. HRMS (EI, 70 eV) calcd for $C_{13}H_{20}O$ $[M]^+$: 192.1509, found 192.1510; calcd for $C_{12}{}^{13}CH_{20}O$ $[M]^+$: 193.1542, found 193.1541.

(4aS,9aS*)-2-/-3-Methyl-1,4,4a,6,7,8,9,9a-octahydro-5H-benzo[7]annulen-5-one* ***(3d/3d′)***. Following the general procedure, 110 mg cyclohept-2-en-1-one (1.00 mmol, 1.0 equiv) were converted with 2.00 mL isoprene (20.0 mmol, 20 equiv). After purification by column chromatography (2.0 cm × 15 cm, P/Et_2O = 9/1), 129.7 mg ketones **3d**/**3d′** (728 μmol, 73%, *rr* = 50:50) were obtained as a colorless oil. *Mixture of* **3d**/**3d′** (assignments to a specific isomer not possible): TLC R_f = 0.66 (Hex/EtOAc = 3/1) [$KMnO_4$]. ^{1}H NMR (500 MHz, $CDCl_3$, 300 K) δ [ppm] = 5.40−5.33 (m, 2H), 2.71−2.59 (m, 2H), 2.40−2.15 (m, 4H), 2.15−1.58 (m, 22H), 1.54−1.41 (m, 4H), 1.31−1.17 (m, 2H). ^{13}C NMR{^{1}H} (126 MHz, $CDCl_3$, 300 K) δ [ppm] = 217.2, 216.9, 134.4, 132.8, 121.2, 119.5, 55.5, 55.1, 41.3, 41.2, 38.8, 37.1, 36.8, 35.5, 35.4, 34.2, 34.1, 29.8, 29.3, 29.2, 26.5, 26.4, 23.4, 23.2. IR (ATR) $\tilde{\nu}$ [cm^{-1}] = 2913 (s), 2858 (m), 2830 (w), 1700 (vs). MS (EI, 70 eV) *m*/*z* (%) = 93 (56), 105 (42), 145 (38), 163 (26) $[C_{11}H_{15}O]^+$, 178 (100) $[M]^+$. HRMS (EI, 70 eV) calcd for $C_{12}H_{18}O$ $[M]^+$: 178.1352, found 178.1354; calcd for $C_{11}{}^{13}CH_{18}O$ $[M]^+$: 179.1386, found 179.1392.

(4aS,9aS*)-2-/-3-(3′-Methylbut-2′-en-1′-yl)-1,4,4a,6,7,8,9,9a-octahydro-5H-benzo[7]annulen-5-one* ***(3e/3e′)***. Following the general procedure, 22.0 mg cyclohept-2-en-1-one (200 μmol, 1.0 equiv) were converted with 616 μL myrcene (4.00 mmol, 20 equiv). After purification by column chromatography (1.5 cm × 15 cm, P/Et_2O = 9/1), 45.5 mg ketone **3e**/**3e′** (196 μmol, 98%, *rr* = 50:50) were obtained as a colorless oil. *Mixture of* **3e**/**3e′** (assignments to a specific isomer not possible): TLC R_f = 0.69 (Hex/EtOAc = 3/1) [$KMnO_4$]. ^{1}H NMR (500 MHz, $CDCl_3$, 300 K) δ [ppm] = 5.41−5.35 (m, 2H), 5.13−5.04 (m, 2H), 2.66 (*virt.* tdd, *J* = 11.3, 5.0, 3.2 Hz, 2H), 2.41−2.32 (m, 2H), 2.28 (*virt.* td, *J* = 11.2, 5.5 Hz, 1H), 2.21 (*virt.* td, *J* = 11.2, 5.4 Hz, 1H), 2.16−1.44 (m, 35H), 1.30−1.17 (m, 3H). ^{13}C NMR{^{1}H} (126 MHz, $CDCl_3$, 300 K) δ [ppm] = 217.2, 217.1, 138.1, 136.5, 131.8, 124.2, 120.8, 119.1, 55.5, 55.3, 41.3, 41.2, 37.5, 37.4, 37.2, 37.1, 36.9, 35.6, 35.4, 34.0, 32.7, 29.8, 29.3, 29.2, 26.5, 26.4, 25.9, 17.9 (due to overlapping signals, the number of reported signals is smaller than the number of magnetically inequivalent carbon atoms). IR (ATR) $\tilde{\nu}$ [cm^{-1}] = 2918 (s), 2857 (m), 1702 (vs). MS (EI, 70 eV) *m*/*z* (%) = 91 (99), 105 (100), 159 (73), 177 (27), 203 (78), 232 (4) $[M]^+$. HRMS (EI, 70 eV) calcd for $C_{16}H_{24}O$ $[M]^+$: 232.1822, found 232.1818.

(4aS,9aS*)-Octahydro-1H-benzo[7]annulene-2,5-dione/-2,9-dione* ***(2b/2b′)***. Following the general procedure, 22.0 mg cyclohept-2-en-1-one (200 μmol, 1.0 equiv) were converted with 702 μL (buta-1,3-dien-2-yloxy)trimethylsilane (4.00 mmol, 20 equiv). The reaction mixture was concentrated in vacuo and filtered through a SiO_2 plug (100 mL of P/Et_2O = 4/1 as eluent). After concentrating in vacuo, the crude product (*rr* = 50:50) was dissolved in THF (10 mL) and conc. HCl (aq.) (100 μL) was added. The solution was stirred for 15 min, after which H_2O (5.0 mL) and sat. aq. $NaHCO_3$ (2.0 mL) were added. The layers were separated and the aqueous one extracted with EtOAc (3 × 10 mL). The combined organic layers were washed with brine (10 mL), dried over Na_2SO_4, filtered, and concentrated in

vacuo. After purification by column chromatography (1.5 cm × 20 cm, P/Et$_2$O = 1/1), 15.4 mg ketone **2b** (84.4 μmol, 43%) and 15.6 mg ketone **2b′** (86.6 μmol, 43%) were obtained as colorless oils. *Head-to-tail isomer* (**2b**): TLC R_f = 0.31 (Hex/EtOAc = 1/1) [KMnO$_4$]. ^{1}H NMR (500 MHz, CD$_2$Cl$_2$, 300 K) δ [ppm] = 2.75 (ddd, J = 12.5, 10.7, 4.4 Hz, 1H), 2.63 (ddd, J = 14.8, 12.5, 1.0 Hz, 1H), 2.58−2.49 (m, 2H), 2.42−2.33 (m, 1H), 2.29 (dddd, J = 14.8, 4.8, 3.1, 2.2 Hz, 1H), 2.18 (ddd, J = 14.8, 4.4, 2.1 Hz, 1H), 2.04 (*virt.* ddt, J = 13.1, 6.0, 3.4 Hz, 1H), 1.98−1.86 (m, 3H), 1.75−1.49 (m, 3H), 1.39−1.30 (m, 2H). ^{13}C NMR{^{1}H} (126 MHz, CD$_2$Cl$_2$, 300 K) δ [ppm] = 212.3, 210.8, 54.9, 43.1, 42.0, 40.8, 39.6, 37.2, 34.5, 27.5, 24.0. IR (ATR) $\tilde{\nu}$ [cm^{-1}] = 2923 (m), 2856 (w), 1704 (vs). MS (EI, 70 eV) m/z (%) = 109 (63), 135 (43), 151 (100), 180 (91) [M]$^+$. HRMS (EI, 70 eV) calcd for C$_{11}$H$_{16}$O$_2$ [M]$^+$: 180.1145, found 180.1151. *Head-to-head isomer* (**2b′**): TLC R_f = 0.25 (Hex/EtOAc = 1/1) [KMnO$_4$]. ^{1}H NMR (500 MHz, CD$_2$Cl$_2$, 300 K) δ [ppm] = 2.58−2.50 (m, 2H), 2.50−2.43 (m, 1H), 2.41−2.27 (m, 3H), 2.17 (dd, J = 14.6, 12.8 Hz, 1H), 2.07−1.71 (m, 6H), 1.62−1.51 (m, 1H), 1.47−1.31 (m, 2H). ^{13}C NMR{^{1}H} (126 MHz, CD$_2$Cl$_2$, 300 K) δ [ppm] = 214.6, 210.0, 55.1, 48.6, 42.8, 40.7, 40.1, 37.7, 28.5, 28.4, 25.1. IR (ATR) $\tilde{\nu}$ [cm^{-1}] = 2925 (m), 2859 (w), 1702 (vs). MS (EI, 70 eV) m/z (%) = 110 (43), 125 (40), 152 (11), 180 (100) [M]$^+$. HRMS (EI, 70 eV) calcd for C$_{11}$H$_{16}$O$_2$ [M]$^+$: 180.1145, found 180.1153.

(1R*,4S*,4aR*,9aR*)-/(1S*,4R*,4aR*,9aR*)-1,4,4a,6,7,8,9,9a-Octahydro-5H-1,4-epoxybenzo[7]annulen-5-one (4/4′). Following the general procedure, 110.0 mg cyclohept-2-en-1-one (1.00 mmol, 1.0 equiv) were converted with 1.45 mL furan (4.00 mmol, 20 equiv). After purification of the crude product (*dr* = 65:35) by column chromatography (2.5 cm × 20 cm, P/Et$_2$O = 1/1), 115 mg ketone **4** (645 μmol, 64%) and 61.2 mg ketone **4′** (343 μmol, 34%) were obtained as colorless solids. *Major isomer* (**4**): TLC R_f = 0.32 (P/Et$_2$O = 1/1) [KMnO$_4$]. mp 69.8 °C. ^{1}H NMR (500 MHz, C$_6$D$_6$, 300 K) δ [ppm] = 6.02 (dd, J = 5.8, 1.7 Hz, 1H), 5.78 (dd, J = 5.8, 1.7 Hz, 1H), 5.24 (s, 1H), 4.47−4.42 (m, 1H), 2.23 (ddd, J = 18.7, 6.2, 2.3 Hz, 1H), 2.06 (ddd, J = 18.7, 12.2, 2.6 Hz, 1H), 1.66 (d, J = 7.2 Hz, 1H), 1.58−1.47 (m, 2H), 1.38 (*virt.* ddt, J = 12.7, 5.1, 2.6 Hz, 1H), 1.33−1.23 (m, 1H), 1.06 (*virt.* dtt, J = 14.5, 12.2, 2.0 Hz, 1H), 1.00−0.83 (m, 1H), 0.46−0.34 (m, 1H). ^{13}C NMR{^{1}H} (126 MHz, C$_6$D$_6$, 300 K) δ [ppm] = 208.8, 138.4, 131.2, 81.1, 77.0, 57.6, 43.8, 42.8, 31.0, 30.2, 23.8. IR (ATR) $\tilde{\nu}$ [cm^{-1}] = 2925 (s), 2856 (m), 1709 (vs). MS (EI, 70 eV) m/z (%) = 68 (100) [C$_4$H$_4$O]$^+$, 81 (47), 178 (7) [M]$^+$. HRMS (EI, 70 eV) calcd for C$_{11}$H$_{14}$O$_2$ [M]$^+$: 178.0988, found 178.0989; calcd for C$_{10}$^{13}CH$_{14}$O$_2$ [M]$^+$: 179.1022, found 179.1023. *Minor isomer* (**4′**): TLC R_f = 0.39 (P/Et$_2$O = 1/1) [KMnO$_4$]. mp 88.1 °C. ^{1}H NMR (500 MHz, C$_6$D$_6$, 300 K) δ [ppm] = 6.48 (dd, J = 5.8, 1.6 Hz, 1H), 6.05 (dd, J = 5.8, 1.7 Hz, 1H), 4.94−4.89 (m, 1H), 4.21−4.17 (m, 1H), 2.59 (dd, J = 6.9, 3.6 Hz, 1H), 2.15−2.06 (m, 1H), 1.86−1.75 (m, 1H), 1.68−1.50 (m, 2H), 1.31 (*virt.* qd, J = 12.3, 4.2 Hz, 1H), 1.26−1.13 (m, 2H), 1.06−0.94 (m, 1H), 0.94−0.85 (m, 1H). ^{13}C NMR{^{1}H} (126 MHz, C$_6$D$_6$, 300 K) δ [ppm] = 210.0, 137.6, 133.2, 82.5, 79.3, 58.8, 45.7, 43.1, 33.6, 30.4, 24.0. IR (ATR) $\tilde{\nu}$ [cm^{-1}] = 2924 (s), 2854 (m), 1707 (vs). MS (EI, 70 eV) m/z (%) = 81 (100), 178 (6) [M]$^+$. HRMS (EI, 70 eV) calcd for C$_{11}$H$_{14}$O$_2$ [M]$^+$: 178.0988, found 178.0988; calcd for C$_{10}$^{13}CH$_{14}$O$_2$ [M]$^+$: 179.1022, found 179.1025. Crystals for X-ray analysis were obtained through preparing a concentrated solution of **4′** in CH$_2$Cl$_2$ and allowing the solvent to slowly evaporate at room temperature (see SI for information on crystal measurement).

(1R*,4S*,4aS*,5R*,9aR*)-4,4a,5,6,7,8,9,9a-Octahydro-1H-1,4-epoxybenzo[7]annulen-5-ol (5). To a solution of 35.7 mg **4** (200 μmol, 1.0 equiv) in dry MeOH (2.0 mL) was added 15.1 mg NaBH$_4$ (400 μmol, 2.0 equiv) and the solution stirred at rt for 2 h. A small amount of SiO$_2$ was added and the volatiles removed in vacuo. After purification by column chromatography (dry load, 1.5 cm × 15 cm, Hex/EtOAc = 1/4), 35.5 mg alcohol **5** (197 μmol, 98%) were obtained as a colorless oil. TLC R_f = 0.38 (Hex/EtOAc = 1/4) [KMnO$_4$]. ^{1}H NMR (500 MHz, C$_6$D$_6$, 300 K) δ [ppm] = 6.00 (dd, J = 5.9, 1.8 Hz, 1H), 5.83 (dd, J = 5.9, 1.6 Hz, 1H), 4.42 (d, J = 4.8 Hz, 1H), 4.39 (s, 1H), 4.08−4.02 (m, 1H), 2.19 (*virt.* ddt, J = 12.8, 5.9, 4.0 Hz, 1H), 2.06 (br s, 1H), 1.74 (ddd, J = 12.8, 8.1, 4.8 Hz, 1H), 1.66−1.09 (m, 7H), 0.90 (dd, J = 5.9, 2.6 Hz, 1H). ^{13}C NMR{^{1}H} (126 MHz, C$_6$D$_6$, 300 K) δ [ppm] = 137.4, 131.8, 81.6, 81.1, 69.8, 48.3, 38.4, 36.2, 29.2, 27.8, 22.0. IR (ATR) $\tilde{\nu}$ [cm^{-1}] = 3430 (*br* m), 2988 (w), 2921 (s), 2855 (m). MS (EI, 70 eV) m/z (%) = 97 (100), 111 (72), 125 (42), 180 (5) [M]$^+$. HRMS (EI, 70 eV) calcd for C$_{11}$H$_{16}$O$_2$ [M]$^+$: 180.1145, found 180.1144.

(1aR*,2R*,2aR*,7aR*,8S*,8aS*)-Decahydro-3H-2,8-epoxycyclohepta[4,5]benzo[1,2-b]oxiren-3-one (6). A solution of 35.7 mg **4** (200 μmol, 1.0 equiv) in dry CH$_2$Cl$_2$ (2.0 mL) was cooled at 0 °C and 89.6 mg *meta*-chloroperoxybenzoic acid (77% w/w, 400 μmol, 2.0 equiv) were added. After stirring the mixture at rt for 24 h, CH$_2$Cl$_2$ (5.0 mL) was added, the solution washed with sat. aq. Na$_2$S$_2$O$_3$ (50 mL) and the aqueous layer extracted with CH$_2$Cl$_2$ (50 mL). The combined organic layers were washed with sat. aq. NaHCO$_3$ (50 mL), brine (20 mL), dried over MgSO$_4$, filtered, and concentrated in vacuo. After purification by column chromatography (1.5 cm × 15 cm, EtOAc), 33.1 mg epoxide **6** (170 μmol, 85%) were obtained as colorless crystals. TLC R_f = 0.47 (EtOAc) [KMnO$_4$]. mp 125.8 °C. ^{1}H NMR (500 MHz, CD$_3$CN, 300 K) δ [ppm] = 4.62 (s, 1H), 4.23 (d, J = 4.3 Hz, 1H), 3.42 (d, J = 3.4 Hz, 1H), 3.33 (d, J = 3.4 Hz, 1H), 2.65 (d, J = 8.1 Hz, 1H), 2.41 (ddd, J = 19.3, 6.1, 3.0 Hz, 1H), 2.33 (ddd, J = 19.3, 11.5, 3.0 Hz, 1H), 2.11−2.04 (m, 1H), 2.03−1.96 (m, 2H), 1.88−1.68 (m, 2H), 1.56−1.37 (m, 2H). ^{13}C NMR{^{1}H} (126 MHz, CD$_3$CN, 300 K) δ [ppm] = 210.2, 77.4, 73.3, 58.6, 50.7, 50.0, 48.5, 42.7, 30.7, 28.8, 24.2. IR (ATR) $\tilde{\nu}$ [cm^{-1}] = 2981 (w), 2927 (m), 2861 (w), 1707 (vs).MS (EI, 70 eV) m/z (%) = 97 (100), 135 (61), 165 (44), 194 (6) [M]$^+$. HRMS (EI, 70 eV) calcd for C$_{11}$H$_{14}$O$_3$ [M]$^+$: 194.0937, found 194.0941. Crystals for X-ray analysis were obtained through preparing a concentrated solution of **6** in CH$_2$Cl$_2$ and allowing the solvent to slowly evaporate at room temperature (see SI for information on crystal measurement).

(1R*,4S*,4aS*,9aS*)-/(1S*,4R*,4aS*,9aS*)-1,4,4a,6,7,8,9,9a-Octahydro-5H-1,4-methanobenzo[7]annulen-5-one (7a/7a′). Following the general procedure, 22.0 mg cyclohept-2-en-1-one (200 μmol, 1.0 equiv) were converted with 336 μL cyclopentadiene (4.00 mmol, 20 equiv). After purification by column chromatography (1.5 cm × 15 cm, P/Et$_2$O = 9/1) 32.1 mg ketones **7a**/**7a′** (182 μmol, 91%, *dr* = 71:29) were obtained as a colorless oil. TLC R_f = 0.67 (Hex/EtOAc = 3/1) [KMnO$_4$]. *Major isomer* (**7a**): ^{1}H NMR (500 MHz, CDCl$_3$, 300 K) δ [ppm] = 6.26 (dd, J = 5.7, 3.1 Hz, 1H), 6.03 (dd, J = 5.7, 2.9 Hz, 1H), 2.96 (s, 1H), 2.78 (s, 1H), 2.50 (ddd, J = 19.0, 5.7, 3.0 Hz, 1H), 2.40 (dd, J = 11.8, 3.0 Hz, 1H), 2.15 (dd, J = 7.6, 1.8 Hz, 1H), 2.06−1.98 (m, 1H), 1.91 (*virt.* ddt, J = 13.0, 4.8, 2.7 Hz, 1H), 1.87−1.76 (m, 2H), 1.71 (*virt.* dtt, J = 14.5, 12.2, 2.3 Hz, 1H), 1.54−1.43 (m, 2H), 1.37−1.32 (m, 1H), 1.04 (*virt.* qd, J = 12.2, 4.4 Hz, 1H). ^{13}C NMR{^{1}H} (126 MHz, CDCl$_3$, 300 K) δ [ppm] = 215.0, 138.4, 133.1, 58.2, 48.5, 47.8, 45.7, 43.2, 41.6, 33.6, 30.3, 24.1. *Minor isomer* (**7a′**): ^{1}H NMR (500 MHz, CDCl$_3$, 300 K) δ [ppm] = 6.19−6.11 (m, 2H), 3.01−2.97 (m, 1H), 2.86 (dd, J = 7.2, 2.7 Hz, 1H), 2.45−2.41 (m, 3H), 2.35 (dd, J = 11.8, 3.0 Hz, 1H), 2.29−2.18 (m, 1H), 2.15−2.06 (m, 1H), 2.05−2.00 (m, 1H), 1.88−1.80 (m, 2H), 1.58−1.39 (m, 2H), 1.35−1.29 (m, 1H). ^{13}C NMR{^{1}H} (126 MHz, CDCl$_3$, 300 K) δ [ppm] = 214.0, 138.1, 134.2, 59.8, 47.0, 46.4, 46.2, 43.4, 43.3, 35.7, 30.9, 24.5. The data obtained matched those reported in the literature.[6]

(1R*,4S*,4aS*,9aS*)-/(1S*,4R*,4aS*,9aS*)-1,4,4a,6,7,8,9,9a-Octahydro-5H-1,4-ethanobenzo[7]annulen-5-one (7b/7b′). Following the general procedure, 22.0 mg cyclohept-2-en-1-one (200 μmol, 1.0 equiv) were converted with 381 μL cyclohexa-1,3-diene (4.00 mmol, 20 equiv). After purification of the crude product (*dr* = 33:67) by column chromatography (1.5 cm × 15 cm, P/Et$_2$O = 9/1), 9.7 mg ketone **7b** (50.7 μmol, 25%) and 12.5 mg ketone **7b′** (65.4 μmol, 33%) were obtained as colorless oils. *Minor isomer* (**7b**): TLC R_f = 0.59 (P/Et$_2$O = 9/1) [KMnO$_4$]. ^{1}H NMR (500 MHz, CDCl$_3$, 300 K) δ [ppm] = 6.32 (ddd, J = 8.0, 6.6, 1.3 Hz, 1H), 6.18 (ddd, J = 8.0, 6.3, 1.2 Hz, 1H), 2.79−2.70 (m, 1H), 2.55−2.46 (m, 1H), 2.45−2.30 (m, 2H), 2.19−2.10 (m, 1H), 2.06−1.95 (m, 1H), 1.90−1.74 (m, 3H), 1.72−1.58 (m, 1H), 1.57−1.38 (m, 2H), 1.35−1.05 (m, 4H). ^{13}C NMR{^{1}H} (126 MHz, CDCl$_3$, 300 K) δ [ppm] = 214.8, 135.0, 132.5, 57.6, 43.9, 41.8, 38.6, 38.0, 30.5, 30.0, 27.9, 24.2, 18.6. IR (ATR) $\tilde{\nu}$ [cm^{-1}] = 3046 (w), 2923 (s), 2866 (m), 1702 (vs). MS (EI, 70 eV) *m*/*z* (%) = 85 (71), 97 (51), 111 (34), 141 (26), 149 (100), 167 (23), 190 (3) $[M]^+$. HRMS (EI, 70 eV) calcd for $C_{13}H_{18}O$ $[M]^+$: 190.1352, found 190.1345. *Major isomer* (**7b′**): TLC R_f = 0.47 (P/Et_2O = 9/1) [$KMnO_4$]. ^1H NMR (500 MHz, $CDCl_3$, 300 K) δ [ppm] = 6.35−6.15 (m, 2H), 2.78−2.74 (m, 1H), 2.52−2.23 (m, 4H), 2.19−2.05 (m, 1H), 1.87−1.61 (m, 4H), 1.55−1.37 (m, 2H), 1.33−1.10 (m, 4H). ^{13}C NMR{^1H} (126 MHz, $CDCl_3$, 300 K) δ [ppm] = 213.8, 135.2, 133.1, 57.1, 44.1, 42.4, 36.5, 35.8, 30.6, 29.9, 26.9, 24.2, 18.3. IR (ATR) $\tilde{\nu}$ [cm^{-1}] = 3042 (w), 2923 (s), 2863 (m), 1701 (vs). MS (EI, 70 eV) *m*/*z* (%) = 91 (52), 161 (7), 111 (100), 190 (11) $[M]^+$. HRMS (EI, 70 eV) calcd for $C_{13}H_{18}O$ $[M]^+$: 190.1352, found 190.1348; calcd for $C_{12}{}^{13}CH_{18}O$: 191.1386, found 191.1387.

(1′R,4′S*,4a′R*,9a′S*)-/(1′S*,4′R*,4a′R*,9a′S*)-1′,4′,4a′,6′,7′,8′,9′,9a′-Octahydro-5′H-spiro[cyclopropane-1,10′-[1,4]methanobenzo[7]annulen]-5′-one* (***7c/7c′***). Following the general procedure, 22.0 mg cyclohept-2-en-1-one (200 μmol, 1.0 equiv) were converted with 401 μL spiro[2.4]hepta-4,6-diene (4.00 mmol, 20 equiv). After purification of the crude product (*dr* = 72:28) by column chromatography (1.5 cm × 20 cm, P/Et_2O = 9/1), 31.3 mg ketones **7c**/**7c′** (155 μmol, 77%) were obtained as colorless oil. TLC R_f = 0.30 (P/Et_2O = 9/1) [$KMnO_4$]. *Major isomer* (**7c**): ^1H NMR (500 MHz, $CDCl_3$, 300 K) δ [ppm] = 6.35 (dd, *J* = 5.8, 3.1 Hz, 1H), 6.12 (dd, *J* = 5.8, 2.1 Hz, 1H), 2.54−2.38 (m, 3H), 2.27−2.22 (m, 1H), 2.15−2.00 (m, 3H), 1.96−1.80 (m, 2H), 1.76−1.62 (m, 1H), 1.55−1.44 (m, 1H), 1.21−1.08 (m, 1H), 0.68−0.60 (m, 1H), 0.48−0.39 (m, 2H), 0.33−0.25 (m, 1H). ^{13}C NMR{^1H} (126 MHz, $CDCl_3$, 300 K) δ [ppm] = 213.9, 138.0, 133.0, 60.0, 53.1, 46.5, 45.9, 44.9, 43.4, 33.6, 30.6, 24.3, 8.8, 5.4. *Minor isomer* (**7c′**): ^1H NMR (500 MHz, $CDCl_3$, 300 K) δ [ppm] = 6.34 (dd, *J* = 5.8, 3.1 Hz, 1H), 6.11 (dd, *J* = 5.8, 2.7 Hz, 1H), 2.59−2.37 (m, 3H), 2.28−2.21 (m, 1H), 2.16−1.99 (m, 2H), 1.95−1.79 (m, 2H), 1.77−1.63 (m, 1H), 1.55−1.41 (m, 1H), 1.25 (s, 1H), 1.22−1.07 (m, 1H), 0.68−0.59 (m, 1H), 0.48−0.39 (m, 2H), 0.33−0.24 (m, 1H). ^{13}C NMR{^1H} (126 MHz, $CDCl_3$, 300 K) δ [ppm] = 214.1, 137.8, 134.4, 60.3, 52.5, 48.9, 48.2, 43.4, 43.1, 34.7, 31.2, 24.5, 8.5, 4.0. *Mixture of* **7c**/**7c′**: IR (ATR) $\tilde{\nu}$ [cm^{-1}] = 3060 (w), 2924 (s), 2855 (m), 1705 (vs). MS (EI, 70 eV) *m*/*z* (%) = 91 (51), 92 (100), 105 (21), 117 (12), 130 (6), 202 (5) $[M]^+$. HRMS (EI, 70 eV) calcd for $C_{14}H_{18}O$ $[M]^+$: 202.1352, found 202.1353; calcd for $C_{13}{}^{13}CH_{18}O$: 203.1386, found 203.1392.

(1R,4S*,4aS*,9aS*)-/(1S*,4R*,4aS*,9aS*)-9a-Methyl-1,4,4a,6,7,8,9,9a-octahydro-5H-1,4-methanobenzo[7]annulen-5-one* (***9a/9a′***). Following the general procedure, 24.8 mg enone **8a** (200 μmol, 1.0 equiv) were converted with 336 μL cyclopentadiene (4.00 mmol, 20 equiv). After purification by column chromatography (1.5 cm × 15 cm, P/Et_2O = 9/1), 33.9 mg ketones **9a**/**9a′** (178 μmol, 89%, *dr* = 61:39) were obtained as a colorless oil. TLC R_f = 0.63 (Hex/EtOAc = 3/1) [$KMnO_4$]. *Minor isomer* (**9a**): ^1H NMR (500 MHz, $CDCl_3$, 300 K) δ [ppm] = 6.33 (dd, *J* = 5.8, 3.1 Hz, 1H), 6.10 (dd, *J* = 5.8, 3.0 Hz, 1H), 2.85 (s, 1H), 2.51 (s, 1H), 2.45 (s, 1H), 2.29−2.16 (m, 1H), 1.95−1.69 (m, 6H), 1.65−1.60 (m, 1H), 1.43−1.38 (m, 1H), 1.30−1.21 (m, 1H), 1.05 (s, 3H). ^{13}C NMR{^1H} (126 MHz, $CDCl_3$, 300 K) δ [ppm] = 215.1, 140.2, 134.3, 60.9, 55.7, 45.2, 43.3, 42.6, 41.5, 39.5, 25.8, 24.6, 22.8. *Major isomer* (**9a′**): ^1H NMR (500 MHz, $CDCl_3$, 300 K) δ [ppm] = 6.27 (dd, *J* = 5.8, 3.0 Hz, 1H), 6.15 (dd, *J* = 5.8, 3.1 Hz, 1H), 3.31 (d, *J* = 2.3 Hz, 1H), 2.89 (s, 1H), 2.44−2.36 (m, 2H), 2.29−2.17 (m, 1H), 2.04−1.69 (m, 6H), 1.67 (d, *J* = 8.5 Hz, 1H), 1.48 (d, *J* = 8.5 Hz, 1H), 0.80 (s, 3H). ^{13}C NMR{^1H} (126 MHz, $CDCl_3$, 300 K) δ [ppm] = 213.9, 138.2, 133.9, 62.2, 53.2, 48.4, 46.6, 45.0, 42.7, 41.1, 26.2, 25.1, 20.2. *Mixture of* **9a**/**9a′**: IR (ATR) $\tilde{\nu}$ [cm^{-1}] = 3060 (w), 2930 (s), 2864 (m), 1704 (vs). MS (EI, 70 eV) *m*/*z* (%) = 91 (44), 105 (41), 125 (100), 171 (16), 190 (16) $[M]^+$. HRMS (EI, 70 eV) calcd for $C_{13}H_{18}O$ $[M]^+$: 190.1352, found 190.1369.

(1R,4S*,4aS*,9aS*)-/(1S*,4R*,4aS*,9aS*)-9,9-Dimethyl-1,4,4a,6,7,8,9,9a-octahydro-5H-1,4-methanobenzo[7]annulen-5-one* (***9b/9b′***). Following the general procedure, 13.8 mg enone **8b** (100 μmol, 1.0 equiv) were converted with 168 μL cyclopentadiene (2.00 mmol, 20 equiv). After purification by column chromatography (1.5 cm × 15 cm, P/Et_2O = 9/1), 20.0 mg ketone **9b**/**9b′** (97.9 μmol, 98%, *dr* = 80:20) were obtained as a colorless oil. TLC R_f = 0.60 (Hex/EtOAc = 3/1) [$KMnO_4$]. *Major isomer* (**9b**): ^1H NMR (500 MHz, $CDCl_3$, 300 K) δ [ppm] = 6.13 (dd, *J* = 5.7, 3.2 Hz, 1H), 6.03 (dd, *J* = 5.7, 2.9 Hz, 1H), 3.03−2.97 (m, 1H), 2.93−2.88 (m, 1H), 2.51−2.42 (m, 1H), 2.42−2.32 (m, 2H), 1.85−1.72 (m, 2H), 1.71−1.51 (m, 2H), 1.49−1.39 (m, 1H), 1.37−1.21 (m, 2H), 1.02 (s, 3H), 0.74 (s, 3H). ^{13}C NMR{^1H} (126 MHz, $CDCl_3$, 300 K) δ [ppm] = 215.2, 135.9, 135.0, 53.8, 52.1, 49.7, 46.6, 45.6, 43.7, 42.0, 34.9, 31.2, 22.2, 19.8. *Minor isomer* (**9b′**): ^1H NMR (500 MHz, $CDCl_3$, 300 K) δ [ppm] = 6.21 (dd, *J* = 5.6, 2.7 Hz, 1H), 6.17 (dd, *J* = 5.6, 3.2 Hz, 1H), 3.01−2.96 (m, 2H), 2.64−2.59 (m, 1H), 2.46−2.43 (m, 1H), 2.40−2.31 (m, 1H), 2.28−2.19 (m, 1H), 1.71−1.51 (m, 1H), 1.49−1.39 (m, 1H), 1.37−1.22 (m, 4H), 1.04 (s, 3H), 0.99 (s, 3H). ^{13}C NMR{^1H} (126 MHz, $CDCl_3$, 300 K) δ [ppm] = 214.0, 138.4, 135.4, 53.2, 52.7, 46.5, 45.9, 44.0, 42.8, 42.8, 34.5, 31.0, 29.8, 22.3. *Mixture of* **9b**/**9b′**: IR (ATR) $\tilde{\nu}$ [cm^{-1}] = 2955 (s), 2928 (s), 2870 (m), 1702 (vs). MS (EI, 70 eV) *m*/*z* (%) = 111 (100), 139 (61), 189 (22) $[M-CH_3]^+$, 204 (15) $[M]^+$. HRMS (EI, 70 eV) calcd for $C_{14}H_{20}O$ $[M]^+$: 204.1509, found 204.1512.

(1R,4S*,4aS*,9aS*)-/(1S*,4R*,4aS*,9aS*)-6,6-Dimethyl-1,4,4a,6,7,8,9,9a-octahydro-5H-1,4-methanobenzo[7]annulen-5-one* (***9c/9c′***). Following the general procedure, 13.8 mg enone **8c** (100 μmol, 1.0 equiv) were converted with 168 μL cyclopentadiene (2.00 mmol, 20 equiv). After purification by column chromatography (1.5 cm × 15 cm, P/Et_2O = 95/5), 17.4 mg ketone **9c**/**9c′** (85.0 μmol, 85%, *dr* = 71:29) were obtained as a colorless oil. TLC R_f = 0.63 (Hex/EtOAc = 3/1) [$KMnO_4$]. *Major isomer* (**9c**): ^1H NMR (500 MHz, $CDCl_3$, 300 K) δ [ppm] = 6.27 (*virt.* dt, *J* = 5.3, 2.3 Hz, 1H), 6.01 (*virt.* dt, *J* = 5.3, 2.3 Hz, 1H), 2.86 (s, 1H), 2.77 (s, 1H), 2.18 (d, *J* = 7.6 Hz, 1H), 1.92−1.71 (m, 3H), 1.71−1.51 (m, 3H), 1.50−1.38 (m, 2H), 1.17 (s, 3H), 1.04 (s, 3H), 1.00−0.87 (m, 1H). ^{13}C NMR{^1H} (126 MHz, $CDCl_3$, 300 K) δ [ppm] = 218.9, 138.8, 133.0, 55.8, 48.3, 47.7, 46.7, 45.7, 42.4, 39.2, 33.3, 29.9, 24.9, 24.9. *Minor isomer* (**9c′**): ^1H NMR (500 MHz, $CDCl_3$, 300 K) δ [ppm] = 6.22−6.18 (m, 1H), 6.17−6.12 (m, 1H), 2.99−2.90 (m, 2H), 2.43 (s, 1H), 2.00−1.79 (m, 3H), 1.64−1.51 (m, 1H), 1.50−1.38 (m, 3H), 1.28−1.17 (m, 2H), 1.07 (s, 3H), 1.04 (s, 3H). ^{13}C NMR{^1H} (126 MHz, $CDCl_3$, 300 K) δ [ppm] = 217.9, 137.3, 134.5, 57.6, 46.9, 46.5, 46.4, 46.2, 44.3, 39.4, 34.9, 30.0, 24.8 [*n.b.*: due to overlapping signals, number of reported signals is smaller than number of carbon atoms]. *Mixture of* **9c**/**9c′**: IR (ATR) $\tilde{\nu}$ [cm^{-1}] = 2963 (m), 2925 (s), 2859 (m), 1701 (vs). MS (EI, 70 eV) *m*/*z* (%) = 111 (98), 126 (100), 139 (61), 189 (7) $[M-CH_3]^+$, 204 (66) $[M]^+$. HRMS (EI, 70 eV) calcd for $C_{14}H_{20}O$ $[M]^+$: 204.1509, found 204.1508; calcd for $C_{13}{}^{13}CH_{20}O$ $[M]^+$: 205.1542, found 205.1540.

(1R,4S*,4aS*,9aS*)-/(1S*,4R*,4aS*,9aS*)-6,6-Difluoro-1,4,4a,6,7,8,9,9a-octahydro-5H-1,4-methanobenzo[7]annulen-5-one* (***9d/9d′***). Following the general procedure, 14.6 mg **8d** (100 μmol, 1.0 equiv) were converted with 168 μL cyclopentadiene (2.00 mmol, 20 equiv). After purification by column chromatography (1.5 cm × 15 cm, P/Et_2O = 95/5), 17.8 mg ketone **9d**/**9d′** (83.7 μmol, 84%, *dr* = 72:28) were obtained as a colorless oil. TLC R_f = 0.59 (Hex/EtOAc = 3/1) [$KMnO_4$]. *Major isomer* (**9d**): ^1H NMR (500 MHz, $CDCl_3$, 300 K) δ [ppm] = 6.32 (dd, *J* = 5.8, 3.1 Hz, 1H), 6.08 (dd, *J* = 5.8, 2.9 Hz, 1H), 3.08 (s, 1H), 2.90−2.86 (m, 1H), 2.28−1.77 (m, 7H), 1.60−1.39 (m, 2H), 1.12−0.99 (m, 1H). ^{13}C NMR{^1H} (126 MHz, $CDCl_3$, 300 K) δ [ppm] = 200.2 (dd, *J* = 27.1, 23.9 Hz), 138.5, 133.6, 116.2 (dd, *J* = 255.1, 249.4 Hz), 54.9, 48.4, 47.6, 45.4, 41.5, 33.3 (*virt.* t, *J* = 23.6 Hz), 30.8, 22.1 (dd, *J* = 7.8, 4.1 Hz). ^{19}F NMR{^1H} (376 MHz, $CDCl_3$, 300 K) δ [ppm] = −97.7 (d, *J* = 286.0 Hz), −105.2 (d, *J* = 286.0 Hz). *Minor isomer* (**9d′**): ^1H NMR (500 MHz, $CDCl_3$, 300 K) δ [ppm] = 6.24−6.18 (m, 2H), 3.12−3.09 (m, 1H), 2.83 (*virt.* dt, *J* = 6.9, 2.2 Hz, 1H), 2.55−2.51 (m, 1H), 2.27−1.76 (m, 5H), 1.62−1.41 (m, 4H). ^{13}C NMR{^1H} (126 MHz, $CDCl_3$, 300 K) δ [ppm] = 198.4 (*virt.* t, *J* = 25.4 Hz), 138.2, 133.9, 56.3, 46.6, 46.5, 45.3, 43.2, 33.5 (*virt.* t, *J* = 23.7 Hz), 32.6, 22.3 (dd, *J* = 7.7, 3.7 Hz) [*n.b.*: due to low intensity, signal of CF_2 could not be detected]. ^{19}F NMR{^1H} (376 MHz, $CDCl_3$, 300 K) δ [ppm]

= −97.5 (d, *J* = 287.6 Hz), −104.4 (d, *J* = 287.6 Hz). *Mixture of* **9d**/**9d′**: IR (ATR) $\tilde{\nu}$ [cm^{-1}] = 2943 (m), 2871 (w), 1742 (vs). MS (EI, 70 eV) *m*/*z* (%) = 81 (100), 91 (63), 105 (26), 134 (34), 147 (18), 212 (14) [M]$^+$. HRMS (EI, 70 eV) calcd for $C_{12}H_{14}OF_2$ [M]$^+$: 212.1007, found 212.0993; calcd for $C_{11}{}^{13}CH_{14}OF_2$ [M]$^+$: 213.1041, found 213.1036.

(1R*,4S*,4aS*,10aS*)-/(1S*,4R*,4aS*,10aS*)-4,4a,6,7,8,9,10,10a-Octahydro-1,4-methanobenzo[8]annulen-5(1H)-one (**9e**/**9e′**). Following the general procedure, 24.8 mg enone **8e** (200 μmol, 1.0 equiv) were converted with 336 μL cyclopentadiene (4.00 mmol, 20 equiv). After purification by column chromatography (1.5 cm × 15 cm, P/Et_2O = 9/1), 35.8 mg ketone **9e**/**9e′** (188 μmol, 94%, *dr* = 80:20) were obtained as a colorless oil. TLC R_f = 0.74 (Hex/EtOAc = 3/1) [$KMnO_4$]. *Major isomer* (**9e**): ^{1}H NMR (500 MHz, $CDCl_3$, 300 K) δ [ppm] = 6.22 (dd, *J* = 5.7, 3.1 Hz, 1H), 6.07 (dd, *J* = 5.7, 2.9 Hz, 1H), 3.00 (s, 1H), 2.74 (s, 1H), 2.63−2.44 (m, 2H), 2.14−2.06 (m, 2H), 1.96−1.34 (m, 9H), 1.07−0.96 (m, 1H). ^{13}C NMR{^{1}H} (126 MHz, $CDCl_3$, 300 K) δ [ppm] = 216.7, 137.8, 135.1, 55.9, 48.4, 48.2, 46.0, 45.3, 44.6, 34.9, 28.1, 27.0, 25.8. *Minor isomer* (**9e′**): ^{1}H NMR (500 MHz, $CDCl_3$, 300 K) δ [ppm] = 6.16−6.10 (m, 2H), 3.14 (s, 1H), 2.65 (dd, *J* = 5.6, 3.2 Hz, 1H), 2.62−2.44 (m, 3H), 2.33 (ddd, *J* = 13.9, 6.6, 2.6 Hz, 1H), 1.97−1.33 (m, 10H). ^{13}C NMR{^{1}H} (126 MHz, $CDCl_3$, 300 K) δ [ppm] = 215.1, 137.0, 135.5, 57.2, 48.7, 45.9, 44.9, 43.9, 43.1, 35.9, 27.1, 26.8, 25.4. The data obtained matched those reported in the literature.[12]

(1R*,4S*,4aS*,11aS*)-/(1S*,4R*,4aS*,11aS*)-1,4,4a,10,11,11a-Hexahydro-5H-1,4-methanodibenzo[a,d][7]annulen-5-one (**9f**/**9f′**). Following the general procedure, 31.6 mg enone **8f** (200 μmol, 1.0 equiv) were converted with 336 μL cyclopentadiene (4.00 mmol, 20 equiv). After purification of the crude product (*dr* = 62:38) by column chromatography (1.5 cm × 20 cm, P/Et_2O = 95/5), 20.8 mg ketone **9f** (92.7 μmol, 46%) and 15.3 mg ketone **9f′** (68.0 μmol, 34%) were obtained as viscous yellowish oils. *Major isomer* (**9f**): TLC R_f = 0.43 (P/Et_2O = 95/5) [UV, $KMnO_4$]. ^{1}H NMR (400 MHz, $CDCl_3$, 300 K) δ [ppm] = 8.13 (dd, *J* = 7.8, 1.6 Hz, 1H), 7.45 (*virt.* td, *J* = 7.4, 1.6 Hz, 1H), 7.35 (*virt.* td, *J* = 7.6, 1.3 Hz, 1H), 7.24 (dd, *J* = 7.5, 1.3 Hz, 1H), 6.40 (dd, *J* = 5.7, 3.1 Hz, 1H), 6.14 (dd, *J* = 5.7, 2.9 Hz, 1H), 3.40 (d, *J* = 2.9 Hz, 1H), 3.05−2.91 (m, 2H), 2.80 (d, *J* = 3.1 Hz, 1H), 2.19 (dd, *J* = 8.2, 1.7 Hz, 1H), 2.04−1.89 (m, 2H), 1.62−1.56 (m, 1H), 1.38−1.24 (m, 2H). ^{13}C NMR{^{1}H} (101 MHz, $CDCl_3$, 300 K) δ [ppm] = 203.1, 141.6, 139.0, 136.9, 133.6, 133.0, 132.0, 129.2, 127.0, 56.4, 49.9, 45.5, 42.5, 42.0, 35.7, 27.5. *Minor isomer* (**9f′**): TLC R_f = 0.32 (P/Et_2O = 95/5) [UV, $KMnO_4$]. ^{1}H NMR (500 MHz, $CDCl_3$, 300 K) δ [ppm] = 7.99 (dd, *J* = 7.8, 1.6 Hz, 1H), 7.42 (*virt.* td, *J* = 7.4, 1.6 Hz, 1H), 7.31 (*virt.* td, *J* = 7.2, 1.2 Hz, 1H), 7.25−7.20 (m, 1H), 6.19−6.12 (m, 2H), 3.35 (s, 1H), 3.22 (ddd, *J* = 14.5, 11.6, 8.3 Hz, 1H), 3.04−2.91 (m, 2H), 2.53 (dd, *J* = 2.8, 1.5 Hz, 1H), 2.07 (*virt.* tt, *J* = 12.4, 6.6 Hz, 1H), 1.70−1.57 (m, 3H), 1.42−1.32 (m, 1H). ^{13}C NMR{^{1}H} (126 MHz, $CDCl_3$, 300 K) δ [ppm] = 207.4, 141.2, 138.9, 137.1, 134.2, 132.9, 131.8, 129.0, 127.0, 57.1, 47.1, 44.5, 42.9, 42.7, 34.8, 28.3. The data obtained matched those reported in the literature.[41c]

(1R*,4aS*,9aS*)-1-Hydroxy-2,9,9-trimethyl-1,4,4a,6,7,8,9,9a-octahydro-5H-benzo[7]annulen-5-one (**11**). Following the general procedure, 69.1 mg enone **8b** (500 μmol, 1.00 equiv) and 3.91 g (25.0 mmol, 50 equiv) trimethyl((2-methylbuta-1,3-dien-1-yl)oxy)silane (**10**) were irradiated for 3 h. Then, the mixture was concentrated in vacuo and filtered through a SiO_2 plug (100 mL of P/Et_2O = 4/1 as eluent). After concentrating in vacuo, the crude product (*rr* = 56:44) was dissolved in THF (50 mL) and conc. HCl(aq.) (500 μL) was added. The solution was stirred for 15 min, after which H_2O (25 mL) and sat. aq. $NaHCO_3$ (10 mL) were added. The layers were separated and the aqueous one extracted with EtOAc (3 × 50 mL). The combined organic layers were washed with brine (50 mL), dried over Na_2SO_4, filtered, and concentrated in vacuo. After purification by column chromatography (2.5 cm × 20 cm, P/Et_2O = 2/1), 39.9 mg ketone **11** (179 μmol, 36%) and 31.4 mg ketone **11′** (141 μmol, 28%) were obtained as colorless oils. *Major isomer* (**11**): TLC R_f = 0.38 (P/Et_2O = 1/1) [$KMnO_4$]. ^{1}H NMR (500 MHz, $CDCl_3$, 300 K) δ [ppm] = 5.53−5.47 (m, 1H), 4.12 (d, *J* = 3.1 Hz, 1H), 2.67 (ddd, *J* = 13.5, 10.5, 2.9 Hz, 1H), 2.59 (*virt.* td, *J* = 12.0, 5.2 Hz, 1H), 2.34−2.26 (m, 1H), 2.20−2.10 (m, 1H), 2.10−1.91 (m, 1H), 1.85−1.75 (m, 4H), 1.68−1.41 (m, 4H), 1.17 (s, 3H), 0.96 (s, 3H). ^{13}C NMR{^{1}H} (126 MHz, $CDCl_3$, 300 K) δ [ppm] = 216.5, 136.5, 122.6, 70.1, 48.1, 47.5, 47.2, 40.5, 36.5, 31.0, 30.5, 22.8, 21.6, 21.2. IR (ATR) $\tilde{\nu}$ [cm^{-1}] = 3442 (*br* m), 2933 (s), 2871 (m), 1695 (vs). MS (EI, 70 eV) *m*/*z* (%) = 134 (100), 147 (79), 161 (53), 189 (24), 204 (31), 207 (9) [M−CH_3]$^+$, 222 (8) [M]$^+$. HRMS (EI, 70 eV) calcd for $C_{14}H_{22}O_2$ [M]$^+$: 222.1614, found 222.1595. *Minor isomer* (**11′**) *epimerized upon acid treatment.*

(1R*,4aS*,9aS*)-1-Methoxy-2,9,9-trimethyl-1,4,4a,6,7,8,9,9a-octahydro-5H-benzo[7]annulen-5-one (**12**). Based on a literature procedure.[45] A mixture of 133 mg trimethyloxonium tetrafluoroborate (900 μmol, 6.0 equiv) and 289 mg 1,8-bis(dimethylamino)-naphthalene (1.35 mmol, 9.0 equiv) was suspended in dry CH_2Cl_2 (9.0 mL). A solution of 33.4 mg ketone **11** (150 μmol, 1.00 equiv) in dry CH_2Cl_2 (1.0 mL) was added and the mixture stirred at rt for 16 h. Then, sat. aq. $NaHCO_3$ (5.0 mL) and CH_2Cl_2 (10 mL) were added. The layers were separated, and the organic layer was washed with 1.0 M aq. $KHSO_4$ (3 × 6.0 mL) and brine (6.0 mL), dried over $MgSO_4$, filtered, and concentrated in vacuo. After purification by column chromatography (1.5 cm × 15 cm, P/Et_2O = 4/1), 28.3 mg ketone **12** (127 μmol, 85%) were obtained as a pale yellow oil. TLC R_f = 0.26 (P/Et_2O = 4/1) [$KMnO_4$]. ^{1}H NMR (500 MHz, $CDCl_3$, 300 K) δ [ppm] = 5.57−5.51 (m, 1H), 3.74 (d, *J* = 2.8 Hz, 1H), 3.45 (s, 3H), 2.84 (*virt.* td, *J* = 11.8, 5.8 Hz, 1H), 2.63 (ddd, *J* = 13.4, 10.7, 3.0 Hz, 1H), 2.29−2.16 (m, 2H), 2.00−1.88 (m, 1H), 1.86 (d, *J* = 1.7 Hz, 3H), 1.83−1.72 (m, 1H), 1.65−1.52 (m, 3H), 1.50−1.39 (m, 1H), 1.08 (s, 3H), 0.92 (s, 3H). ^{13}C NMR{^{1}H} (126 MHz, $CDCl_3$, 300 K) δ [ppm] = 216.7, 135.2, 123.8, 78.9, 58.1, 48.6, 47.4, 47.1, 40.3, 36.6, 30.9, 30.8, 24.0, 22.7, 21.3. IR (ATR) $\tilde{\nu}$ [cm^{-1}] = 2926 (s), 2827 (w), 1698 (vs). MS (EI, 70 eV) *m*/*z* (%) = 98 (99), 111 (85), 119 (80), 134 (98), 147 (100), 161 (87), 189 (44), 204 (77), 221 (9) [M−CH_3]$^+$, 236 (10) [M]$^+$. HRMS (EI, 70 eV) calcd for $C_{15}H_{24}O_2$ [M]$^+$: 236.1771, found 236.1765.

(1R*,4aS*,9aS*)-1-Methoxy-2,9,9-trimethyl-5-methylene-1,4,4a,6,7,8,9,9a-octahydro-1H-benzo[7]annulen-5-one (**13**). Based on a literature procedure.[16] To a solution of 70.1 mg Ph_3PCH_3Br (196 μmol, 2.0 equiv) in THF (2.5 mL) at 0 °C was added 79 μL of a 2.5 M *n*-BuLi solution in hexanes (196 μmol, 2.0 equiv). After stirring for 30 min, a solution of 23.2 mg **12** (98.2 μmol, 1.0 equiv) in THF (1.0 mL) was added and the mixture stirred at rt for 18 h. Then, H_2O (2.5 mL) was added dropwise. The layers were separated and the aqueous one extracted with EtOAc (3 × 5.0 mL). The combined organic layers were washed with brine (5.0 mL), dried over Na_2SO_4, filtered, and concentrated in vacuo. After purification by column chromatography (1.5 cm × 15 cm, P/Et_2O = 95/5), 19.9 mg ether **13** (84.9 μmol, 87%) were obtained as a pale yellow liquid. TLC R_f = 0.78 (P/Et_2O = 9/1) [$KMnO_4$]. ^{1}H NMR (500 MHz, $CDCl_3$, 300 K) δ [ppm] = 5.52 (d, *J* = 2.2 Hz, 1H), 4.73 (d, *J* = 2.4 Hz, 1H), 4.70 (d, *J* = 2.4 Hz, 1H), 3.70 (d, *J* = 2.8 Hz, 1H), 3.53 (s, 3H), 2.74 (*virt.* td, *J* = 11.4, 5.6 Hz, 1H), 2.25−2.16 (m, 1H), 2.05−1.95 (m, 1H), 1.95−1.88 (m, 1H), 1.85 (*virt.* q, *J* = 1.8 Hz, 3H), 1.80−1.72 (m, 1H), 1.51−1.40 (m, 2H), 1.35 (dd, *J* = 11.8, 2.8 Hz, 1H), 1.31−1.23 (m, 2H), 1.04 (s, 3H), 1.03 (s, 3H). ^{13}C NMR{^{1}H} (126 MHz, $CDCl_3$, 300 K) δ [ppm] = 156.9, 134.9, 126.0, 110.6, 81.3, 58.8, 50.8, 48.5, 40.1, 37.2, 36.9, 33.2, 31.6, 28.6, 23.8, 21.6. IR (ATR) $\tilde{\nu}$ [cm^{-1}] = 2921 (vs), 2858 (m), 2823 (w), 1638 (w). MS (EI, 70 eV) *m*/*z* (%) = 83 (97), 97 (100), 111 (59), 125 (33), 234 (25) [M]$^+$. HRMS (EI, 70 eV) calcd for $C_{16}H_{26}O$ [M]$^+$: 234.1978, found 234.1978.

(4aS*,9aS*)-3,5,5-Trimethyl-9-methylene-2,4a,5,6,7,8,9,9a-octahydro-1H-benzo[7]annulene (trans-α-Himachalene, **14**). Based on a literature procedure.[29] To liquid NH_3 (25 mL) at −78 °C were added 3.5 mg Li (500 μmol, 10 equiv), turning the solution dark blue. Then a solution of 11.7 mg **13** (50 μmol, 1.0 equiv) in dry THF (2.5 mL) was added dropwise. The cooling bath was removed and the mixture was stirred at reflux for 30 min, using a dry ice reflux condenser. Afterward, 267 mg NH_4Cl (5.00 mmol, 100 equiv) were added in small portions. NH_3 was slowly evaporated and bubbled through conc. HCl(aq.). H_2O (5.0 mL) was added to the residue and the mixture was extracted with CH_2Cl_2 (3 × 5.0 mL). The combined organic layers were washed with brine (5.0 mL), dried over Na_2SO_4, filtered, and concentrated in vacuo. After purification of the crude product (*rr* = 61:39) by column chromatography ($AgNO_3$-impregnated SiO_2, 10% w/w; 1.5 cm × 20 cm, P/Et_2O = 199/1), 4.6 mg **14** (22.5 μmol, 54% based on 17% recovered starting material) were obtained as a pale yellow oil. TLC R_f = 0.80 (P) [$KMnO_4$]. ^{1}H NMR (500 MHz, $CDCl_3$, 300 K) δ [ppm] = 5.31 (dd, *J* = 2.3, 1.2 Hz, 1H), 4.79 (*virt.* dt, *J* = 2.1, 0.9 Hz, 1H), 4.72 (*virt.* dt, *J* = 2.1, 1.2 Hz, 1H), 2.34−2.18 (m, 2H), 2.07−1.95 (m, 2H), 1.92−1.81 (m, 2H), 1.74−1.56 (m, 6H), 1.50−1.40 (m, 1H), 1.33−1.20 (m, 2H), 0.96 (s, 3H), 0.71 (s, 3H). ^{13}C NMR{^{1}H} (126 MHz, $CDCl_3$, 300 K) δ [ppm] = 156.3, 134.2, 123.6, 109.3, 50.5, 40.6, 40.5, 36.3, 34.7, 31.8, 30.8, 29.6, 24.0, 22.9, 20.2. The data obtained matched those reported in the literature.[29] *Minor regioisomer*: ^{1}H NMR (500 MHz, $CDCl_3$, 300 K) δ [ppm] = 5.40−5.30 (m, 1H), 4.71−4.67 (m, 1H), 4.67−4.64 (m, 1H), 2.25−2.15 (m, 2H), 2.07−1.74 (m, 6H), 1.68−1.63 (m, 3H), 1.54−1.27 (m, 4H), 0.88 (s, 3H), 0.84 (s, 3H). ^{13}C NMR {^{1}H} (126 MHz, $CDCl_3$, 300 K) δ [ppm] = 157.6, 134.6, 120.9, 110.2, 46.8, 46.5, 45.3, 37.4, 36.4, 34.1, 33.1, 31.4, 28.2, 23.7, 19.6. HRMS (EI, 70 eV) calcd for $C_{15}H_{24}$ $[M]^+$: 204.1873, found 204.1854.

■ ASSOCIATED CONTENT

Supporting Information

The Supporting Information is available free of charge at https://pubs.acs.org/doi/10.1021/acs.joc.2c00186.

Data sheets of light sources; ^{1}H and ^{13}C{^{1}H} NMR spectra for all new compounds; spectroscopic and computational studies; X-ray crystallographic details (compounds **3b**, **4′**, **6**) (PDF)

FAIR data, including the primary NMR FID files, for compounds **2b**, **2b′**, **3b**, **3c**, **3d**/**3d′**, **3e**/**3e′**, **5**, **6**, **7b**, **7b′**, **7c**/**7c′**, **8d**, **9a**/**9a′**, **9b**/**9b′**, **9c**/**9c′**, **9d**/**9d′**, **11**, **12**, **13**, 3-hydroxy-4,4-dimethylcycloheptan-1-one (ZIP)

Cartesian coordinates of computationally optimized molecular structures (all calculated structures as part of the manuscript and the supporting information, e.g. minima in the ground and excited states but also transition states, 48 in total) (XYZ)

Accession Codes

CCDC 2130527−2130529 contain the supplementary crystallographic data for this paper. These data can be obtained free of charge via www.ccdc.cam.ac.uk/data_request/cif, or by emailing data_request@ccdc.cam.ac.uk, or by contacting The Cambridge Crystallographic Data Centre, 12 Union Road, Cambridge CB2 1EZ, UK; fax: +44 1223 336033.

■ AUTHOR INFORMATION

Corresponding Author

Thorsten Bach − *School of Natural Sciences, Department of Chemistry and Catalysis Research Center (CRC), Technical University of Munich, 85747 Garching, Germany*; orcid.org/0000-0002-1342-0202; Email: thorsten.bach@ch.tum.de

Authors

Daniel P. Schwinger − *School of Natural Sciences, Department of Chemistry and Catalysis Research Center (CRC), Technical University of Munich, 85747 Garching, Germany*; orcid.org/0000-0002-3144-462X

Martin T. Peschel − *Department Chemie, Ludwig-Maximilians-Universität München, 81377 München, Germany*

Constantin Jaschke − *Department Chemie, Ludwig-Maximilians-Universität München, 81377 München, Germany*

Christian Jandl − *School of Natural Sciences, Department of Chemistry and Catalysis Research Center (CRC), Technical University of Munich, 85747 Garching, Germany*

Regina de Vivie-Riedle − *Department Chemie, Ludwig-Maximilians-Universität München, 81377 München, Germany*; orcid.org/0000-0002-7877-5979

Complete contact information is available at: https://pubs.acs.org/10.1021/acs.joc.2c00186

Notes

The authors declare no competing financial interest.

■ ACKNOWLEDGMENTS

Financial support by the Deutsche Forschungsgemeinschaft (DFG, German Research Foundation)—TRR 325 (B1, C5)—444632635 is gratefully acknowledged. D.P.S. thanks the Studienstiftung des deutschen Volkes for a Ph.D. fellowship.

■ REFERENCES

(1) Reviews: (a) Kärkäs, M. D.; Porco, J. A.; Stephenson, C. R. J. Photochemical Approaches to Complex Chemotypes: Applications in Natural Product Synthesis. *Chem. Rev.* **2016**, *116*, 9683−9747. (b) Bach, T.; Hehn, J. P. Photochemical Reactions as Key Steps in Natural Product Synthesis. *Angew. Chem., Int. Ed.* **2011**, *50*, 1000−1045. (c) Hoffmann, N. Photochemical Reactions as Key Steps in Organic Synthesis. *Chem. Rev.* **2008**, *108*, 1052−1103.

(2) Reviews: (a) Neveselý, T.; Wienhold, M.; Molloy, J. J.; Gilmour, R. Advances in the *E* → *Z* Isomerization of Alkenes Using Small Molecule Photocatalysts. *Chem. Rev.* **2022**, *122*, 2650−2694. (b) Turque, O.; Greer, A.; Wauchope, O. R. Synthetic feasibility of oxygen-driven photoisomerizations of alkenes and polyenes. *Org. Biomol. Chem.* **2020**, *18*, 9181−9190. (c) Cameron, D.; Eisler, S. Photoswitchable double bonds: Synthetic strategies for tunability and versatility. *J. Phys. Org. Chem.* **2018**, *31*, No. e3858. (d) Arai, T.; Tokumaru, K. Photochemical one-way adiabatic isomerization of aromatic olefins. *Chem. Rev.* **1993**, *93*, 23−39.

(3) (a) Inoue, Y.; Yokoyama, T.; Yamasaki, N.; Tai, A. An optical yield that increases with temperature in a photochemically induced enantiomeric isomerization. *Nature* **1989**, *341*, 225−226. (b) Hoffmann, R.; Inoue, Y. Trapped Optically Active (*E*)-Cycloheptene Generated by Enantiodifferentiating *Z*−*E* Photoisomerization of Cycloheptene Sensitized by Chiral Aromatic Esters. *J. Am. Chem. Soc.* **1999**, *121*, 10702−10710. (c) Maeda, R.; Wada, T.; Mori, T.; Kono, S.; Kanomata, N.; Inoue, Y. *Planar-to-Planar* Chirality Transfer in the Excited State. Enantiodifferentiating Photoisomerization of Cyclooctenes Sensitized by Planar-Chiral Paracyclophane. *J. Am. Chem. Soc.* **2011**, *133*, 10379−10381.

(4) For related recent work and additional references on the synthesis of (*E*)-cycloalkenes, see: Singh, K.; Trinh, W.; Weaver, J. D. An elusive thermal [2 + 2] cycloaddition driven by visible light photocatalysis: tapping into strain to access C2-symmetric tricyclic rings. *Org. Biomol. Chem.* **2019**, *17*, 1854−1861.

(5) Recent examples: (a) Ruivo, E.; Elvas, F.; Adhikari, K.; Vangestel, C.; Van Haesendonck, G.; Lemière, F.; Staelens, S.; Stroobants, S.; Van der Veken, P.; Wyffels, L.; Augustyns, K. Preclinical Evaluation of a Novel ^{18}F-Labeled dTCO-Amide Derivative for Bioorthogonal Pretargeted Positron Emission Tomography Imaging. *ACS Omega* **2020**, *5*, 4449−4456. (b) Ferreira, V. F. C.; Oliveira, B. L.; D'Onofrio, A.; Farinha, C. M.; Gano, L.; Paulo, A.; Bernardes, G. J. L.; Mendes, F. In Vivo Pretargeting Based on Cysteine-Selective Antibody Modification with IEDDA Bioorthogonal Handles for Click Chemistry. *Bioconjugate Chem.* **2021**, *32*, 121−132. (c) Liu, X.; Xiang, M.-H.; Zhou, W.-J.; Wang, F.; Chu, X.; Jiang, J.-H.

Clicking of organelle-enriched probes for fluorogenic imaging of autophagic and endocytic fluxes. *Chem. Sci.* **2021**, *12*, 5834−5842. (d) Fairhall, J. M.; Camilli, J. C.; Gibson, B. H.; Hook, S.; Gamble, A. B. EGFR-targeted prodrug activation using bioorthogonal alkene-azide click-and-release chemistry. *Bioorg. Med. Chem.* **2021**, *46*, 116361.

(6) Corey, E. J.; Tada, M.; LaMahieu, R.; Libit, L. *trans*-2-Cycloheptenone. *J. Am. Chem. Soc.* **1965**, *87*, 2051−2052.

(7) Eaton, P. E.; Lin, K. *trans*-2-Cycloheptenone. *J. Am. Chem. Soc.* **1965**, *87*, 2052−2054.

(8) For further references on the dimerization of (*E*)-cycloalkenones, see: (a) Vallée, M. R. J.; Inhülsen, I.; Margaretha, P. Photoannelation Reactions of 3-(Alk-1-ynyl)cyclohept-2-en-1-ones. *Helv. Chim. Acta* **2010**, *93*, 17−24. (b) Schmidt, K.; Margaretha, P. Photocyclodimers of 'Made-to-Measure' Seven- and Six-Membered Cyclic Enones. *Helv. Chim. Acta* **2012**, *95*, 423−427.

(9) For an additional early contribution to the photochemical isomerization of cycloalk-2-enones, see: Lange, G. L.; Neidert, E. Photochemistry of 2,4-Cyclooctadienone I. In Benzene and Toluene. *Can. J. Chem.* **1973**, *51*, 2207−2214.

(10) For a recent example, see: Kumar, S. N.; Yu, I. F.; Chein, R.-J. Oxathiaborolium: A Type of Chiral Lewis Acid Catalyst and Its Application in Catalytic and Highly Enantioselective Diels−Alder Reactions. *Org. Lett.* **2017**, *19*, 22−25.

(11) For thermal formation of *trans*-fused Diels−Alder reaction by base-induced isomerization, see: Fringuelli, F.; Pizzo, F.; Taticchi, A.; Halls, T. D. J.; Wenkert, E. Diels-Alder Reactions of Cycloalkenones. 1. Preparation and Structure of the Adducts. *J. Org. Chem.* **1982**, *47*, 5056−5065.

(12) Shinozaki, H.; Arai, S.; Tada, M. The Photoinduced Diels-Alder Reaction of 2-Cycloocten-1-one and 2-Cyclohepten-1-one. *Bull. Chem. Soc. Jpn.* **1976**, *49*, 821−822.

(13) Dorr, H.; Rawal, V. H. The Intramolecular Diels−Alder Reactions of Photochemically Generated trans-Cycloalkenones. *J. Am. Chem. Soc.* **1999**, *121*, 10229−10230.

(14) Nikolai, J.; Loe, Ø.; Dominiak, P. M.; Gerlitz, O. O.; Autschbach, J.; Davies, H. M. L. Mechanistic Studies of UV Assisted [4 + 2] Cycloadditions in Synthetic Efforts toward Vibsanin E. *J. Am. Chem. Soc.* **2007**, *129*, 10763−10772.

(15) Ghosh, S.; Bose, S.; Jana, A.; Nijamudheen, A.; Datta, A. Influence of ring fusion stereochemistry on the stereochemical outcome in photo-induced Diels−Alder reaction of fused bicycloheptenone derivatives. *Tetrahedron* **2014**, *70*, 9783−9790.

(16) Wang, R.-B.; Ma, S.-G.; Jamieson, C. S.; Gao, R.-M.; Liu, Y.-B.; Li, Y.; Wang, X.-J.; Li, Y.-H.; Houk, K. N.; Qu, J.; Yu, S.-S. Library construction of stereochemically diverse isomers of spirooliganin: their total synthesis and antiviral activity. *Chem. Sci.* **2021**, *12*, 7003−7011.

(17) For accounts on contributions from our group to the field, see: (a) Schwinger, D. P.; Bach, T. Chiral 1,3,2-Oxazaborolidine Catalysts for Enantioselective Photochemical Reactions. *Acc. Chem. Res.* **2020**, *53*, 1933−1943. (b) Burg, F.; Bach, T. Lactam Hydrogen Bonds as Control Elements in Enantioselective Transition-Metal-Catalyzed and Photochemical Reactions. *J. Org. Chem.* **2019**, *84*, 8815−8836.

(18) Peschel, M. T.; Kabaciński, P.; Schwinger, D. P.; Thyrhaug, E.; Cerullo, G.; Bach, T.; Hauer, J.; de Vivie-Riedle, R. Activation of 2-Cyclohexenone by BF_3 Coordination: Mechanistic Insights from Theory and Experiment. *Angew. Chem., Int. Ed.* **2021**, *60*, 10155−10163.

(19) García-Expósito, E.; Bearpark, M. J.; Ortuño, R. M.; Branchadell, V.; Robb, M. A.; Wilsey, S. The $T_1{}^3(\pi-\pi^*)/S_0$ Intersections and Triplet Lifetimes of Cyclic *α,β*-Enones. *J. Org. Chem.* **2001**, *66*, 8811−8814.

(20) (a) Stephenson, L. M.; Hammond, G. S. Fate of the excitation energy in the quenching of fluorescence by conjugated dienes. *Pure Appl. Chem.* **1968**, *16*, 125−136. (b) Schuster, D. I.; Fabian, A. C.; Kong, N. P.; Barringer, W. C.; Curran, W. V.; Sussman, D. H. Photochemistry of unsaturated ketones in solution. XVIII. Efficiencies of quenching of short-lived excited triplet states of ketones with dienes. *J. Am. Chem. Soc.* **1968**, *90*, 5027−5028. (c) Schuster, D. I.; Dunn, D. A.; Heibel, G. E.; Brown, P. B.; Rao, J. M.; Woning, J.; Bonneau, R. Enone Photochemistry. Dynamic Properties of Triplet Excited States of Cyclic Conjugated Enones as Revealed by Transient Absorption Spectroscopy. *J. Am. Chem. Soc.* **1991**, *113*, 6245−6255.

(21) (a) Shiozaki, T.; Györffy, W.; Celani, P.; Werner, H.-J. Communication: Extended multi-state complete active space second-order perturbation theory: Energy and nuclear gradients. *J. Chem. Phys.* **2011**, *135*, 081106. As implemented in BAGEL, see: (b) Shiozaki, T. BAGEL: Brilliantly Advanced General Electronic-structure Library. *WIRE's Comput. Mol. Sci.* **2018**, *8*, No. e1331.

(22) Review: Margaretha, P. Retrospective View on Recent Developments in Cyclobutane Synthesis via [2 + 2] Photocycloaddition of Unsaturated Ketones to Acyclic Dienes. *Helv. Chim. Acta* **2014**, *97*, 1027−1035.

(23) (a) Inukai, T.; Kojima, T. Aluminum Chloride Catalyzed Diene Condensation. VI. Partial Rate Factors of 2-Phenyl-, 2-Chloro-, 2-Trifluoromethyl-, and 2-Cyanobutadienes in Reactions with Methyl Acrylate. Differential Hammett Correlation. *J. Org. Chem.* **1971**, *36*, 924−928. (b) Alston, P. V.; Ottenbrite, R. M.; Shillady, D. D. Secondary Orbital Interactions Determining Regioselectivity in the Diels-Alder Reaction. *J. Org. Chem.* **1973**, *38*, 4075−4077.

(24) Laugraud, S.; Guingant, A.; d'Angelo, J. Synthesis of (±) 11-Deoxydaunomycinone and 4-Demethoxy Analogue by Sequential Diels-Alder Cycloadditions. *Tetrahedron Lett.* **1989**, *30*, 83−86.

(25) (a) Guo, Y.; Riplinger, C.; Becker, U.; Liakos, D. G.; Minenkov, Y.; Cavallo, L.; Neese, F. Communication: An improved linear scaling perturbative triples correction for the domain based local pair-natural orbital based singles and doubles coupled cluster method [DLPNO-CCSD(T)]. *J. Chem. Phys.* **2018**, *148*, 011101. As implemented in ORCA, see: (b) Neese, F.; Wennmohs, F.; Becker, U.; Riplinger, C. The ORCA quantum chemistry program package. *J. Chem. Phys.* **2020**, *152*, 224108.

(26) (a) Chai, J.-D.; Head-Gordon, M. Long-range corrected hybrid density functionals with damped atom-atom dispersion corrections. *Phys. Chem. Chem. Phys.* **2008**, *10*, 6615−6620. As implemented in GAUSSIAN: (b) Frisch, M. J.; Trucks, G. W.; Schlegel, H. B.; Scuseria, G. E.; Robb, M. A.; Cheeseman, J. R.; Scalmani, G.; Barone, V.; Petersson, G. A.; Nakatsuji, H.; Li, X.; Caricato, M.; Marenich, A. V.; Bloino, J.; Janesko, B. G.; Gomperts, R.; Mennucci, B.; Hratchian, H. P.; Ortiz, J. V.; Izmaylov, A. F.; Sonnenberg, J. L.; Williams-Young, D.; Ding, F.; Lipparini, F.; Ergidi, F.; Goings, J.; Peng, B.; Ehara, M.; Toyota, K.; Fukuda, R.; Hasegawa, J.; Ishida, M.; Nakajima, T.; Honda, Y.; Kitao, O.; Nakai, H.; Vreven, T.; Throssell, K.; Montgomery, J. A.; Peralta, J. E.; Ogliaro, F.; Baerpark, M. J.; Heyd, J. J.; Brothers, E. N.; Kudin, K. N.; Staroverov, V. N.; Keith, T. A.; Kobayashi, R.; Normand, J.; Raghavari, K.; Rendell, A. P.; Burant, J. C.; Iyengar, S. S.; Tomasi, J.; Cossi, M.; Milliam, J. M.; Klene, M.; Adamo, C.; Cammi, R.; Ochterski, J. W.; Martin, R. L.; Morokuma, K.; Farkas, O.; Foresman, J. B.; Fox, D. J. *Gaussian 16*, Revision A.03; Gaussian, Inc.: Wallingford, CT, 2016.

(27) Levandowski, B. J.; Houk, K. N. Theoretical Analysis of Reactivity Patterns in Diels−Alder Reactions of Cyclopentadiene, Cyclohexadiene, and Cycloheptadiene with Symmetrical and Unsymmetrical Dienophiles. *J. Org. Chem.* **2015**, *80*, 3530−3537.

(28) Bartelt, R. J.; Cossé, A. A.; Zilkowski, B. W.; Weisleder, D.; Momany, F. A. Male-Specific Sesquiterpenes from Phyllotreta and Aphthona Flea Beetles. *J. Chem. Ecol.* **2001**, *27*, 2397−2423.

(29) (a) Srikrishna, A.; Kumar, R. Enantiospecific synthesis of (+)-*trans*-*α*-himachalene via an intramolecular type II carbonyl ene reaction. *Tetrahedron Lett.* **2004**, *45*, 6867−6870. (b) Srikrishna, A.; Kumar, P. R. Enantiospecific synthesis of (+)-*trans*-*α*-himachalene via an intramolecular type II carbonyl ene reaction. *Indian J. Chem.* **2008**, *47B*, 1414−1422.

(30) Balcells, S.; Haughey, M. B.; Walker, J. C. L.; Josa-Culleré, L.; Towers, C.; Donohoe, T. J. Asymmetric Total Synthesis of (−)-(3*R*)-Inthomycin C. *Org. Lett.* **2018**, *20*, 3583−3586.

(31) (a) Groesbeek, M.; van Galen, A. J. J.; Ippel, J. H.; Berden, J. A.; Lugtenburg, J. Three Bacteriorhodopsins with Ring-Didemethylated

6-s-Locked Chromophores and Their Properties. *Recl. Trav. Chim. Pays-Bas* **1993**, *112*, 237−246. (b) Brinker, U. H.; Lin, G.; Xu, L.; Smith, W. B.; Mieusset, J.-L. Dihalocarbene Insertion Reactions into C−H Bonds of Compounds Containing Small Rings: Mechanisms and Regio- and Stereoselectivities. *J. Org. Chem.* **2007**, *72*, 8434−8451.

(32) Balcells, S.; Haughey, M. B.; Walker, J. C. L.; Josa-Culleré, L.; Towers, C.; Donohoe, T. J. Asymmetric Total Synthesis of (−)-(3*R*)-Inthomycin C. *Org. Lett.* **2018**, *20*, 3583−3586.

(33) Leverenz, M.; Merten, C.; Dreuw, A.; Bach, T. Lewis Acid Catalyzed Enantioselective Photochemical Rearrangements on the Singlet Potential Energy Surface. *J. Am. Chem. Soc.* **2019**, *141*, 20053−20057.

(34) Müller, D.; Tissot, M.; Alexakis, A. New Experimental Conditions for Tandem hydroalumination/Cu-Catalyzed Asymmetric Conjugate Additions to β-Substituted Cyclic Enones. *Org. Lett.* **2011**, *13*, 3040−3043.

(35) Burton, G. W.; Daroszewski, J.; Nickerson, J. G.; Johnston, J. B.; Mogg, T. J.; Nikiforov, G. B. β-Carotene autoxidation: oxygen copolymerization, non-vitamin A products, and immunological activity. *Can. J. Chem.* **2014**, *92*, 305−316.

(36) (a) For the $LiAlH_4$ reduction, see ref 26b. (b) For the DMP oxidation, see: Wienhold, S.; Fritz, L.; Judt, T.; Hackl, S.; Neubauer, T.; Sauerer, B.; Bach, T. Studies towards the Synthesis of (−)-Pulvomycin: Construction of the C12−C40 Segment by a Stereoselective Aldol Reaction. *Synthesis* **2021**, *53*, 4246−4262.

(37) O'Brien, E. M.; Li, J.; Carroll, P. J.; Kozlowski, M. C. Synthesis of the Cores of Hypocrellin and Shiraiachrome: Diastereoselective 1,8-Diketone Aldol Cyclization. *J. Org. Chem.* **2010**, *75*, 69−73.

(38) Economou, C.; Tomanik, M.; Herzon, S. B. Synthesis of Myrocin G, the Putative Active Form of the Myrocin Antitumor Antibiotics. *J. Am. Chem. Soc.* **2018**, *140*, 16058−16061.

(39) Bartelt, R. J.; Weisleder, D.; Momany, F. A. Total Synthesis of Himachalene Sesquiterpenes of *Aphthona* and *Phyllotreta* Flea Beetles. *Synthesis* **2003**, 117−123.

(40) Tanemura, K.; Suzuki, T.; Nishida, Y.; Satsumabayashi, K.; Horaguchi, T. A mild and efficient procedure for α-bromination of ketones using *N*-bromosuccinimide catalysed by ammonium acetate. *Chem. Commun.* **2004**, 470−471.

(41) (a) Roosen, P. C.; Vanderwal, C. D. Investigations into an Anionic Oxy-Cope/Transannular Conjugate Addition Approach to 7,20-Diisocyanoadociane. *Org. Lett.* **2014**, *16*, 4368−4371. (b) Paquette, L. A.; Stepanian, M.; Mallavadhani, U. V.; Cutarelli, T. D.; Lowinger, T. B.; Klemeyer, H. J. Definition of Several Control Elements Relevant to the Stereodefined Serial Elaboration of Belted Poly(spirotetrahydrofurans) Fitted with a Cyclohexane Core. *J. Org. Chem.* **1996**, *61*, 7492−7507. (c) Ghosh, S.; Saha Roy, S.; Saha, G. An expeditious route to trans fused 5−7−6 and 6−7−6 carbocycles through photoisomerisation-cycloaddition of benzocycloheptenone. *Tetrahedron* **1988**, *44*, 6235−6240.

(42) Moriyama, K.; Hamada, T.; Nakamura, Y.; Togo, H. Catalytic dehydrogenative dual functionalization of ethers: dealkylation−oxidation−bromination accompanied by C−O bond cleavage *via* aerobic oxidation of bromide. *Chem. Commun.* **2017**, *53*, 6565−6568.

(43) Kuga, T.; Sasano, Y.; Iwabuchi, Y. IBX as a catalyst for dehydration of hydroperoxides: green entry to α,β-unsaturated ketones *via* oxygenative allylic transposition. *Chem. Commun.* **2018**, *54*, 798−801.

(44) Beltran, F.; Bergamaschi, E.; Funes-Ardoiz, I.; Teskey, C. J. Photocontrolled Cobalt Catalysis for Selective Hydroboration of α,β-Unsaturated Ketones. *Angew. Chem., Int. Ed.* **2020**, *132*, 21362−21368.

(45) Poock, C.; Kalesse, M. Total Synthesis of Nannocystin Ax. *Org. Lett.* **2017**, *19*, 4536−4539.

Recommended by ACS

Base-Catalyzed [1,*n*]-Proton Shifts in Conjugated Polyenyl Alcohols and Ethers

Nagaraju Molleti, Belén Martín-Matute, *et al.*

AUGUST 26, 2019
ACS CATALYSIS
READ

An Integrated Building Block for Cascade Diels–Alder and Hetero-Diels–Alder Reactions

Shuheng Xu, Sunliang Cui, *et al.*

APRIL 01, 2022
ORGANIC LETTERS
READ

Catalytic Asymmetric Spirocyclizing Diels–Alder Reactions of Enones: Stereoselective Total and Formal Syntheses of α-Chamigrene, β-Chamigrene, Laurenc...

Santanu Ghosh, Benjamin List, *et al.*

APRIL 07, 2022
JOURNAL OF THE AMERICAN CHEMICAL SOCIETY
READ

Bisketene Equivalents as Diels–Alder Dienes

Isuru Dissanayake, Christopher G. Newton, *et al.*

JULY 18, 2020
JOURNAL OF THE AMERICAN CHEMICAL SOCIETY
READ

Get More Suggestions >

https://doi.org/10.1021/acs.joc.2c00186
J. Org. Chem. 2022, 87, 4838−4851

B Photoinduced B–Cl Bond Fission in Aldehyde-BCl_3 Complexes as a Mechanistic Scenario for C–H Bond Activation

Reprinted (adapted) with permission from D. P. Schwinger, M. T. Peschel, T. Rigotti, P. Kabaciński, T. Knoll, E. Thyrhaug, G. Cerullo, J. Hauer, R. de Vivie-Riedle, T. Bach, *J. Am. Chem. Soc.* **2022**, *144*, 18927–18937. Copyright 2022 American Chemical Society.

JOURNAL OF THE AMERICAN CHEMICAL SOCIETY

pubs.acs.org/JACS Article

Photoinduced B−Cl Bond Fission in Aldehyde-BCl_3 Complexes as a Mechanistic Scenario for C−H Bond Activation

Daniel P. Schwinger,[#] Martin T. Peschel,[#] Thomas Rigotti,[#] Piotr Kabaciński, Thomas Knoll, Erling Thyrhaug, Giulio Cerullo, Jürgen Hauer,* Regina de Vivie-Riedle,* and Thorsten Bach*

Cite This: J. Am. Chem. Soc. 2022, 144, 18927−18937 Read Online

ACCESS | Metrics & More | Article Recommendations | SI Supporting Information

Downloaded via TU MUENCHEN on November 14, 2022 at 16:00:12 (UTC).
See https://pubs.acs.org/sharingguidelines for options on how to legitimately share published articles.

ABSTRACT: In concert with carbonyl compounds, Lewis acids have been identified as a versatile class of photocatalysts. Thus far, research has focused on activation of the substrate, either by changing its photophysical properties or by modifying its photochemistry. In this work, we expand the established mode of action by demonstrating that UV photoexcitation of a Lewis acid−base complex can lead to homolytic cleavage of a covalent bond in the Lewis acid. In a study on the complex of benzaldehyde and the Lewis acid BCl_3, we found evidence for homolytic B−Cl bond cleavage leading to formation of a borylated ketyl radical and a free chlorine atom only hundreds of femtoseconds after excitation. Both time-dependent density functional theory and transient absorption experiments identify a benzaldehyde-BCl_2 cation as the dominant species formed on the nanosecond time scale. The experimentally validated B−Cl bond homolysis was synthetically exploited for a BCl_3-mediated hydroalkylation reaction of aromatic aldehydes (19 examples, 42−76% yield). It was found that hydrocarbons undergo addition to the C═O double bond via a radical pathway. The photogenerated chlorine radical abstracts a hydrogen atom from the alkane, and the resulting carbon-centered radical either recombines with the borylated ketyl radical or adds to the ground-state aldehyde-BCl_3 complex, releasing a chlorine atom. The existence of a radical chain was corroborated by quantum yield measurements and by theory. The photolytic mechanism described here is based on electron transfer between a bound chlorine and an aromatic π-system on the substrate. Thereby, it avoids the use of redox-active transition metals.

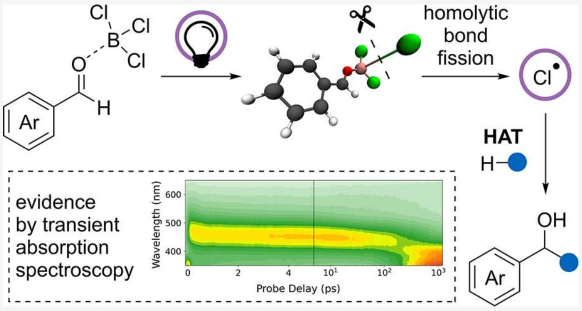

■ INTRODUCTION

Lewis acids represent the most frequently used class of catalysts in conventional (thermal) C−C bond forming reactions.[1] They act by coordination to a Lewis basic entity of the substrate, frequently the oxygen atom of a carbonyl group. In α,β-unsaturated carbonyl compounds the energy of the lowest unoccupied molecular orbital (LUMO) decreases upon Lewis acid coordination, rendering them more electrophilic. A major benefit of Lewis acid catalysis is the plethora of chiral Lewis acids available that enable enantioselective catalysis of a given reaction.[2] In contrast to the great success Lewis acids have encountered in thermal reactions, their influence on photochemical reactions has not been appreciated for many years. In the photochemical case, the stabilization of the LUMO also plays a key role, as it renders α,β-unsaturated carbonyl compounds more amenable to photoexcitation in the near UV. Thus, there has recently been an increased interest in chiral Lewis acids in the context of enantioselective photochemical reactions.[3] Formation of an assembly with a Lewis acid alters the reactivity pattern of a substrate and opens up alternative reaction channels that are inaccessible by direct irradiation.[4] The photochemical behavior of 2-naphthaldehyde (**1**) toward olefins such as 2,3-dimethyl-2-butene serves as an illustrative example (Scheme 1).[5]

Direct irradiation of the compound at $\lambda = 366$ nm delivers exclusively products stemming from reactivity at the carbonyl group, for example oxetane **2** as the product of a Paternò−Büchi reaction. This reaction channel is inaccessible upon Lewis acid coordination, and instead a clean [2+2] photocycloaddition with 2,3-dimethyl-2-butene occurs at the aromatic double bond (*ortho* photocycloaddition) to obtain cyclobutane **3**.

In studies initially directed to a related *ortho* photocycloaddition[6] of benzaldehyde and olefins, we have investigated the 1:1 complex of benzaldehyde and the Lewis acid boron trichloride. Although its ground-state properties had been investigated previously,[7] there was no information on its excited-state properties. In earlier work, we had seen that excited-state calculations in combination with transient absorption spectros-

Received: June 25, 2022
Published: October 7, 2022

© 2022 American Chemical Society

Scheme 1. Reactivity of 2-Naphthaldehyde (1) toward 2,3-Dimethylbutene in the Absence and in the Presence of $AlBr_3$ as a Lewis Acid

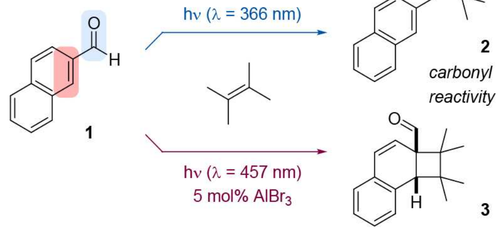

copy provide valuable insights into the nature of Lewis acid complexes in the excited state. We were able to assign excited-state absorptive signals of a 1:1 complex between cyclohex-2-enone and boron trifluoride and to elucidate the photophysical relaxation processes on the singlet and triplet hypersurface.[8] Surprisingly, boron trichloride and benzaldehyde displayed a completely different and unexpected behavior (Scheme 2).

Scheme 2. A 1:1 Complex of Benzaldehyde and Boron Trichloride (4) Is Predicted to Cleave Homolytically after Irradiation and to Undergo a Subsequent Electron Transfer

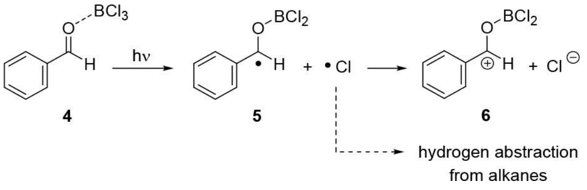

Their 1:1 complex was predicted by theory to be unstable in the excited state, and many trajectories were found in which a homolytic cleavage to a chlorine atom and a borylated ketyl radical **5** occurred. In analogy to observations on benzhydryl radicals,[9] a subsequent electron transfer was suggested, leading to cation **6** with a chloride counterion. Both predictions were corroborated in detailed transient absorption experiments on the fs and ns time scales. The initial step of this pathway is reminiscent of the visible-light-induced homolysis (VLIH) of earth-abundant metal complexes, which has found recently increased synthetic attention.[10,11] It was thus attempted to employ the generated chlorine radical in metal-free C−H activation reactions (hydrogen abstraction), which finally culminated in a procedure for the Lewis acid-mediated addition of hydrocarbons on aromatic aldehydes. Our study establishes a detailed mechanistic picture behind the homolytic photocleavage reaction depicted in Scheme 2, based on a combination of theory and femtosecond UV-pump white-light-probe transient absorption spectroscopy. We tested and utilized the reaction mechanism in synthetic work, establishing a new method for the generation of halogen radicals from main group compounds and their application to the activation of C−H bonds. A coherent mechanistic picture evolved, which reaches beyond current knowledge of transition-metal-based VLIH processes.

The discussion in the following sections commences with a theoretical treatise of the benzaldehyde-BCl_3 complex and its predicted photochemical behavior, most notably the B−Cl bond fission. The second section describes the photochemical dynamics of the complex by transient absorption spectroscopy experiments. It is linked to theory by comparison of calculated and experimentally obtained spectra of the transient intermediates. The final part takes up the results of theory and spectroscopy by devising a synthetic application of the B−Cl bond fission. The suggested reaction pathway involves a release of a chlorine atom upon attack of a carbon-centered radical on the benzaldehyde-BCl_3 complex, which in turn is supported by calculations.

■ RESULTS AND DISCUSSION

Vertical Excitation Energies and Static Absorption Spectra. The small aromatic carbonyl compound benzaldehyde is a relatively strong absorber in the mid- to deep-UV spectral range. Its UV absorption spectrum has been discussed extensively in the literature.[12] In CH_2Cl_2 solution, it features three partially overlapping absorption bands in the region from 400 to 220 nm (Figure 1).

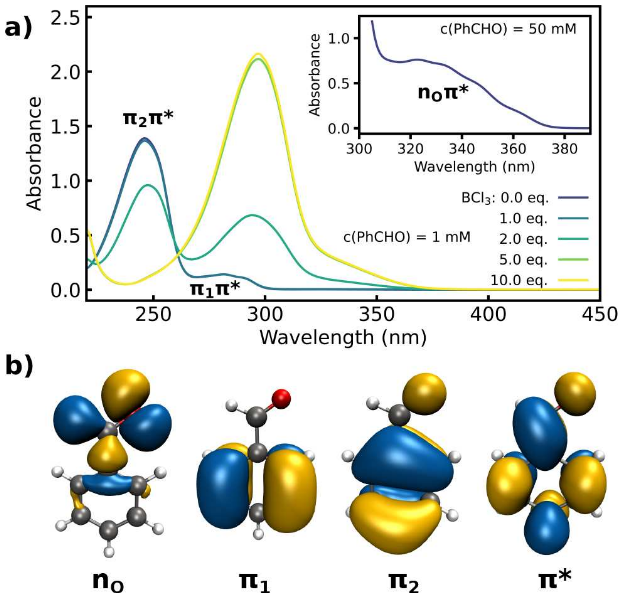

Figure 1. Panel a: UV−vis spectrum of benzaldehyde (dark blue) with varying amounts of BCl_3, showing formation of complex **4** (dark green-yellow). The bright $S_0 \rightarrow S_2(\pi_1\pi^*)$ and $S_0 \rightarrow S_3(\pi_2\pi^*)$ transitions are labeled. The inset shows the UV−vis spectrum of benzaldehyde at a higher concentration, revealing the symmetry-forbidden $S_0 \rightarrow S_1(n_O\pi^*)$ transition. Panel b: Natural transition orbitals (NTOs) for the respective transitions displayed in panel a, calculated using time-dependent ωb97x-D3/ZORA-def2-TZVP.

The first band at $\lambda \cong 330$ nm is very weak and attributed to the symmetry forbidden $S_0 \rightarrow S_1(n_O\pi^*)$ transition out of a lone-pair orbital at the carbonyl oxygen atom. The second (at $\lambda \cong 280$ nm) and third band (at $\lambda \cong 240$ nm) are caused by bright $S_0 \rightarrow S_2(\pi_1\pi^*)$ and $S_0 \rightarrow S_3(\pi_2\pi^*)$ transitions. The excitations originate from two different π-orbitals of the aromatic core. Upon addition of BCl_3, the absorption bands shifted and, after addition of five equivalents, no further changes were observed, indicating that complex formation was complete (see Figure 1). The observed spectral shifts are typical for carbonyl compounds on complexation with Lewis acids.[4,13] The final spectrum of complex **4** displayed a single, broad band with an absorption maximum at $\lambda = 297$ nm including a red-shifted shoulder. The coordination of the Lewis acid strongly stabilizes the oxygen n-

https://doi.org/10.1021/jacs.2c06683
J. Am. Chem. Soc. 2022, 144, 18927−18937

orbital of benzaldehyde and weakly stabilizes its π^*-orbital (LUMO), leaving the π_1- and π_2-orbitals almost unchanged. Thus, we expected the absorption range of **4** to contain all three transitions ($n_O\pi^*$, $\pi_1\pi^*$, and $\pi_2\pi^*$) with the $n_O\pi^*$ transition blue-shifted and both $\pi\pi^*$ transitions red-shifted, as was observed in our earlier study of a cyclohexenone-BF$_3$ complex.[8] Additionally, the chlorine lone pairs n_{Cl} in **4** are close in energy to the π-orbitals, and excitations from these orbitals into the π^*-orbital appear in the near to middle UV region as well. Each chlorine atom contributes two high-lying chlorine lone pairs, so an additional six $n_{Cl}\pi^*$ states have to be considered. This is in contrast to the previously investigated BF$_3$ complex,[8] where transitions from the halogen lone pairs lie significantly below 200 nm and are not relevant for photochemical processes after UV excitation. In Figure 2a, the experimental absorption spectrum of **4** is displayed together with vertical lines indicating the calculated transition energies and oscillator strengths at the Franck–Condon (FC) point. The calculations were performed at the time-dependent (TD) ωB97X-D3/ZORA-def2-TZVP[14,15] level of theory. As this method was found to overestimate the excitation energy, we scaled the energies by a factor of 0.836. This factor is not universal, but was validated for complex **4** by benchmarking to match the experimental absorption spectrum and XMS-CASPT2[16] benchmark calculations in the Franck–Condon region and beyond (see Figure S5 and tables on pages S14 and S15). From now on, we will refer to this as scaled time-dependent density functional theory (TDDFT), and we used it consistently in all TDDFT calculations on complex **4**. There are nine electronic states in the experimental absorption region between 360 and 240 nm, representing the expected six $n_{Cl}\pi^*$ and the three shifted benzaldehyde states $n_O\pi^*$, $\pi_1\pi^*$, and $\pi_2\pi^*$. The natural transition orbitals (NTOs) characterizing these states require further discussion, and a selection of NTOs is displayed in Figure 2b. The lowest lying singlet state is the S$_1$[NTO$_1$(n_{Cl}) → NTO$_6$(π^*)] state. Due to symmetry, it is a dark state and the NTO$_1$(n_{Cl}) orbital does not contain any contribution from orbitals at the aromatic core. The S$_2$[NTO$_2$(π_1) → NTO$_6$(π^*)] is the bright state that corresponds to the S$_2$($\pi_1\pi^*$) observed in free benzaldehyde. S$_3$ and S$_4$ are nearly degenerate at the FC point. S$_3$ is a bright state characterized as NTO$_3$(n_{Cl}) → NTO$_6$(π^*), with NTO$_3$(n_{Cl}) being a linear combination of chlorine lone pairs and the π_2-orbital of benzaldehyde. S$_4$ is a dark state characterized by a transition from an NTO that is a linear combination of the lone pairs of chlorine (n_{Cl}) and oxygen (n_O). The situation for the nearly degenerate states S$_5$ and S$_6$ is similar. While S$_5$ is a dark state characterized by a transition out of a linear combination of n_{Cl}-orbitals and n_O (NTO$_4$(n_O)), S$_6$ has the largest oscillator strength with an NTO that is a linear combination of n_{Cl}-orbitals and π_2 (NTO$_5$(π_2)). The states S$_7$–S$_9$ all have low oscillator strength. S$_7$ and S$_8$ are of $n_{Cl}\pi^*$ character, and S$_9$ contains contributions from σ-orbitals of the aromatic core.

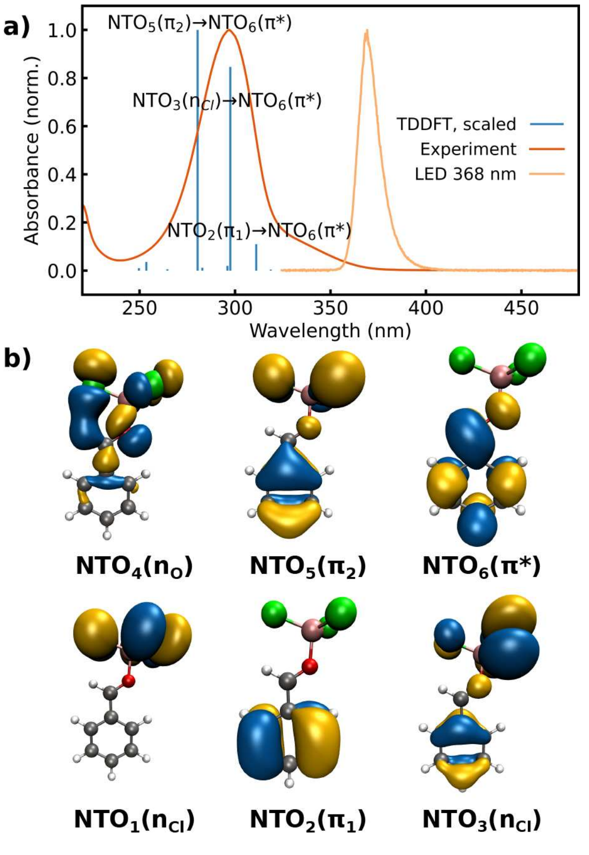

Figure 2. Panel a: UV–vis spectrum of benzaldehyde-BCl$_3$ complex **4** (red), excitation energies (transition wavelengths) and relative oscillator strengths at the FC point (calculated using scaled ωb97x-D3/ZORA-def2-TZVP), and emission spectrum (orange) of the LED used in synthetic and mechanistic studies (vide infra, λ_{max} = 368 nm). For the three brightest states, the natural transition orbitals (NTOs) that characterize these states are indicated. Panel b: NTOs of different excited states in complex **4**. All nine excited states that form the first absorption band are characterized by transitions into the NTO$_6$(π^*) orbital. For the three bright states, S$_2$, S$_3$, and S$_6$, the excitations originate from NTO$_2$(π_1), NTO$_3$(n_{Cl}), and NTO$_5$(π_2), respectively. Excitation from NTO$_1$(n_{Cl}) belongs to the lowest singlet state S$_1$($n_{Cl,1}\pi^*$). NTO$_4$(n_O) has a large contribution from the n_O-orbital of benzaldehyde and forms the adiabatic state S$_5$.

Trajectory Calculations and Mechanism of Dissociation. All nine states contributing to the first absorption band overlap energetically (see Figure S6 in the Supporting Information). Excitation into this broad absorption band might cause nonadiabatic dynamics in a variety of states including additional dark triplet states. The energetic order of the lowest singlet and triplet states is given in the Supporting Information. To elucidate the fate of complex **4** after photoexcitation, we simulated nonadiabatic trajectories at the scaled TDDFT level of theory using the SHARC program.[17] We started sampling trajectories in a spectral window reaching from 0 to 3.85 eV (322 nm), the red shoulder of the absorption spectrum, which is a typical excitation wavelength in photocatalytic applications. The sampling led to a total of 171 trajectories propagated for up to 350 fs and distributed over the states according to their transition dipole moment within the spectral window (for more detailed technical information see the Supporting Information). To our surprise, most of the trajectories led to the dissociation of a chlorine atom (Figure 3).

In all cases, only a single chlorine atom (out of three) dissociates and the mean B–Cl bond distance (shown in Figure 3a) was used to categorize the trajectories into "dissociated" and "not dissociated" based on a cutoff value of 2.15 Å. As the equilibrium B–Cl bond distance is 1.82 Å, this cutoff value roughly corresponds to an elongation of a single B–Cl bond to 2.80 Å. Based on this criterion, 81% of trajectories led to a dissociation. Dissociation occurs over the whole simulation time, although it becomes rarer as the simulation progresses and the most energetic trajectories are already dissociated. Figure 3b

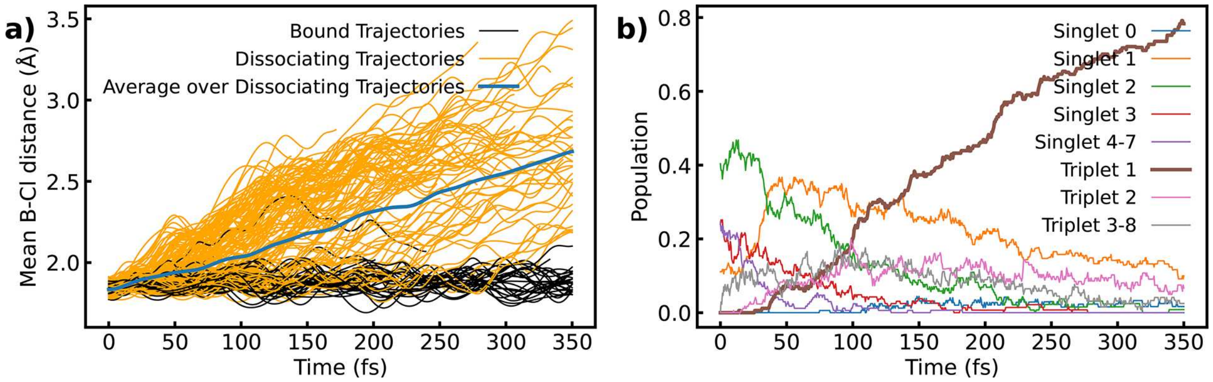

Figure 3. Results of semiclassical nonadiabatic molecular dynamics simulations. Panel a: Mean B−Cl bond distances of dissociating trajectories (orange) and nondissociating trajectories (black) The average bond distance over dissociating trajectories is marked in blue and was only calculated over trajectories that ran for the entire 350 fs simulation. Panel b: Adiabatic state populations.

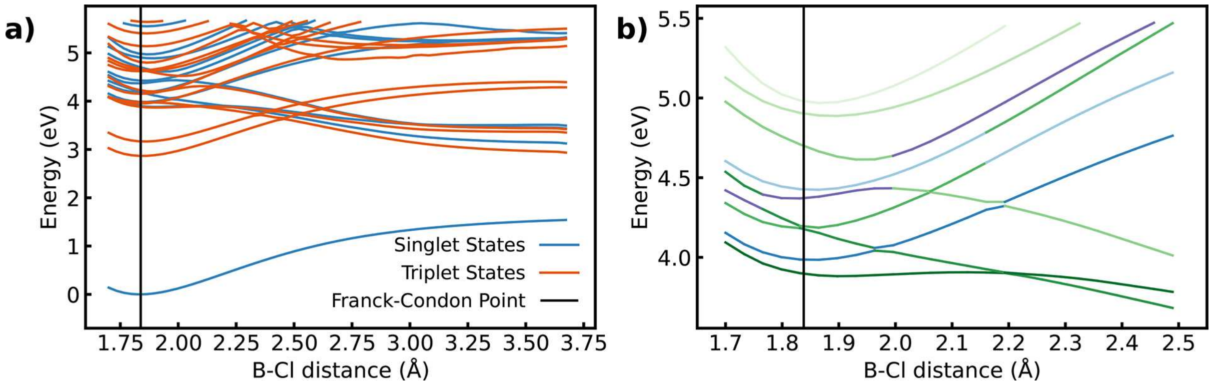

Figure 4. Adiabatic potential energy surfaces of **4** along a ground-state relaxed scan of the B−Cl bond of the chlorine atom in the molecular symmetry plane. The calculations were performed at the scaled TDDFT level of theory. Panel a: Singlet and triplet states. The lowest singlet states show mainly dissociative behavior. The lowest two triplet states are bound in the FC region but after a barrier at 2.50 Å, which is associated with a change from $\pi\pi^*$ to $n\pi^*$ character, become dissociative as well. Panel b: Zoom-in of the FC region, showing the lowest nine excited singlet states forming the first absorption band in the UV spectrum of **4**. The two states with the largest $\pi\pi^*$ contribution are shown in shades of blue, the state with the largest $n_O\pi^*$ contribution is shown in violet, and the other states, which have large contributions from different $n_{Cl}\pi^*$-orbitals, are shown in shades of green.

shows that the initial excitation leads to the population of a multitude of different states, as expected from the broad absorption spectrum featuring many overlapping states. The largest population was found in the bright $S_2(\pi_1\pi^*)$ state. Leaving the FC region, trajectories quickly relax to S_1, leading to a large rise in its population after around 40 fs. Then, population is more slowly transferred from S_1 to T_2 and to T_1. More highly excited states also relax quickly. After 350 fs, most population ends up in the lowest three excited states with 78% in T_1, 10% remaining in S_1, 7% remaining in T_2, and 5% in all other states. Dissociation occurs in all three states.

To explain the dissociation and relate it to the observed population dynamics of the adiabatic states, we performed a relaxed scan in the ground state of complex **4**, and we calculated excitation energies at each point along the scan to obtain the adiabatic potential energy surfaces (PESs). In Figure 4a, the singlet and triplet PESs are shown. The states lying within the experimental absorption band emerge densely packed between 3.8 and 5.2 eV, displaying repulsive and bound-state features and many crossings between states of the same and different multiplicity. Curve crossings between states of bound $\pi\pi^*$- and dissociative $n_{Cl}\pi^*$-character center around 2.1 and 2.5 Å (Figure 4a). Figure 4b highlights the complexity of the situation for the lowest nine excited singlet states. The change in color marks the change in electronic character. The process relevant contributions from the $n_{Cl}\pi^*$-orbitals are shown in shades of green. The two well-separated triplet states $T_1(\pi_2\pi^*)$ and $T_2(\pi_1\pi^*)$ (Figure 4a) may act as trapping states for short bond distances.

Their relatively deep minima visible at 2.9 and 3.2 eV are close to the FC region (for the energy and geometry of the optimized T_1 minimum, see the Supporting Information). Trajectories with fairly low energy crossing into these triplets soon after excitation can become trapped in their minima, which explains the 19% of the trajectories that do not dissociate. All others pass the crossing region at around 2.5 Å, leading to dissociation, which is initiated by six low-lying $n_{Cl}\pi^*$ states (three of the singlet manifold and three of the triplet manifold). They cross with the states of $\pi\pi^*$ character including the bright S_2 state. Upon B−Cl bond elongation, the contributing n_{Cl}-orbitals transform into the three 3p-orbitals of the chlorine radical in accordance with the bond cleavage.

Taken together, the data led us to propose the following dissociation mechanism: Starting from the bright $S_2(\pi_1\pi^*)$ state, the dissociating trajectories can either (1) cross early into $S_1(n_{Cl}\pi^*)$ and dissociate nearly barrierless following the $n_{Cl}\pi^*$ character diabatically or (2) cross a small barrier at 2.0 Å associated with the change in character of S_2 from bound $\pi_1\pi^*$ to dissociative $n_{Cl}\pi^*$. These trajectories will continue to cross into the dissociative part of T_1 at a later point. In summary, the nonadiabatic dynamics predict efficient photoinduced cleavage

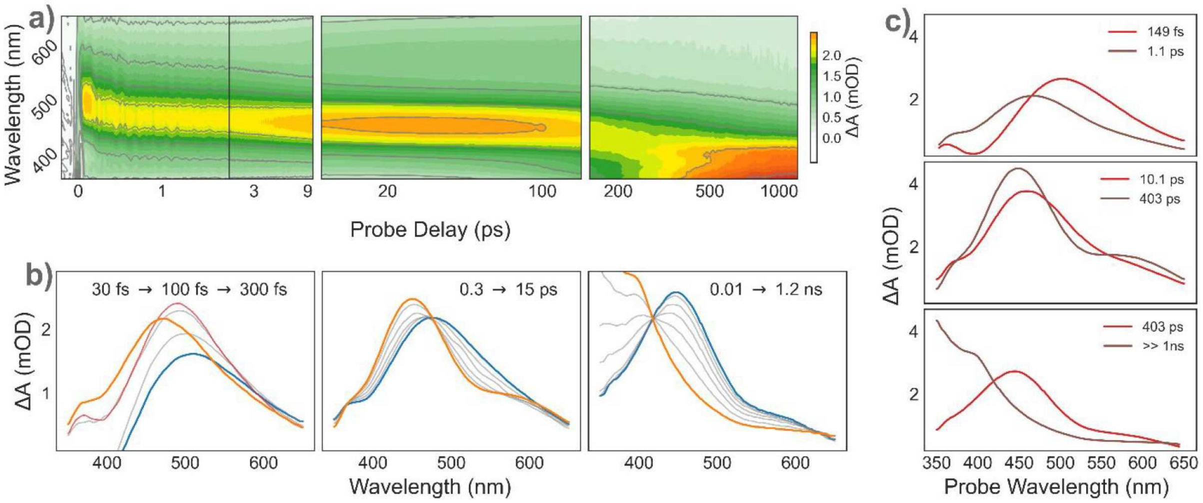

Figure 5. TA data acquired from benzaldehyde-BCl_3 complex **4** in CH_2Cl_2 solution at room temperature. Panel a: 2D representation vs time and detection wavelength of the TA spectra. Data from individual experiments are shown in separate panels. Note the change from linear to logarithmic time scale at 1.8 ps (black vertical line). Panel b: TA spectra at selected probe delays highlight the spectral evolution from early (blue) to late (orange) times at the different time scales. The spectrum at the intermediate time of 100 fs in the left panel is shown in red. Note the isosbestic points, suggesting state-to-state transitions at vastly differing time scales. Panel c: Evolution-associated spectra extracted from global kinetic fits to the data. Component lifetimes are denoted in the figure labels. See the narrative for details.

of **4** into a chlorine radical and the borylated ketyl radical **5** on a time scale of a few 100 fs. The bond cleavage is induced due to the prominent participation of the n_{Cl} lone pairs in the excited electronic wave functions. To provide data for direct comparison with transient absorption experiments, we calculated the absorption spectra for the borylated ketyl radical (**5**) and cation (**6**) using XMS-CASPT2[16,18] (see the Supporting Information for details).

Time-Resolved Optical Properties and Photoinduced Dynamics. The computational work in the preceding section provided detailed predictions about the cascade of relaxation processes taking place within the benzaldehyde-BCl_3 complex (**4**) after absorption of a UV photon. Moreover, these predictions were associated with accessible experimental observables in the form of calculated optical spectra. As such, it was conceptually straightforward to validate the computational predictions by direct comparison to experiment, and we thus undertook a time-domain observation of the photochemical processes triggered by UV photoexcitation of complex **4**. To achieve a detailed picture of these ultrafast dynamics, we made use of ultrafast transient absorption (TA) spectroscopy, where interaction with an excitation ("pump") pulse generates an excited-state wave packet, the fate of which can subsequently be followed by monitoring the time evolution of the probe transmission spectrum. Despite the inherent challenges in generating short pulses in the UV spectral range, this strategy has been proved highly valuable in elucidating light-induced dynamics in complex molecular systems.[9,19] To initiate excited-state dynamics, we used 20 fs pulses with a central wavelength of 275 nm, while the pump-induced changes in optical absorption of the sample were interrogated using a white-light supercontinuum pulse with a spectrum spanning ∼350−725 nm. The total experimental TA data are collected in Figure 5a. Two general observations can be made immediately: (1) As both the excitation pulse and the lowest energy ($S_0 \rightarrow S_1$) transition fall outside the range of the probe spectrum, we observe predominantly excited-state absorption (ESA) signals, and (2) the induced dynamics occur on time scales covering several orders of magnitude. To reach sufficient fidelity at all scales, it was thus necessary to perform three individual experiments, each targeting a subsection of the total time range. In Figure 5a, these results are shown in separate panels for clarity.

A qualitative overview over the dynamics can be gained from the two-dimensional spectra plotted vs detection wavelength and probe delay in Figure 5a and the extracted TA spectra in Figure 5b: Immediately after excitation, we observed predominantly a broad ESA feature around 500 nm, in addition to negative-amplitude signals in the near-UV range associated with the so-called coherent artifact.[20] Within 200 fs, these negative-amplitude signals disappear, and the ESA feature shifts noticeably toward the blue, now being centered at approximately 460 nm. Subsequent to this initial ultrafast relaxation, the excited dynamics take place over two distinct time scales: from approximately 300 fs to 15 ps and from a few tens of picoseconds to nanoseconds.

In the range from approximately 300 fs to 15 ps (central panels of Figure 5a,b) two effects dominate the spectral dynamics: a further blue-shift of the ESA maximum to 440 nm and an overall narrowing of the spectral profile. As a result of this narrowing, a band associated with one or more ESA transitions becomes clearly distinguishable near 600 nm. The appearance of a clean isosbestic point at 480 nm suggests that the underlying dynamics are a transition between two distinct states, with no substantial, if any, contributions from competing decay pathways. In particular, both the few picosecond time scale of this process and the characteristic change in spectral shape from a broad, red-shifted feature toward a more well-defined shape in the blue are typical of vibrational cooling processes.[21] This suggests that the initial ultrafast dynamics leave the system in a vibrationally "hot" electronic state, the excess energy of which dissipates to leave a "cool" product state well before further relaxation processes can take place. In the time interval subsequent to these femto- to picosecond processes, further substantial spectral changes take place. In particular, the spectrum of the "cooled" product state disappears concomitantly with the appearance of an intense absorption band in the UV. Again, we observe a clear isosbestic point, implying the existence of another state-to-state transfer process with insignificant losses or other competing relaxation pathways.

Kinetic Analysis and Comparison with Theory. Quantitative characterization of the photoinduced dynamics in complex **4** requires careful analysis. Here we analyze the dynamics in the standard framework of singular-value decomposition followed by global kinetic fitting to a sum-of-exponential-decays model. The observed kinetics can then be imposed on a particular relaxation model to determine a full relaxation scheme. The transient absorption signals reported in Figure 5b show two clear isosbestic points, suggesting a simple sequential deactivation scheme (A → B → C ...) as a natural starting point for kinetic analysis. This commonly implemented scheme is advantageous in that it contains the exact same number of transfer processes as observable time constants, and thus it allows detailed analysis of the spectral dynamics by extraction of the optical spectra of the individual compartments. These spectra are commonly referred to as evolutionary associated (decay) spectra (EAS).[22] In many practical cases, this simple model is a good approximation to the actual excited-state dynamics of the physical system, in which case the "compartments" correspond to the electronic (or vibrational) states of the system, and the EAS are the spectra of these states. The results of our global kinetic analysis are summarized in Figure 5c. The quantitative fit corroborates our qualitative analysis: the initially observed transition, with a time constant of ~150 fs, occurs from a state absorbing at approximately 500 nm to a state assigned to vibrationally hot radical **5** with an absorption maximum at 460 nm. This is followed by a further slight blue-shift and spectral narrowing with time constants of ~1 and 10 ps, respectively, before a final transfer process into a UV-absorbing state takes place with a time constant of ~400 ps. The phenomenological kinetic model extracted from the experimental kinetics can be compared directly with the predictions from theory (for the calculation of ESA, see the Supporting Information). We show this comparison in Figure 6. In the top panel we observe that the experimental TA spectrum extracted at 15 ps pump−probe delay is in good qualitative agreement with the spectrum calculated for the borylated ketyl radical **5** (Scheme 2). This is consistent with our expectation, in that the radical was predicted to form on ultrafast time scales and that its subsequent decay takes place on much longer time scales. The calculated radical spectrum in the top panel of Figure 6 was calculated at the XMS-CASPT2/cc-pvtz level. Only contributions from the transitions $D_1 \rightarrow D_2$ and $D_1 \rightarrow D_3$ are shown. When including the $D_1 \rightarrow D_4$ transition (dashed line in Figure 6, top panel), a rise in absorption occurs in the blue region that is not observed in the experiment. We attribute this to spuriously large perturbative corrections in the treatment of the D_4 state shifting the $D_1 \rightarrow D_4$ transition to the red. This is confirmed by calculations at the bt-PNO-STEOM-CCSD/def2-SVP[23] level (see the Supporting Information), where the transition appears at much shorter wavelengths.

At longer time scales, TDDFT with a continuum solvation model predicts the pair of the benzaldehyde-BCl_2 cation and the chloride anion to be 113.5 kJ mol^{-1} more stable than the radical pair. It should therefore form by electron transfer via a Marcus-like mechanism.[9] The predicted spectrum of the benzaldehyde-BCl_2 cation features intense absorption bands predominantly in the UV spectral range. This is in good qualitative agreement with the experimental observation of UV absorption and near-negligible absorbance in the visible range at nanosecond pump−probe delays (Figure 6, bottom panel).

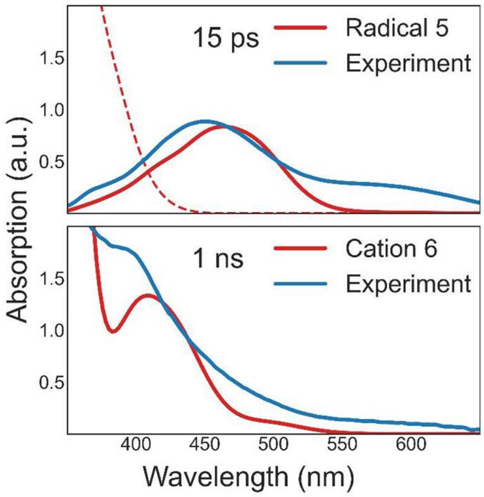

Figure 6. Comparison between calculated (red) and experimentally observed (blue) spectra. Top panel: calculated absorption spectrum of the borylated ketyl radical **5** and the experimental TA spectrum at 15 ps probe delay. The calculated spectrum for the radical only includes the $D_1 \rightarrow D_2$ and $D_1 \rightarrow D_3$ transitions. Including the $D_1 \rightarrow D_4$ transition (dashed line) leads to a rise in the UV that is discussed in the main text. Bottom panel: calculated spectrum of the benzaldehyde-BCl_2 cation **6** compared to the experimental TA spectrum at 1 ns probe delay.

Addition Reaction of Hydrocarbons to Aromatic Aldehydes. With theory and transient absorption spectroscopy suggesting a homolytic B−Cl bond cleavage of complex **4**, it was attempted in synthetic studies to employ the putative chlorine radical for a hydrogen atom transfer (HAT) from an alkane H−R.[24] It was hypothesized that HAT would result in the formation of a carbon-centered radical, which would subsequently undergo C−C bond formation at the carbonyl carbon atom of the aldehyde (Scheme 3, top). The bond dissociation energy (BDE) of HCl is sufficiently high (BDE = 431 kJ mol^{-1})[25] to render this process exothermic. Initially, cyclohexane (BDE = 416 kJ mol^{-1},[26] 20 equiv) was employed as the hydrocarbon that was irradiated together with benzaldehyde (**7a**) and BCl_3 (1.5 equiv) at λ = 300 nm in dichloromethane solution. The reaction was complete after 15 min, and a new product was isolated, which was identified as chloride **8** (Scheme 3, bottom).

Scheme 3. Mechanistic Hypothesis for a Potential C−C Bond Formation (cf. Scheme 2) with a Hydrocarbon H−R and Preliminary Experiment on the UV-Mediated Reaction of Cyclohexane with Benzaldehyde in the Presence of Boron Trichloride

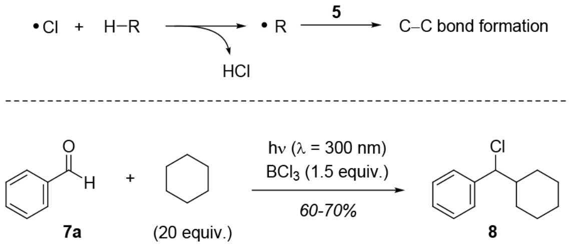

The yields of the reaction were variable, and the isolation of the nonpolar product **8** from minor by-products was difficult.

There were indications that chloride **8** was formed from the respective alcohol by a thermal nucleophilic substitution reaction (vide infra). To support the assumption that the HCl developing in the HAT process was responsible for the formation of the chloride, the reaction was studied in the presence of a base. In addition, we employed for the optimization experiments an irradiation at longer wavelength (λ = 368 nm, cf. Figure 2a), which was found to also trigger the desired transformation. Gratifyingly, the addition of potassium phosphate (Table 1, entry 1) led to a suppression of the consecutive reaction, and alcohol **9a** was isolated in 53% yield.

Table 1. Optimization of the Reaction Conditions for the Light-Mediated Addition of Cyclohexane to Benzaldehyde in the Presence of Boron Trichloride

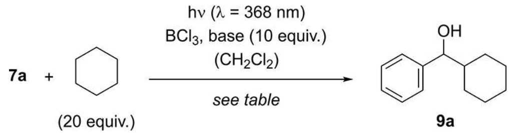

entry[a]	equiv BCl_3	base	T [°C]	t[b] [min]	c [mM]	yield[c] [%]
1	1.5	K_3PO_4	r.t.	2.5	20	53
2	1.0	K_3PO_4	r.t.	10	20	51
3	0.5	K_3PO_4	r.t.	30	20	28
4	1.5	K_2CO_3	r.t.	2.5	20	45
5	1.5	Cs_2CO_3	r.t.	10	20	41
6	1.5	K_3PO_4	r.t.	2.5	40	51
7	1.5	KH_2PO_4	r.t.	5	40	40
8	1.5	K_3PO_4	−78	90	40	53
9	1.5	K_3PO_4	−40	15	40	65
10	1.5	K_3PO_4	−10	10	40	67
11	1.5	K_3PO_4	0	10	40	65

[a]A degassed solution of benzaldehyde (1.0 equiv), cyclohexane (20 equiv), boron trichloride, and base was irradiated by an LED with an emission maximum at λ = 368 nm (see the Supporting Information for details). [b]The reaction was stopped once the reaction was complete based on TLC analysis. [c]Yield of isolated product after column chromatography.

The reaction was complete in 150 s (2.5 min). A decrease of the Lewis acid concentration led to longer reaction times (entries 2, 3) and a lower yield. Other bases were less efficient as acid scavengers (entries 4, 5, 7) compared to potassium phosphate. The influence of the substrate concentration was minimal (entry 6). Given that a lower amount of solvent facilitated the degassing procedure and allowed a more efficient stirring of the reaction mixture, the experiments at lower temperature were performed at c = 40 mM (entries 8−11). At −78 °C, the reaction rate decreased notably, and full conversion was achieved only after 90 min (entry 8). The situation improved at −40 °C (entry 9) and was best at −10 °C (entry 10). For practical reasons (ice bath), we also checked whether 0 °C was a suitable temperature, which turned out to be the case, and the conditions of entry 11 emerged as being optimal. Several modifications that are not listed in Table 1 did not lead to an improvement of the reaction yields (see the Supporting Information for details). Most notably, the use of other Lewis acids such as BBr_3 and $AlBr_3$ resulted in traces of product or no conversion, respectively. The scope of the reaction was first evaluated with regard to the aromatic aldehydes **7** (Scheme 4).

Tolerance toward functional groups such as chlorine (products **9b**, **9d**, **9e**), fluorine (products **9i**, **9j**), and trifluoromethyl (product **9k**) was established. The position of the chlorine substituent (*ortho*, *meta*, or *para*) had no influence on the reaction yield. The same observation was made for the methyl group (products **9c**, **9f**, **9g**), which was remarkably tolerated even in *ortho* position to the formyl group. Typically, *ortho*-methylbenzaldehydes undergo an intramolecular hydrogen abstraction to an *ortho*-quinodimethane intermediate.[27] This reaction was completely suppressed by the Lewis acid, confirming the absence of typical benzaldehyde reactivity emanating from the nπ* triplet state. Other alkyl substituents like *tert*-butyl were well-tolerated (product **9h**). It was attempted to employ nonaromatic aldehydes in the reaction, but neither cinnamic aldehyde nor pivalaldehyde delivered the expected alcohols, even if the irradiation wavelength was altered.

Apart from cyclohexane, other alicyclic hydrocarbons such as cyclopentane (product **9l**) and cycloheptane (product **9m**) were successfully employed in the reaction. Adamantane gave a mixture of two regioisomeric products, the main isomer (product **9n**) of which was shown to display a quaternary carbon atom at the newly formed C−C junction. In a similar fashion, propane reacted preferably at the more highly substituted carbon atom, delivering mainly isopropyl ketone **9o**. Even light, short chain alkanes such as ethane could be

Scheme 4. Light-Mediated Addition of Hydrocarbons (H−R) to Aromatic Aldehydes 7 in the Presence of Boron Trichloride: Formation of Secondary Alcohols 9

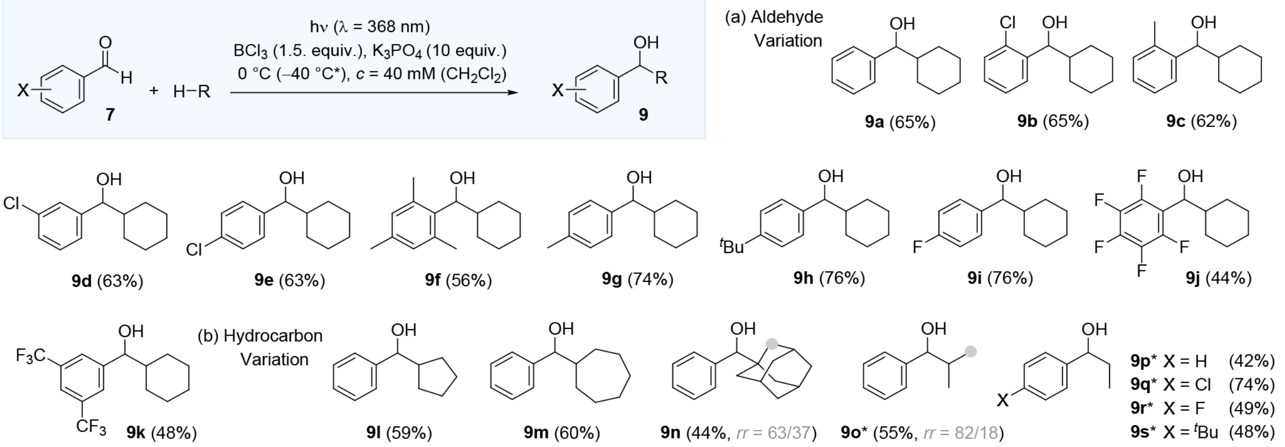

involved in the BCl_3-mediated hydroalkylation reaction. Like for ketone **9o**, ethyl ketones **9p**−**9s** were obtained by irradiating a saturated solution of the hydrocarbon in CH_2Cl_2 at −40 °C instead of 0 °C. The other parameters remained unchanged compared to the optimized conditions. The reactions are amenable to scale-up, which was shown by performing the transformation **7a** (X = H) → **9a** on a scale of 1.0 mmol. The desired product was obtained in 61% yield (117 mg).

Mechanistic Studies and Calculations on the Reaction Pathway. Mechanistic studies were undertaken to elucidate the individual steps responsible for the formation of products **8** and **9**. In a first set of experiments, alcohol **9a** was subjected to typical Lewis acid conditions in the absence of base and light (1.5 equiv of BCl_3 in CH_2Cl_2 at ambient temperature). The reaction occurred smoothly and showed the features of an S_N1-type substitution; that is, a racemization of an enantioenriched alcohol was observed (see the Supporting Information for details). It is therefore reasonable to assume that alcohols **9** or their borylated analogues are the primary products of the reaction and chloride **8** is a consecutive product of **9a**. Similar observations were made by Kabalka et al., who studied the formation of secondary alcohols by addition of alkylboron chlorides to aromatic aldehydes.[28] In the absence of base, they also observed the formation of the respective benzylic chlorides, which likely derived from the primary C−C addition products.

Experiments with deuterated starting materials revealed that deuterium labeling was completely retained and no scrambling occurred (Scheme 5).

Scheme 5. Deuteration Experiments Performed with Fully Deuterated Cyclohexane-d_{12} (Top) and with Monodeuterated Benzaldehyde (7a-d_1, Bottom)

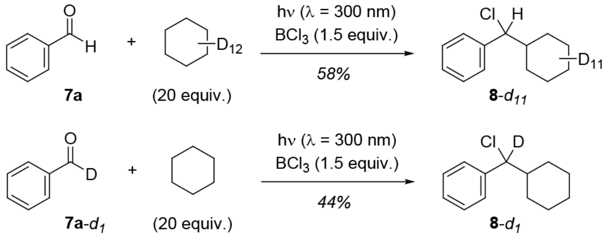

The reaction with cyclohexane-d_{12} delivered exclusively product **8**-d_{11} with no deuterium incorporated at the former benzaldehyde fragment. Vice versa, the monodeuterated benzaldehyde **7a**-d_1 delivered product **8a**-d_1 with exclusive deuterium incorporation at the alcohol carbon atom. In intermolecular competition experiments between nondeuterated cyclohexane (10 equiv) and cyclohexane-d_{12} (10 equiv), products **8** and **8**-d_{11} were isolated in equal amounts (see the Supporting Information for details), suggesting no significant kinetic isotope effect (KIE).[29] This is in line with previous work that found only marginal KIEs of approximately 1.1 for the H/D abstraction by a chlorine radical from cyclohexane.[30]

Quantum yield measurements revealed that the reaction rate was not constant during the reaction but decreased over time (see the Supporting Information for details). We determined the quantum yield at the beginning of the reaction **7a** → **8** by calculating the numerical quotient of benzaldehyde conversion over photon absorption ($\lambda = 368$ nm). An average value for the quantum yield Φ was obtained from three individual runs resulting in $\Phi = 1.04$ (±0.06). The reaction rate increased if the concentration of cyclohexane was increased. Substrate conversion scaled linearly with light intensity. The nonlinear behavior of the quantum yield was corroborated by monitoring the conversion in a light on−light off experiment at $\lambda = 368$ nm (Figure 7).

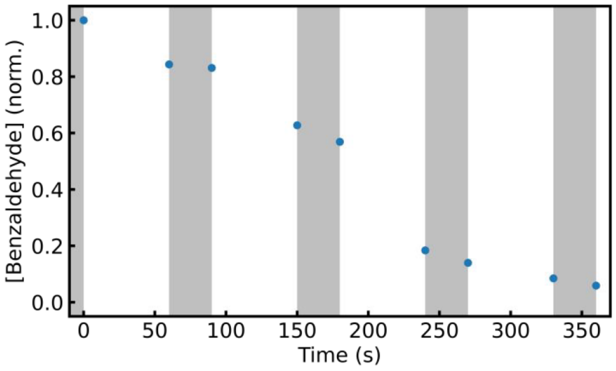

Figure 7. Kinetic profile of the reaction **7a** → **8** under conditions of UV irradiation (cf. Scheme 3: $\lambda = 368$ nm, CH_2Cl_2, 1.5 equiv of BCl_3, 50 equiv of cyclohexane) depicted as a concentration decrease of **7a**. The light beam of the LED was blocked in the gray time intervals.

The reaction progressed even in time periods in which there was no exposure to light (gray bars). Together with the fact that the quantum yield exceeds unity and the cyclohexane concentration leverages the reaction rate, the result suggests that a radical chain process is involved in product formation. A mechanistic scenario often invoked for VLIH involves a chlorine radical that abstracts a hydrogen atom from a hydrocarbon with the resulting radical then entering a closed catalytic cycle. The BCl_3-mediated alkylation occurs—at least partially—along a different reaction channel that leads to the formation of more than one product molecule per absorbed photon. While a recombination of the cyclohexyl radical with borylated ketyl radical **5** is feasible (cf. Scheme 3), a second reaction pathway appears to be competitive, which is responsible for the relatively high quantum yield. We suggest this process to be a radical chain that is mediated by the chlorine radical and that involves addition of the cyclohexyl radical to the benzaldehyde-BCl_3 complex (**4**). The addition is expected to occur at the carbonyl carbon atom, leading to putative intermediate **10**, from which a chlorine atom can dissociate and enter the radical chain (Scheme 6). The chain process can be terminated through radical−radical recombination, e.g., by a productive reaction of a cyclohexyl radical with borylated ketyl radical **5**.

Despite the fact that the addition of a nucleophilic cyclohexyl radical at the electrophilic carbon atom of **4** makes sense, it was not clear whether the proposed bond formation would be favorable, given that intermediate **10** displays a phenyl radical cation. To shed light on this issue, calculations were performed at the unrestricted DLPNO-CCSD(T)[31]/CBS(3/4,cc)//ωb97x-D3/def2-TZVP level of theory. It was found that the addition reaction is indeed feasible via a low-lying transition state **TS1** (Figure 8).

The postulated intermediate **10** was identified as an energy minimum on the reaction hypersurface (**Min2**), lying 17.4 kJ mol^{-1} below the energy of a complex **Min1** of the two starting components (cyclohexyl radical and **4**). Remarkably, the calculations also corroborated the subsequent step, i.e., the dissociation of the chlorine radical. This reaction proceeds again via a readily accessible transition state in which one B−Cl bond

Scheme 6. Mechanistic Pathway for a Potential Radical Chain by Addition of a Cyclohexyl Radical to the Benzaldehyde-BCl_3 Complex (4) and Subsequent Homolytic Cleavage of the B−Cl Bond within Intermediate 10

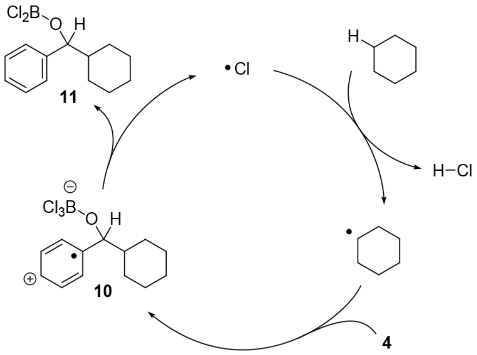

is elongated so that the chlorine atom eventually ends up as a π-complex (**Min3**) with the arene part of intermediate **11**. Although the ensuing reaction pathway was not further analyzed, it is reasonable to assume that the chlorine atom is available for another HAT so that the radical chain is continued. The results of the synthetic study thus correlate well with the predictions made by theory and with the experimental results obtained by transient absorption spectroscopy. They serve to substantiate the existence of the borylated ketyl radical **5** as a key intermediate in this chemistry, and the calculations support the existence of a radical chain as a reaction channel competing with a radical−radical recombination.

It was probed in some preliminary experiments whether there is synthetic evidence for cation **6** as the product of a consecutive electron transfer from radical **5** (Scheme 2). Trapping was attempted by using benzene as a potential nucleophile which would not be amenable to a premature HAT (BDE = 472 kJ mol^{-1}).[26] In the absence of light, the components did not show formation of a product that resulted from aromatic substitution at the benzene core. Upon irradiation, a sluggish conversion was observed and benzhydryl chloride (1,1-diphenylchloromethane) was detectable in low quantities by GLC-MS. However, the product could not be isolated, and the yield was very low, which may be due to the low reactivity of the two components and/or a rapid recombination of cation **6** with the chloride anion to complex **4**.

■ CONCLUSION

We have used a combination of nonadiabatic dynamics simulations and femtosecond transient absorption spectroscopy to elucidate the key process occurring upon irradiation of the complex between an aromatic aldehyde and BCl_3. Rather than activating the aldehyde for a photochemical transformation, the Lewis acid is activated by the aldehyde toward a photoinduced homolytic bond cleavage. The borylated ketyl radical **5** was identified by both experiment and theory as the main intermediate of this process. It is conceivable that related processes are also responsible for homolytic bond cleavage reactions involving Lewis acid−base complexes of other Lewis acids such as $TiCl_4$.[4b,32] A hydroalkylation of aromatic aldehydes was achieved, which was shown to involve a radical chain process. The key step is similar to the observed homolytic M−Cl cleavage occurring in transition metal complexes by ligand-to-metal charge transfer (LMCT) that has been exploited to unlock photochemical HAT-mediated transformations through the generation of a chlorine radical. In our case, no redox-active transition metal is required. Instead, an electron is directly transferred from the bound chlorine atom into the aromatic π-system of the substrate, thereby weakening the B−Cl bond. This Lewis acid−base activation mode may prove to be valuable for future applications that involve the cleavage of other bonds between boron and a given heteroatom.

■ ASSOCIATED CONTENT

SI Supporting Information

The Supporting Information is available free of charge at https://pubs.acs.org/doi/10.1021/jacs.2c06683.

Detailed information on experimental setups, light sources, procedures, and analytical data; characterization data including NMR spectra for new compounds; applied computational methods, calculated orbitals, and energies; further mechanistic studies (PDF)

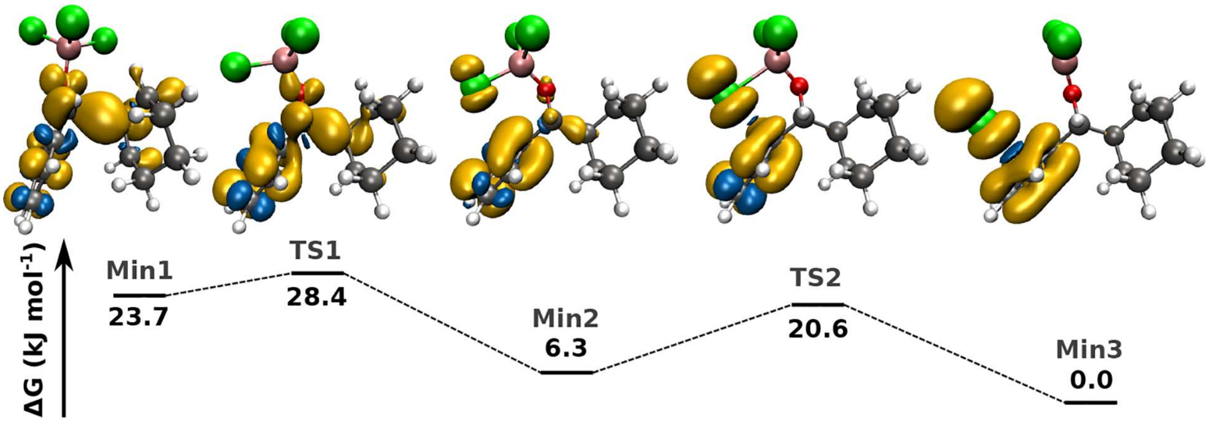

Figure 8. Attack of the cyclohexyl radical on the benzaldehyde-BCl_3 complex (**4**). On the top, structures of critical points along the reaction coordinate are displayed with the alpha spin density in yellow and the beta spin density in blue (isovalue = 0.002). At the bottom the relative Gibbs free energies of these structures are indicated. The structures were optimized at the unrestricted ωb97x-D3/def2-TZVP+CPCM (CH_2Cl_2) level of theory, and spin densities and entropic corrections were evaluated at the optimized points. The electronic contribution to the free energy was refined at the unrestricted DLPNO-CCSD(T)/CBS(3/4,cc) level. An intermediate **Min2** was identified that corresponds to structure **10** in Scheme 6. The free chlorine radical resides on the aromatic π-system (**Min3**) before being released as a free chlorine radical.

NMR data: Primary NMR data of new compounds, including FID files and acquisition data (ZIP)

Geometries and energies: Optimized geometries of the molecules in the computational study as an XYZ file; energies and geometries for the scan presented in Figure 4 as a CSV and XYZ file, respectively (ZIP)

AUTHOR INFORMATION

Corresponding Authors

Jürgen Hauer — *Department Chemie and Catalysis Research Center (CRC) School of Natural Sciences, Technische Universität München, D-85747 Garching, Germany;* orcid.org/0000-0002-6874-6138;
Email: juergen.hauer@tum.de

Regina de Vivie-Riedle — *Department of Chemistry, Ludwig-Maximilians-Universität München, D-81377 München, Germany;* orcid.org/0000-0002-7877-5979;
Email: regina.de_vivie@cup.uni-muenchen.de

Thorsten Bach — *Department Chemie and Catalysis Research Center (CRC) School of Natural Sciences, Technische Universität München, D-85747 Garching, Germany;* orcid.org/0000-0002-1342-0202;
Email: thorsten.bach@ch.tum.de

Authors

Daniel P. Schwinger — *Department Chemie and Catalysis Research Center (CRC) School of Natural Sciences, Technische Universität München, D-85747 Garching, Germany;* orcid.org/0000-0002-3144-462X

Martin T. Peschel — *Department of Chemistry, Ludwig-Maximilians-Universität München, D-81377 München, Germany*

Thomas Rigotti — *Department Chemie and Catalysis Research Center (CRC) School of Natural Sciences, Technische Universität München, D-85747 Garching, Germany*

Piotr Kabaciński — *IFN-CNR and Dipartimento di Fisica, Politecnico di Milano, I-20133 Milano, Italy;* orcid.org/0000-0003-4591-5100

Thomas Knoll — *Department of Chemistry, Ludwig-Maximilians-Universität München, D-81377 München, Germany;* orcid.org/0000-0002-8509-571X

Erling Thyrhaug — *Department Chemie and Catalysis Research Center (CRC) School of Natural Sciences, Technische Universität München, D-85747 Garching, Germany*

Giulio Cerullo — *IFN-CNR and Dipartimento di Fisica, Politecnico di Milano, I-20133 Milano, Italy;* orcid.org/0000-0002-9534-2702

Complete contact information is available at:
https://pubs.acs.org/10.1021/jacs.2c06683

Author Contributions

[#]D.P.S., M.T.P., and T.R. contributed equally. The manuscript was written through contributions by all authors.

Notes

The authors declare no competing financial interest.

ACKNOWLEDGMENTS

Financial support by the Deutsche Forschungsgemeinschaft (DFG, German Research Foundation), TRR 325 (projects B1, B8, C5) and 444632635, is gratefully acknowledged. D.P.S. thanks the Studienstiftung des Deutschen Volkes for a Ph.D. fellowship, J. Kudermann (TUM) for help with GC analyses, and S. Breitenlechner (TUM) for fruitful discussions regarding the mechanism.

REFERENCES

(1) (a) *Lewis Acids in Organic Synthesis*; Yamamoto, H., Ed.; Wiley-VCH: Weinheim, 2000. (b) *Lewis Acids and Selectivity in Organic Synthesis*; Santelli, M.; Pons, J.-M., Eds.; CRC Press: Boca Raton, 1996.

(2) (a) *Chiral Lewis Acids in Organic Synthesis*; Mlynarski, J., Ed.; Wiley-VCH: Weinheim, 2017. (b) Sha, Q.; Deng, Y.; Doyle, M. P. The Future of Catalysis by Chiral Lewis Acids. *Top. Organomet. Chem.* **2015**, *62*, 1−26.

(3) Recent reviews: (a) Genzink, M. J.; Kidd, J. B.; Swords, W. B.; Yoon, T. P. Chiral Photocatalyst Structures in Asymmetric Photochemical Synthesis. *Chem. Rev.* **2022**, *122*, 1654−1716. (b) Prentice, C.; Morrisson, J.; Smith, A. D.; Zysman-Colman, E. Recent developments in enantioselective photocatalysis. *Beilstein J. Org. Chem.* **2020**, *16*, 2363−2441. (c) Schwinger, D. P.; Bach, T. Chiral 1,3,2-Oxazaborolidine Catalysts for Enantioselective Photochemical Reactions. *Acc. Chem. Res.* **2020**, *53*, 1933−1943. (d) Silvi, M.; Melchiorre, P. Enhancing the potential of enantioselective organocatalysis with light. *Nature* **2018**, *554*, 41−49.

(4) For pioneering studies, see: (a) Griffiths, J.; Hart, H. A new general photochemical reaction of 2,4-cyclohexadienones. *J. Am. Chem. Soc.* **1968**, *90*, 5296−5298. (b) Sato, T.; Yoshiie, S.; Imamura, T.; Hasegawa, K.; Miyahara, M.; Yamamura, S.; Ito, O. Metal-catalyzed Organic Photoreactions. Photoreactions of Compounds Containing a Carbon-oxygen or Carbon-nitrogen Multiple Bond with Alcohols in the Presence of Titanium(IV) Chloride or Uranyl Chloride. *Bull. Chem. Soc. Jpn.* **1977**, *50*, 2714−2730. (c) Lewis, F. D.; Howard, D. K.; Oxman, J. D. Lewis acid catalysis of coumarin photodimerization. *J. Am. Chem. Soc.* **1983**, *105*, 3344−3345. (d) Lewis, F. D.; Barancyk, S. V.; Burch, E. L. Conformations, Spectroscopy, and Photochemistry of Methyl Phenanthrene-9-carboxylate, Phenanthrene-9-carboxamides, and Their Lewis Acid Complexes. *J. Am. Chem. Soc.* **1992**, *114*, 3866−3870. (e) Fukuzumi, S.; Okamoto, T.; Otera, J. Addition of Organosilanes with Aromatic Carbonyl Compounds via Photoinduced Electron Transfer in the Presence of Magnesium Perchlorate. *J. Am. Chem. Soc.* **1994**, *116*, 5503−5504. (f) Ischay, M. A.; Anzovino, M. E.; Du, J.; Yoon, T. P. Efficient Visible Light Photocatalysis of [2 + 2] Enone Cycloadditions. *J. Am. Chem. Soc.* **2008**, *130*, 12886−12887.

(5) Stegbauer, S.; Jeremias, N.; Jandl, C.; Bach, T. Reversal of reaction type selectivity by Lewis acid coordination: the *ortho* photocycloaddition of 1- and 2-naphthaldehyde. *Chem. Sci.* **2019**, *10*, 8566−8570.

(6) For reviews on the *ortho* photocycloaddition reaction, see: (a) Remy, R.; Bochet, C. Arene-Alkene Cycloaddition. *Chem. Rev.* **2016**, *116*, 9816−9849. (b) Hoffmann, N. Photochemical reactions of aromatic compounds and the concept of the photon as a traceless reagent. *Photochem. Photobiol. Sci.* **2012**, *11*, 1613−1641. (c) Wagner, P. J. Photoinduced Ortho [2 + 2] Cycloaddition of Double Bonds to Triplet Benzenes. *Acc. Chem. Res.* **2001**, *34*, 1−17.

(7) Mayr, H.; Gorath, G. Kinetics of the Reactions of Carboxonium Ions and Aldehyde Boron Trihalide Complexes with Alkenes and Allylsilanes. *J. Am. Chem. Soc.* **1995**, *117*, 7862−7868.

(8) Peschel, M. T.; Kabaciński, P.; Schwinger, D. P.; Thyrhaug, E.; Cerullo, G.; Bach, T.; Hauer, J.; de Vivie-Riedle, R. Activation of 2-Cyclohexenone by BF_3 Coordination: Mechanistic Insights from Theory and Experiment. *Angew. Chem., Int. Ed.* **2021**, *60*, 10155−10163.

(9) Sailer, C. F.; Thallmair, S.; Fingerhut, B. P.; Nolte, C.; Ammer, J.; Mayr, H.; Pugliesi, I.; de Vivie-Riedle, R.; Riedle, E. A Comprehensive Microscopic Picture of the Benzhydryl Radical and Cation Photogeneration and Interconversion through Electron Transfer. *ChemPhysChem* **2013**, *14*, 1423−1437.

(10) Recent review: Abderrazak, Y.; Bhattacharyya, A.; Reiser, O. Visible-Light-Induced Homolysis of Earth-Abundant Metal-Substrate Complexes: A Complementary Activation Strategy in Photoredox Catalysis. *Angew. Chem., Int. Ed.* **2021**, *60*, 21100−21115.

(11) For selected contributions, see: (a) Kochi, J. K. Photolyses of Metal Compounds: Cupric Chloride in Organic Media. *J. Am. Chem. Soc.* **1962**, *84*, 2121−2127. (b) Shields, B. J.; Doyle, A. G. Direct C(sp^3)-H Cross Coupling Enabled by Catalytic Generation of Chlorine Radicals. *J. Am. Chem. Soc.* **2016**, *138*, 12719−12722. (c) Ackerman, L. K. G.; Martinez Alvarado, J. I.; Doyle, A. G. Direct C-C Bond Formation from Alkanes Using Ni-Photoredox Catalysis. *J. Am. Chem. Soc.* **2018**, *140*, 14059−14063. (d) Hu, A.; Guo, J.-J.; Pan, H.; Zuo, Z. Selective functionalization of methane, ethane, and higher alkanes by cerium photocatalysis. *Science* **2018**, *361*, 668−672. (e) Treacy, S. M.; Rovis, T. Copper Catalyzed C(sp^3)-H Bond Alkylation via Photoinduced Ligand-to-Metal Charge Transfer. *J. Am. Chem. Soc.* **2021**, *143*, 2729−2735. (f) Kang, Y. C.; Treacy, S. M.; Rovis, T. Iron-Catalyzed Photoinduced LMCT: A 1° C-H Abstraction Enables Skeletal Rearrangements and C(sp^3)-H Alkylation. *ACS Catal.* **2021**, *11*, 7442−7449. (g) Jin, Y.; Zhang, Q.; Wang, L.; Wang, X.; Meng, C.; Duan, C. Convenient C(sp^3)-H Bond Functionalisation of Light Alkanes and other Compounds by Iron Photocatalysis. *Green Chem.* **2021**, *23*, 6984−6989. (h) Yang, Q.; Wang, Y.-H.; Qiao, Y.; Gau, M.; Carroll, P. J.; Walsh, P. J.; Schelter, E. J. Photocatalytic C-H Activation and the Subtle Role of Chlorine Radical Complexation in Reactivity. *Science* **2021**, *372*, 847−852.

(12) (a) Silva, C. R.; Reilly, J. P. Theoretical Calculations on Excited Electronic States of Benzaldehyde and Observation of the S2←S0 Jet-Cooled Spectrum. *J. Phys. Chem.* **1996**, *100*, 17111−17123. (b) Molina, V.; Merchán, M. Theoretical Analysis of the Electronic Spectra of Benzaldehyde. *J. Phys. Chem. A* **2001**, *15*, 3745−3751. (c) Cui, G.; Lu, Y.; Thiel, W. Electronic excitation energies, three-state intersections, and photodissociation mechanisms of benzaldehyde and acetophenone. *Chem. Phys. Lett.* **2012**, *537*, 21−26. (d) Ou, Q.; Subotnik, J. E. Electronic Relaxation in Benzaldehyde Evaluated via TD-DFT and Localized Diabatization: Intersystem Crossings, Conical Intersections, and Phosphorescence. *J. Phys. Chem. C* **2013**, *117*, 19839−19849.

(13) For examples in the context of enantioselective photocatalysis, see: (a) Brimioulle, R.; Bauer, A.; Bach, T. Enantioselective Lewis Acid Catalysis in Intramolecular [2 + 2] Photocycloaddition Reactions: A Mechanistic Comparison between Representative Coumarin and Enone Substrates. *J. Am. Chem. Soc.* **2015**, *137*, 5170−5176. (b) Huang, X.; Quinn, T. R.; Harms, K.; Webster, R. D.; Zhang, L.; Wiest, O.; Meggers, E. Direct Visible-Light-Excited Asymmetric Lewis Acid Catalysis of Intermolecular [2 + 2] Photocycloadditions. *J. Am. Chem. Soc.* **2017**, *139*, 9120−9123. (c) Stegbauer, S.; Jandl, C.; Bach, T. Enantioselective Lewis Acid Catalyzed *ortho* Photocycloaddition of Olefins to Phenanthrene-9-carboxaldehydes. *Angew. Chem., Int. Ed.* **2018**, *75*, 14593−14596. (d) Yu, H.; Dong, S.; Yao, Q.; Chen, L.; Zhang, D.; Liu, X.; Feng, X. Enantioselective [2 + 2] Photocycloaddition Reactions of Enones and Olefins with Visible Light Mediated by *N,N′*-Dioxide-Metal Complexes. *Chem.—Eur. J.* **2018**, *24*, 19361−19367.

(14) For the density functional: (a) Chai, J.-D.; Head-Gordon, M. Long-range corrected hybrid density functionals with damped atom-atom dispersion corrections. *Phys. Chem. Chem. Phys.* **2008**, *10*, 6615−6620. Dispersion correction: (b) Grimme, S.; Antony, J.; Ehrlich, S.; Krieg, H. A consistent and accurate ab initio parametrization of density functional dispersion correction (DFT-D) for the 94 elements H-Pu. *J. Chem. Phys.* **2010**, *132*, 154104.

(15) For the ORCA program, see: Neese, F.; Wennmohs, F.; Becker, U.; Riplinger, C. The ORCA quantum chemistry program package. *J. Chem. Phys.* **2020**, *152*, 224108.

(16) (a) Granovsky, A. A. Extended multi-configuration quasi-degenerate perturbation theory: The new approach to multi-state multi-reference perturbation theory. *J. Chem. Phys.* **2011**, *134*, 214113. (b) Shiozaki, T.; Győrffy, W.; Celani, P.; Werner, H.-J. Communication: Extended multi-state complete active space second-order perturbation theory: Energy and nuclear gradients. *J. Chem. Phys.* **2011**, *135*, 081106.

(17) Mai, S.; Marquetand, P.; González, L. Nonadiabatic dynamics: The SHARC approach. *Wiley Interdiscip. Rev.: Comput. Mol. Sci.* **2018**, *8* (6), No. e1370.

(18) (c) For the BAGEL program, see BAGEL, Brilliantly Advanced General Electronic-structure Library. http://www.nubakery.org under the GNU General Public License. (d) Shiozaki, T. BAGEL: Brilliantly Advanced General Electronic-structure Library. *Wiley Interdiscip. Rev.: Comput. Mol. Sci.* **2018**, *8*, No. e1331.

(19) (a) Cannizzo, A. Ultrafast UV spectroscopy: from a local to a global view of dynamical processes in macromolecules. *Phys. Chem. Chem. Phys.* **2012**, *14*, 11205−11223. (b) Bauer, B.; Sharma, R.; Chergui, M.; Oppermann, M. Exciton decay mechanism in DNA single strands: back-electron transfer and ultrafast base motions. *Chem. Sci.* **2022**, *13*, 5230−5242. (c) Riedle, E.; Roos, M. K.; Thallmair, S.; Sailer, C. F.; Krebs, N.; Fingerhut, B. P.; de Vivie-Riedle, R. Ultrafast photochemistry with two product channels: wavepacket motion through two distinct conical intersections. *Chem. Phys. Lett.* **2017**, *683*, 128−134. (d) Fingerhut, B. P.; Sailer, C. F.; Ammer, J.; Riedle, E.; de Vivie-Riedle, R. Build-up and Decay of the Optical Absorption in the Ultrafast Photo-Generation and Reaction of Benzhydryl Cations in Solution. *J. Phys. Chem. A* **2012**, *116*, 11064−11074.

(20) Dobryakov, A. L.; Kovalenko, S. A.; Ernsting, N. P. Electronic and vibrational coherence effects in broadband transient absorption spectroscopy with chirped supercontinuum probing. *J. Chem. Phys.* **2003**, *119*, 988−1002.

(21) Balevičius, V.; Pour, A. G.; Savolainen, J.; Lincoln, C. N.; Lukes, V.; Riedle, E.; Valkunas, L.; Abramavicius, D.; Hauer, J. Vibronic energy relaxation approach highlighting deactivation pathways in carotenoids. *Phys. Chem. Chem. Phys.* **2015**, *17*, 19491−19499.

(22) van Stokkum, I. H. M.; Larsen, D. S.; van Grondelle, R. Global and target analysis of time-resolved spectra. *Biochim. Biophys. Acta* **2004**, *1657*, 82−104.

(23) Dutta, A. K.; Nooijen, M.; Neese, F.; Izsák, R. Exploring the Accuracy of a Low Scaling Similarity Transformed Equation of Motion for Vertical Excitation Energies. *J. Chem. Theory Comput.* **2018**, *14*, 72−91.

(24) (a) Capaldo, L.; Ravelli, D.; Fagnoni, M. Direct Photocatalyzed Hydrogen Atom Transfer (HAT) for Aliphatic C-H Bonds Elaboration. *Chem. Rev.* **2022**, *122*, 1875−1924. (b) Cao, H.; Tang, X.; Tang, H.; Yuan, Y.; Wu, J. Photoinduced intermolecular hydrogen atom transfer reactions in organic synthesis. *Chem. Catal.* **2021**, *1*, 523−598.

(25) Luo, Y.-R. *Comprehensive Handbook of Chemical Bond Energies*; CRC Press, 2007.

(26) Luo, Y.-R. *Handbook of Bond Dissociation Energies in Organic Compounds*; CRC Press, 2003.

(27) (a) Klán, P.; Wirz, J.; Gudmundsdottir, A. D. Photoenolization and Its Applications. In *CRC Handbook of Organic Photochemistry and Photobiology*, 3rd ed.; Griesbeck, A.; Oelgemöller, M.; Ghetti, F., Eds.; CRC Press, 2012. (b) Yang, N. C.; Rivas, C. A New Photochemical Primary Process, the Photochemical Enolization of o-Substituted Benzophenones. *J. Am. Chem. Soc.* **1961**, *83*, 2213−2213.

(28) Kabalka, G. W.; Wu, Z.; Ju, Y. Alkylation of aromatic aldehydes with alkylboron chloride derivatives. *Tetrahedron* **2001**, *57*, 1663−1670.

(29) Simmons, E. M.; Hartwig, J. F. On the Interpretation of Deuterium Kinetic Isotope Effects in C-H Bond Functionalizations by Transition-Metal Complexes. *Angew. Chem., Int. Ed.* **2012**, *51*, 3066−3072.

(30) Li, Z.; Pirasteh, A. Kinetic study of the reactions of atomic chlorine with several volatile organic compounds at 240−340 K. *Int. J. Chem. Kinet.* **2006**, *38*, 386−398.

(31) Guo, Y.; Riplinger, C.; Liakos, D. G.; Becker, U.; Saitow, M.; Neese, F. Linear scaling perturbative triples correction approximation for open-shell domain-based local pair natural orbital coupled cluster singles and doubles theory [DLPNO-CCSD(T$_0$/T)]. *J. Chem. Phys.* **2020**, *152*, 024116.

(32) Yamane, M.; Kanzaki, Y.; Mitsunuma, H.; Kanai, M. Titanium(IV) Chloride-Catalyzed Photoalkylation via C(sp^3)-H Bond Activation of Alkanes. *Org. Lett.* **2022**, *24*, 1486−1490.